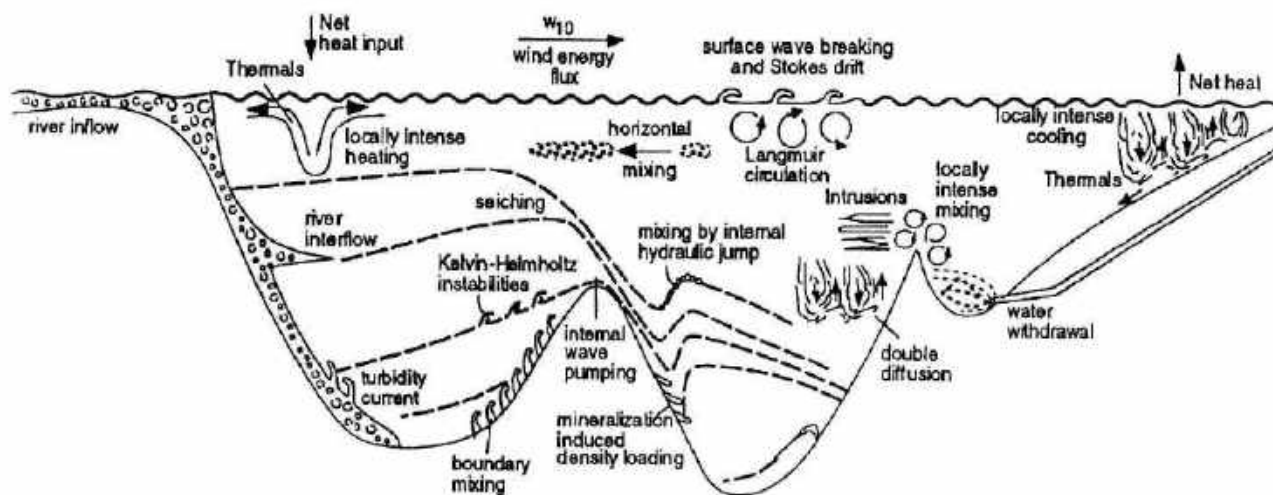


ISBN 9985-9058-9-X

ISSN 1406-023X



4TH WORKSHOP ON
PHYSICAL PROCESSES IN NATURAL WATERS
13-17 SEPTEMBER 1999
ROOSTA, ESTONIA

Edited by Madis-Jaak Lilover and Anu Reinart

ESTONIAN MARINE INSTITUTE

Report series, No. 10

TALLINN, 1999

DOCUMENT DATA SHEET

EDITORS Madis-Jaak Lilover, Ph. D. Anu Reinart, M. Sc.	E-MAIL madis@phys.sea.ee anur@physic.ut.ee	PUBLICATION DATE 29 August 1999
TITLE 4 th Workshop on Physical Processes in Natural Waters, 13-17 September 1999, Roosta, Estonia		
REFERENCE Estonian Marine Institute, Report No.10 , 1XX pp.		
ABSTRACT <i>This report contains contributions to the Fourth Workshop on Physical Processes in Natural Waters. The scope of the workshop includes wide range of aspects of environmental research, including aspects of water quality, transport, mixing processes, flows and stratification as well as interaction between physics, chemistry and biology in the natural water bodies and their remote sensing. The meeting have been held annually in different countries to provide continuous exchange of knowledge and to strengthen the institutional relationship between scientific organizations in Europe.</i>		
ISSUING ORGANISATION Estonian Marine Institute Viljandi mnt. 18B 11216 ESTONIA	TELEPHONE 372 6 281 561	
Director	Toomas Saat	TELEFAX 372 6 281 563
KEYWORDS MIXING WATER EXCHANGE LAKES MODELLING BIO-OPTICS IN LAKES	CONTRACT PROJECT ORDER PRICE 30 DEM	

Copies of this report can be ordered from the library of the Estonian Marine Institute

Editors' Preface

The workshop "Physical Processes in Natural Waters" belongs to a series of workshops on this topic that have been held annually for three last years (Kastanienbaum, 1996; Ispra, 1997; Magdeburg, 1998). The scope of the workshop includes a wide range of aspects of environmental research, including water quality, transport, mixing processes, flows and stratification as well as interaction between physics, chemistry and biology in natural water bodies and their remote sensing. The ultimate goal of the Forth Workshop on this topic is to improve the water quality of the natural waters by sharing information, expertise, and pursuing co-ordinated research between institutions of East-, Middle- and West-Europe.

The coastal and inland waters have received increasing attention during the last few years, because of their importance to human needs (fresh water supply, recreation, tourism, and fisheries). The coastal seas and lakes are the most influenced by human activities when compared to the open ocean. Contaminants in the surface run-off, airborne contaminants, pollutants from industrial, agricultural and urban sources and the dense shipping traffic all pose an increasing threat to the marine environment. The meso-, fine- and micro-scale physical processes are responsible for horizontal and vertical transport as well as distribution/redistribution of substance (contaminants, nutrients in the euphotic layer, toxic substances) in water bodies. Therefore, the knowledge of the physical processes in natural waters would pile up the basis for the environment protection.

This report contains contributions to the Fourth Workshop on Physical Processes in Natural Waters. Many of the presentations were submitted for this volume by their authors as the latest results of their activities to facilitate collaboration.

The workshop is partly financially supported by East East Program of the Open Estonian Foundation. The editors acknowledge the valuable help of Anu Kivilo (OEF) and Aleksander Toompuu (EMI).

Madis-Jaak Lilover and Anu Reinart

Tallinn, August 1999.

**4TH WORKSHOP ON
PHYSICAL PROCESSES IN NATURAL WATERS**

**13-17 SEPTEMBER 1999
ROOSTA, ESTONIA**

Program

Tuesday September 14, 1999

Mixing in Natural Water Bodies

Chair: Dr. A. Toompuu
Dr. A. J. Wüest

Wednesday September 15, 1999

Waves and Circulation in Natural Water Bodies

Chair: Dr. B. Boehrer
Dr. P. Hamblin

Thursday September 16, 1999

Coupling of Biological, Chemical and Physical Processes in Water

Chair: Dr. V. M. Kuchnir

Bio-optics and Remote Sensing of Lakes

Chair: Dr. T. Heege

Agenda of the Fourth Workshop on "Physical Processes in Natural Waters"

Tuesday September 14, 1999

10:00 **Welcome address. Prof. Jüri Elken, Head of Department of Marine Physics,
Estonian Marine Institute**

E.Kaup

A some consequences of physical conditions in lakes for their biology

Mixing in Natural Water Bodies

Chair: Dr. A. Toompuu

10:30 **J. Heinloo**

Turbulence mechanics principles revisited

11:30 **K. Rannat and J. Heinloo**

Double diffusion and turbulence modelling in sea

12:00 **A. J. Wüest and E. Carmack**

A priori estimates of mixing and circulation in the hard-to-reach water body of Lake Vostok

12:15 **A. J. Wüest and A. Simon**

Is the surface boundary layer in lakes laminar at low wind speeds?

12:30-14:00 **Lunch**

Chair: Dr. A. J. Wüest

14:00 **J. Tobias**

Investigation of convective mixing under ice covered lake in spring

14:30 **P. Hamblin and C. He**

Preliminary validation of a model of stratified exchange flow with field observations

15:00-15:30 **Coffee break**

15:30 **J. Virta and K. Pulkkinen**

Modelling vertical mixing in the hypolmion of a lake

16:00 **A.-R. Elo**

The use of a physically based lake model

16:30 **K. Pulkkinen**

Under-ice currents as measured by high frequency 3-D velocimeter

17:00-18:00 Discussion and summary by conveners

Wednesday September 15, 1999

Waves and Circulation in Natural Water Bodies

Chair: Dr. B. Boehrer

10:00 **E. Tsvetova**

Application of inverse modeling to lake investigation

10:30 **E. Bäuerle**

No inertial oscillations in stratified lakes - the dilemma of one-dimensional modelling of wind-induced mixing in lakes.

11:00 **A. Lorke**

Wind- and internal seiche-driven exchange between the basins of a shallow mining lake

11:30 **U. Lemmin** and C.H. Mortimer

Internal seiche climate in the Lake of Geneva

12:00 **S. Semovski**, M.N. Shimarev, W. Alpers and C. Schrum

Lake Baikal internal waves manifestation on ERS SAR imagery

12:30-14:00 **Lunch**

Chair: Dr. P. Hamblin

14:00 **A. Toompuu** and U. Raudsepp

A stochastic model for the sea level data analysis

14:30 **T. Stipa**

Instabilities and along-shore variability in the Finnish coastal current

15:00-15:30 **Coffee break**

15:30 **J. Laanearu** and M. J. Lilover

Hydraulic control of flow through the combination of a sill and horizontal contraction

16:00 **B. Boehrer**, A. Matzinger and M. Schimmelle

Predicting the stratification of future mining lakes

16:30-17:30 Discussion and summary by conveners

Thursday September 16, 1999

Coupling of Biological, Chemical and Physical Processes in Water

Chair: V. M. Kushnir

9:00 **V. M. Kushnir**, B.S. Shtainman and I.A. Danilova

Vertical nutrients fluxes in conditions of sharp density stratification

- 9:30 **L.Umlauf and K. Jöhnk**
Modelling the oxygen stratification of Lake Ammer
- 10:00 **V. Botte and A. Kay**
A numerical study on the effect of the spring warming and the thermal bar on the plankton ecosystem of a deep lake
- 10:30 **L. Falkowska, D. Burska, Z. Klusek and J. Jakacki**
Some periodic dependencies between dissolved and suspended substances in the sea surface micro-layer and gas bubble concentrations in the Baltic Sea
- 11:00 **T. Nõges , Ä. Bilaletdin, T. Frisk, T. Huttula, A. Järvet, H. Kaipainen, R. Kivimaa, O. Malve, M. Möls and P. Nõges**
Results of ecohydrodynamical investigations and modelling on Lake Võrtsjärv in 1994-1997
- 11:30 **V. Y. Zaharov**
The ecosystem approach to an assessment of quality superficial drinking reservoirs
- 12:00-13.30 **Lunch**
- Bio-optics and Remote Sensing of Lakes*
Chair: T. Heege
- 13:30 **T. Heege**
Optical remote sensing of natural waters: some remarks on its principles, possibilities and restrictions
- 14:00 **H. Arst, A. Erm, T. Kutser, A. Reinart**
Optical remote sensing and contact measurements in Estonian and Finnish lakes in 1992-1998
- 14:30-15:00 **Coffee break**
- 15:00 **P. Nõges and T.Nõges**
Seasonal dynamics of phytoplankton, suspended solids and humic substances in Lake Võrtsjärv and their reflection in optical parameters
- 15:30 **L. Falkowska, S. Kaczmarek, and D. Burska**
Diel variability of UV absorption coefficient in the sea surface mikrolayer in the Gdańsk basin.
- 16:00 **A. Herlevi**
About scattering in Nordic waters
- 16:30-17.30 Discussion and summary by conveners. Closing of workshop

TURBULENCE MECHANICS PRINCIPLES REVISITED

(*Lecture for Fourth Workshop on "Physical Processes in Natural Waters",
13.-16. 09. 99. Roosta, Estonia*)

Jaak Heinloo

Estonian Marine Institute

Paldiski Road 1, 10137 Tallinn, Estonia

Prologue

The term "turbulence" is undoubtedly one of the most frequently used term in hydromechanics and the associated specialties, including oceanography and environment physics – the problems under discussion at the present workshop. Disregarding the wide use of the term, the understanding of the essence of turbulence is rather disperse. The situation is much like with an aesthetic term – "beauty": it is pretty hard to give any unique definition but everybody believes recognizing it when seeing.

What are the turbulence properties that make one sure of recognizing it? For some people the essence lies in the stochastic character of motion. Other people are convinced that whatever the mechanical form of motion, including turbulence, it is at least in principle deterministic and that the only difference between the turbulent and non-turbulent motions stands in the degree of the motion complicity. It is also common to tie the turbulence properties with a specific division of a motion field into the mean and fluctuating components and so on.

The notion "turbulence", however, has also another "dimension" – that of an abstraction expressing something general present in all manifestations of the turbulent form of motion independent of particular aims and language chosen to describe it. This abstraction lies in perception of turbulence as of a certain organizational form of liquid media motion, which qualitatively differs from all other forms (shift, laminar flow, undulating motions). It is the presence of this common qualitative basis in the idea of the motion called "turbulent" that explains keeping the term despite the differences in the interpretation of its details.

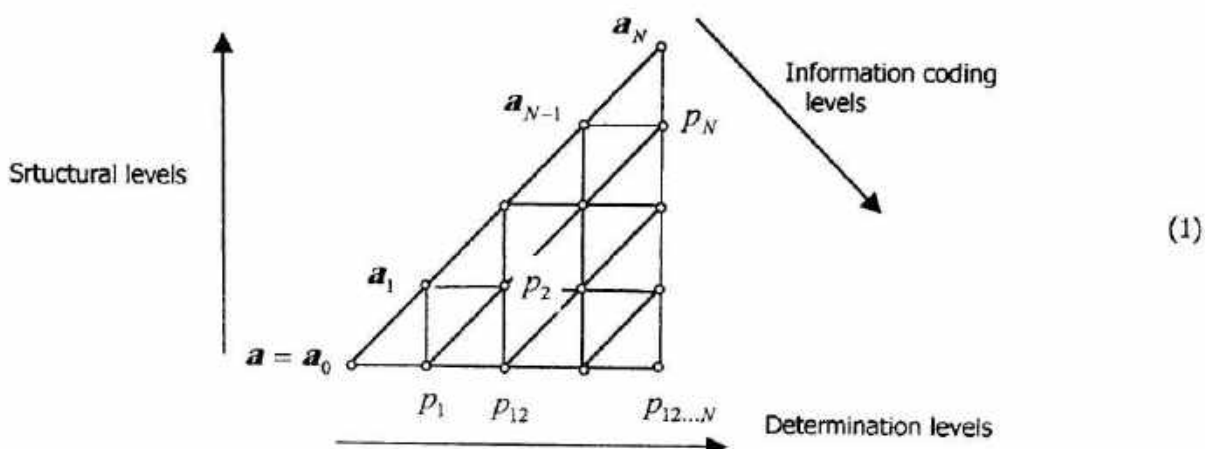
How can we reconcile the notion of turbulence on the above-mentioned level of abstraction with the understanding of its peculiarities? Where is the turbulence situated in the hierarchy of qualitatively differently organized motions in the physical world? What property of turbulent motion is worthy to be upraised into the definition of turbulence quality? What are the requirements following from this quality for formulating turbulence mechanics? How does this turbulence mechanics look like? These are the questions, I hope you will find answers within the next thirty-forty minutes.

1. The theory of hierachic stochastic systems and the location of turbulence in the physical world description as a whole

The theory of hierachic stochastic systems determines as a metatheory. It unites different descriptions of a system (as a material body) and formulates its complete description through a system of theories, describing the initial system on different codes. Thereby, the code defines a complete set of notions, characteristics, variables, measures etc. (named "signs") the quantitative determinacy of which unequivocally fixes the system's state. As fixing the

system's state the codes are defined with the precision up to an arbitrary transformation of their signs, as long as the information they convey remains invariant. The number of different codes and the particular theories formulated on them (named as node theories) are determined by the system's decomposition level. The operations converting the system's description on one decomposition level to descriptions on other levels are defined and all descriptions of a system corresponding to its different decomposition levels are constituted to be equivalent in the metatheoretical sense. The situation is similar to the demand for formulation of any physical law in a form invariant in respect to the choice of the coordinate system.

In more detail. The description of a hierachic stochastic system on its arbitrary fixed decomposition level is organized according to the following code set



The codes of the lowest information coding level ($a = a_0, \dots, a_N$) fix the system's states on its different structural levels. The codes of higher informative coding levels fix the system states as the probability distributions, determined on the signs of codes of the lowest determination levels and formed in the conditions formulated in terms of the codes of higher structural levels.

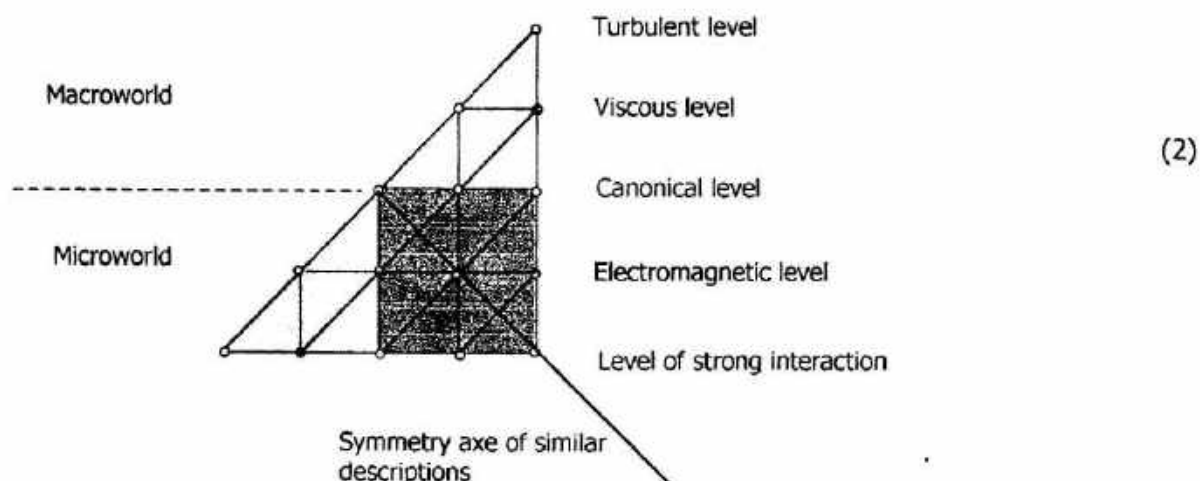
The code set (1) organizes not only different codes. It also presents the whole structure of the system description: the nodes – the node theories, defined as the theories formulated on the fixed codes; the lines between the nodes - recording theories, defined as the theories binding the “neighboring” node theories and so on up to the system theory, binding all node theories of a fixed system decomposition level into a single description.

Let us note that a system described in terms of different node theories can prove mutually exclusive properties. We shall refer to such properties as complementary ones. Thus, a system behaving stochastically according to one node theory (on the level of one code), may behave in a completely determined way according to another node theory (on the level of another code), etc.

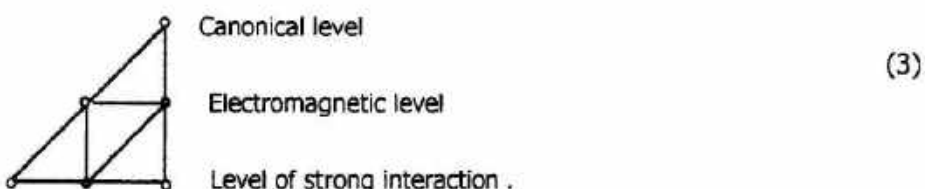
The metatheoretical level of description operates with the system descriptions (1) on different system decomposition levels. The operations of contraction and expansion of system descriptions as the means converting one level of system description into another are defined. The system descriptions following from each other through operations of contraction and expansion are considered coinciding at the metatheoretical level. So, the metatheoretical level

reunites all descriptions of a system, described initially on different system decomposition levels, into a single one.

Let us be more concrete. Considering the physical world as a hierachic stochastic system and decomposing it into five qualitatively different structural levels, the full description of the physical world will be based of the following code set:



The system description (2) can be contracted into different system descriptions of lower order or expanded to system descriptions of higher order (for example, the decomposition of the turbulent level into the motions of different scales). When concerning the purely physical problems the mechanical levels of the system description are traditionally contracted into the Hamilton's description and the description (2) reduces to



When concerning the purely mechanical problems all microlevels are contracted into the same, Hamilton's description:



Confining, dependent on the field of activity, oneself with descriptions (3) or (4) one finds himself with understanding of physics or mechanics as completely separated fields of activity with just the Hamilton mechanics common for both. As it can be seen from (2), the mechanics and physics are not only closely connected to each other but actually constitute a single theory. In other words, the physical world description forms a metatheory with the turbulence

description as a part of it. Moreover, the contractions of the description (2) are contractions into the node theories on the lower information coding level (but not into the node theories of the higher information coding levels). Therefore, the node theories on the lowest information coding level play a fundamental role. The theory of turbulence is involved into this "Club of Five". This point is very important to understand but it says nothing about what the "turbulence" actually is.

2. What actually is "turbulence" ?

Unlike the term "beauty", which is entirely sensual notion and has never pretended to the role of a notion of exact science, the determination of turbulence has to be the cornerstone of any theory of turbulence pretending to have a place among the theories of exact science.

On the way of looking for the answer to the question it appears useful to start from a C.F. Weizäcker's suggestion "those who ask about the bases of the problems of New Age in physics, will discover again the same structures that once had already been discovered by Greek philosophy, although from another point of view". What was important in turbulence for ancient thinkers? It is understanding of turbulence as a motion with permanent creation and disappearance of eddies. Such sort of understanding was essential for the whole ancient period in science, starting from Tahles (625-547 BC). Just the mentioned understanding leads Tales to water in the discussion about the primary matter of the world. In complete form the ancient turbulence understanding is formulated in a didactic poem by Lukrèce (99-55 BC) "De rerum natura". According to M. Serge (1977) this work of Lukrèce is appreciable as the first systematic turbulence description.

In the period of modern science L.F. Richardson (1922) actually formulated the same understanding. What is essential in the concept of L.F. Richardson and his ancient precursors? The most important is the understanding of turbulent character of motion as continuous transmutations of its eddy structure as a specific form of spatial organization of a flow field. It is characteristic that declaration about the transmutations having a role of physical form of motion (Y.I. Frenkel, 1949) in another field of physics – relativistic theory of quantum fields - was later raised into the quality of the most radical idea of the 20th century physics by B.G. Kuznetsov (1968), while the same understanding declared many years earlier in mechanics remained unnoticed.

The understanding of the essence of turbulent motion as transmutations of its eddy structure is undoubtedly substantial. It is worthy to be promoted into the role of definition of turbulence as a qualitatively independent form of motion.

Let us note, that while the metatheoretical treatment of physical world outlook integrates the turbulence problem into the physical world description as a whole organizationally, then the definition of turbulence through transmutations of its structure does it substantially. This way the turbulence problem obtains a fundamental meaning in science.

3. The eddy structure of turbulence and the symmetry of turbulent continuum

In the mechanical sense the main role of eddies stands in carrying the rotational degrees of freedom of environment motion. How these rotational degrees of freedom influence the properties of turbulent continuum?

According to A.N. Kolmogorov the external flow conditions influence the orientation of eddies only of relatively large scale while the small-scale eddies, formed in a cascade process, due to the stochastic character of the latter, are not oriented. A.N. Kolmogorov used this assumption to build the theory of locally isotropic and homogeneous turbulence (1941). What follows from this assumption for us? Firstly, the mean rotational effect of eddies is not zero and, secondly, the mean kinematic effect of the eddy rotation cannot be determined by the velocity of the mean flow only. In other words, the motion of every flow point of turbulent flow field is characterized in addition to the translatory degrees of freedom, described by the mean velocity, also by the independent from the latter rotational degrees of freedom. It is the main property of turbulent continuum, qualitatively separating it from the continuums described in the frame of the classical hydrodynamics (having translatory degrees of freedom only).

Let us note that the classical turbulence mechanics does not ignore the eddy structure of turbulence. Postulating the symmetry of the turbulent stress tensor the classical turbulence mechanics unintentionally connects the mean kinematic effect of the eddy rotation with one of the two assumptions: either the mean kinematic effect of the eddy rotation is absent or it is defined by as - the curl of the averaged velocity field. The first statement belongs to Th. von Kármán, L. Prandtl and their followers, the second – to R.J. Taylor.

4. Turbulence mechanics

4.1. The general theory

Rotational degrees of freedom independent of turbulent continuum mean velocity changes entirely all turbulence treatment. The equation of balance of moment of momentum for turbulent environment doesn't reduce to the condition of symmetry of stress tensor and the motion description has to be based on the laws of conservation of momentum and moment of momentum as independent laws.

Equations for conservation of momentum and moment of momentum have following forms

$$\rho \frac{d}{dt} \mathbf{u} = \{\sigma_{ij}\} + \rho \mathbf{f},$$

$$\rho \frac{d}{dt} \mathbf{M} = \{m_{ij}\} - \boldsymbol{\sigma} + \rho \mathbf{m}, \quad (5)$$

where \mathbf{u} - flow velocity, σ_{ij} - components of stress tensor, \mathbf{f} - density of body forces, \mathbf{M} - internal moment of momentum, m_{ij} - components of moment stress tensor, $\boldsymbol{\sigma}$ - dual vector of the antisymmetric part of stress tensor, \mathbf{m} - body moments.

In the case of turbulent flow

$$\mathbf{u} = \langle \mathbf{v} \rangle. \quad (6)$$

To determine \mathbf{M} through the characteristics of instantaneous flow field we depart from the visual perception of the turbulent field eddy structure and express \mathbf{M} in the form

$$\mathbf{M} = \langle \mathbf{v}' \times \mathbf{R} \rangle, \quad (7)$$

where \mathbf{v}' fluctuating constituent of the flow velocity field, \mathbf{R} curvature radius of streamline of \mathbf{v}' :

$$\mathbf{R} = \frac{\partial \mathbf{e}}{\partial s} \left| \frac{\partial \mathbf{e}}{\partial s} \right|^{-2}. \quad (8)$$

In (8): $\mathbf{e} = \mathbf{v}' / v'$, and s - length of the arc of the streamline of \mathbf{v}' . The definition (7) is the key for expressing all the quantities in equation of moment of momentum through the characteristics of the instantaneous flow field. All these quantities are determined for every point of the flow field as local statistical characteristics of the field's eddy structure.

The kinematic characteristic of the flow field, the velocity of internal rotation Ω , corresponding to \mathbf{M} , defines as

$$\Omega = \left\langle \mathbf{v}' \times \frac{\mathbf{R}}{R^2} \right\rangle. \quad (9)$$

The definitions (7) and (9) determine the moment of inertia of turbulent flow field J ,

$$J\Omega = \mathbf{M}. \quad (10)$$

If J is a scalar then it defines the internal length scale l ,

$$l = \sqrt{J}. \quad (11)$$

Let us now consider how the rotational degrees of freedom of turbulent continuum, independent of the mean velocity, modify the energy situation. It is easy to see that turbulent energy K' , defined as

$$K' = \frac{1}{2} \langle v'^2 \rangle \quad (12)$$

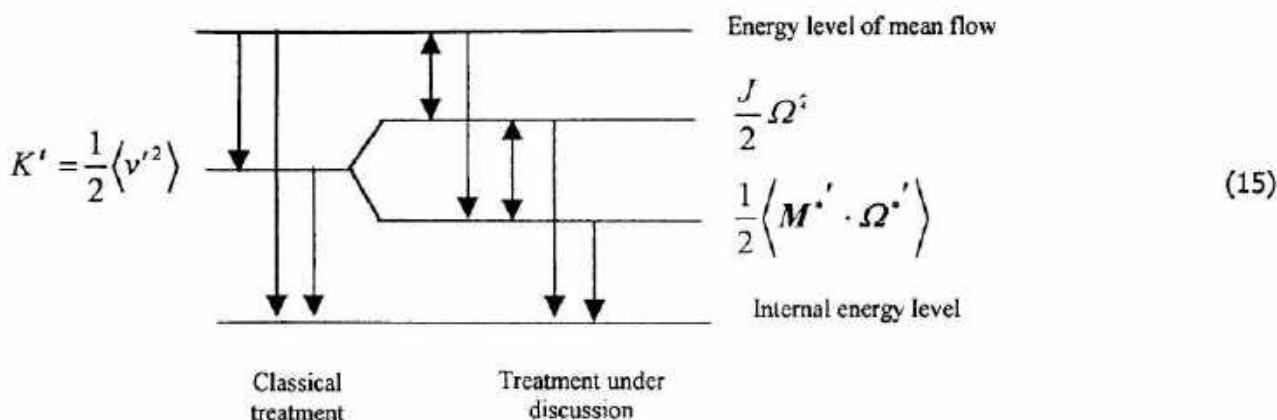
is split in our case into two constituents

$$K' = \frac{J}{2} \Omega^2 + \frac{1}{2} \left\langle \mathbf{M}' \cdot \mathbf{M}' \right\rangle, \quad (13)$$

where \mathbf{M}' and Ω' are defined as fluctuating parts of the instant moment of momentum and velocity of internal rotation,

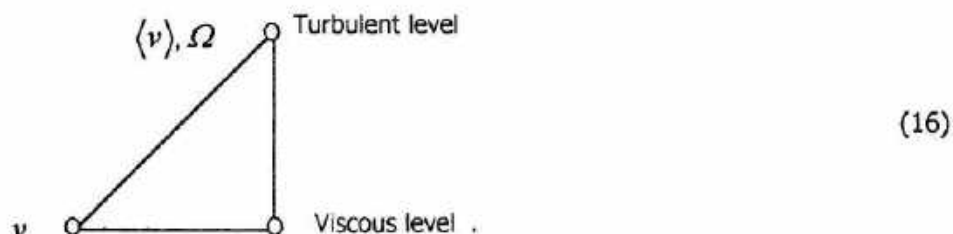
$$\mathbf{M}' = \mathbf{v}' \times \mathbf{R}, \quad \Omega' = \mathbf{v}' \times \frac{\mathbf{R}}{R^2}. \quad (14)$$

With no writing the equations for both constituents of turbulent energy in detail let us confine with an illustration of the situation in the following graph:

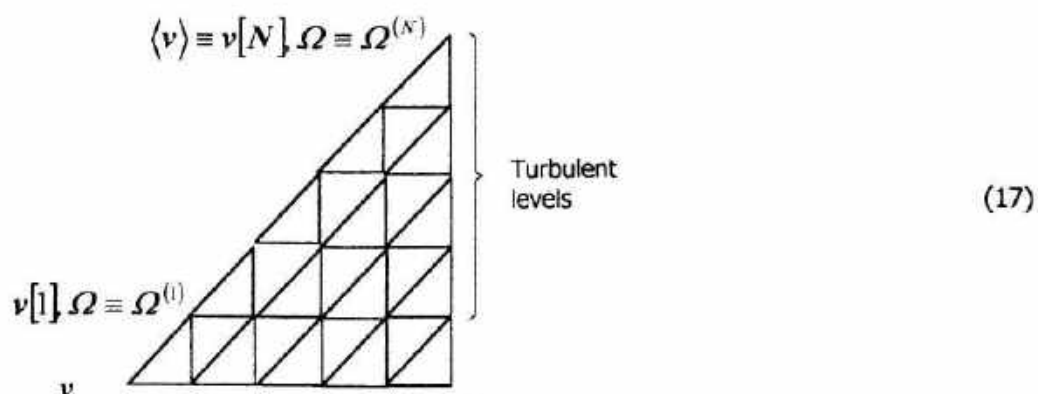


While in the case of classical treatment the physically correct energy interaction between the mean flow and turbulence has unidirectional character, then the treatment under discussion makes two-way energy interaction between the mean flow and turbulence physically well founded.

The description discussed above is based on consideration of the turbulent environment on the level of elementary stochastic system,



If the turbulent level in (16) is decomposed into a set of N levels with different scales of motion, the system description (16) decomposes into the description



Dealing with just mechanical description of turbulence it is sufficient to consider an approximation of the system description (7) accounting for only the two lowest information

coding levels. In the case the graph (17) the full description reduces into a chain of descriptions on the level of elementary stochastic systems, shown in (17).

In the latter case the internal moment of momentum decomposes into the sum

$$\mathbf{M} = \sum_{n=1}^{N=N} \mathbf{M}^{[n]} . \quad (18)$$

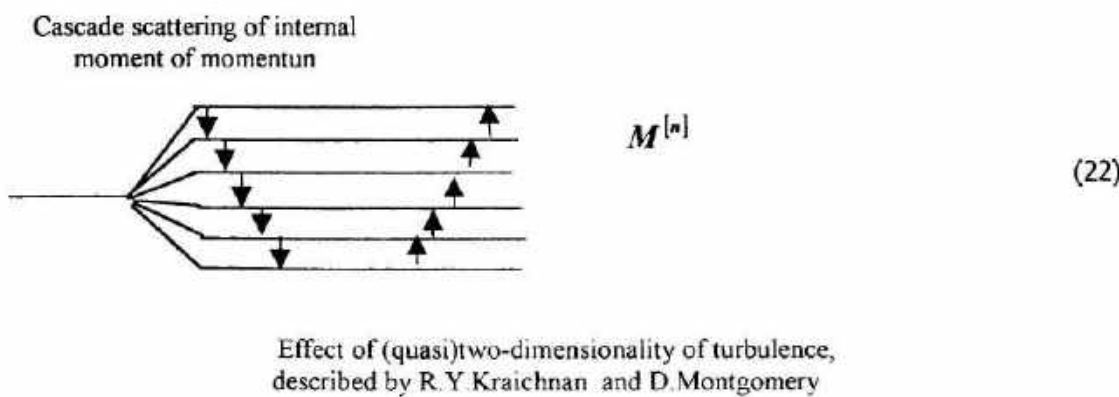
In (18)

$$\mathbf{M}^{[n]} = \left\langle \mathbf{v}[n]' \times \mathbf{R} \right\rangle , \quad (19)$$

where $\mathbf{v}[n]'$ - the n-th constituent of fluctuation velocity field in the expansion into fluctuations of different scales

$$\mathbf{v}' = \sum_{n=1}^{N=N} \mathbf{v}[n]' . \quad (20)$$

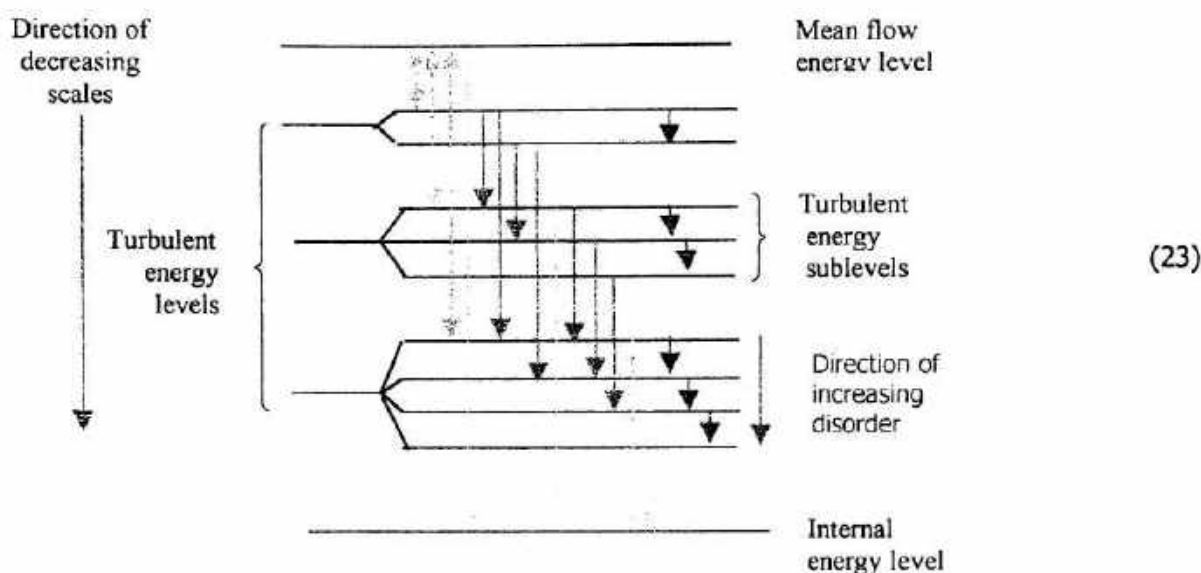
In accordance with (18) the set of equations (5) decomposes into a set defining $\langle \mathbf{v} \rangle$ and $\mathbf{M}^{[n]}$. For example, a special case if only "neighboring" levels of $\mathbf{M}^{[n]}$ interact, is presented on the following graph:



Decomposition of the turbulent energy into the double sum, corresponding to (18), is

$$K' = \sum_{n=1}^N \sum_{p=n}^{N+1} K^{[n:p]} . \quad (22)$$

A graphic example of energy interactions, corresponding to (22) for $N=3$, is:



The suggested technique of hierachic stochastic systems can be applied not only to the description of turbulent motion and energy processes, but also to the description of transport processes of an arbitrary substance in turbulent medium.

The theory I just told about is actually not more than a complete realization of the Richardson-Kolmogorov's conception about hierachic eddy structure of turbulent flow field on the level of balance equations. The formulated theory is well founded and flexible but not applicable for calculation of concrete turbulent flows and processes. Constitutive relations, closing the formulated set of the balance equations have to be formulated.

4.2. The phenomenological theory of turbulence

The phenomenological theory of turbulence bases on the formulated above general theory, complemented with constitutive principles of two types. According to the principle of the first type, widely used in continuum mechanics, the generalized forces of the theory depend only on these generalized velocities on which they act. The principle of the second type (that is essential for the descriptions where $N > 1$) touches the process of R.Y. Kraichnan and D. Montgomery playing important role in interaction of internal moment of momentums but not influencing the energy interactions. All the constitutive relations have to be formulated in the form preserving the properties of balance equations in regard to the contractions and expansions of the system description.

The simplest and presumably the only reasonable constitutive relations are linear. Let us restrict our further discussion with the case of $N=1$. The theory of this type is traditionally

called the theory of Rotationally Anisotropic Turbulence (RAT). The set of motion equations of the theory of RAT has the form

$$\rho \frac{D}{Dt} \langle v \rangle = -\nabla p + \mu \Delta \langle v \rangle + \gamma \nabla \times (2\Omega - \nabla \times \langle v \rangle) + \rho \langle f \rangle \quad (24)$$

$$\begin{aligned} \rho J \frac{D}{Dt} \Omega &= (\Theta_1 + \Theta_2) \nabla \nabla \cdot \Omega + \Theta_1 \Delta \Omega - \\ &- 2\gamma (2\Omega - \nabla \times \langle v \rangle) - 4\kappa \Omega + \rho J (\nabla \langle v \rangle \cdot \Omega) + \rho m^{\infty} \end{aligned} \quad (25)$$

where $\mu, \gamma, \Theta_1, \Theta_2, \kappa$ the coefficients of the theory introduced by linear constitutive relations; m^{∞} - the mass moment generated by external forces. The concrete expressions for $\langle f \rangle$ and m^{∞} depend on the nature of the momentary external force field f . Dependently on the nature of f additional equations may be required. For example, if we describe the transport processes, the set of equations (24), (25) has to be coupled with the equation of turbulent transport and with the energy equation for the small-scale turbulence, having forms

$$\frac{D}{Dt} C = k^{mol} \Delta C + \nabla \cdot (k^{turb} \cdot \nabla C) + q_C \quad (26)$$

$$\rho \frac{D}{Dt} K'_0 = \nabla \cdot (k^{turb} \cdot \nabla K'_0) + Q - \psi + q_K \quad (27)$$

where k^{mol} - the coefficient of molecular diffusivity,

$$k^{turb} = k_0 K'_0 I - k_1 E \cdot \Omega + k_2 (\Omega^2 I + \Omega \Omega) \quad (28)$$

- the tensor of turbulent diffusivity, q_C and q_K denote density of internal sources of C and K'_0 , Q denotes the interaction term of energy K'_0 with the energy of mean flow,

$$\psi = \frac{1}{\tau} K'_0 \quad (29)$$

the dissipative function of energy K'_0 (τ - characteristic time of decay of K'_0 due to the dissipation ; $\tau = const$). In (28) k_0, k_1 and k_2 the coefficients of diffusion ($k_0 = c\tau, k_1 = c_2\tau_{\Omega}J$; c, c_1 and c_2 - dimensionless parameters). Let us note that the tensor of turbulent transport k^{turb} also appears to be asymmetrical. A.Toompuu *et. al.* (A.Toompuu, J.Heinloo, T.Soomere, *Okeanolooogia*, v. 29, N.6., 1989) illustrated the effect caused by the asymmetry of tensor k^{turb} by describing the generation of the Gibraltar Salinity Anomaly in the north Atlantic Ocean.

4.3. The RAT theory and the Classical Semi-Empirical Theory of Turbulence

Assuming the body force and body moment in (24) and (25) are absent, the equations (24), (25) permit three different situations when the media's description is realized in the frame of

momentum conservation law (24) only, as it is assumed in the Classical Semi-Empirical Theory of Turbulence.

a) The first situation is determined by the condition

$$\nabla \times \langle v \rangle \equiv 0. \quad (30)$$

When condition (30) holds, and if

$$\Omega = 0 \quad (31)$$

in some initial time instant, then it follows from equation (25), that Ω remains equal to zero for every time instant in future. In this case the set of equations (24) and (25) reduces into a single equation

$$\rho \frac{D}{Dt} \langle v \rangle = -\nabla p + \rho \langle f \rangle, \quad (32)$$

the expression for k^{turb} in (28) reduces to

$$k^{\text{turb}} = k_0 K_0^2 I, \quad (33)$$

Q in the equation of turbulent energy vanishes and the equations (26) and (27) reduce into the equations, differing from the corresponding equations of classical semi-empirical theory, based on assumption

$$k^{\text{turb}} \sim \ell \sqrt{K} I \text{ and } \psi \sim \ell^{-1} K^{3/2}, \quad (34)$$

where ℓ - the mixing length, by defining ℓ as

$$\ell \sim \tau \sqrt{K}. \quad (35)$$

The assumption (30) is justified, for example, for describing the stratification process of temperature, salinity and density fields due to double-diffusivity (*Ü.Võsumaa and J.Heinloo, JGR, v.101, No 11, 1996; J.Heinloo and Ü.Võsumaa, Annales Geophysicae. V.10, 1992*). The used model is physically well-founded but computationally rather complicated. The investigations of the associated computational problems are in progress (*K.Rannat, P.Miidla, Algebra ja analüüsmeetodid, Tartu Ülikool, Tartu 1998*).

b) We meet the second situation if

$$\nabla \times \langle v \rangle \neq 0. \quad (36)$$

and

$$\gamma \equiv 0. \quad (37)$$

The condition (37) means that there is no friction in eddy rotation.

Analogously to the previous situation, from the validity of the condition (31) at any initial time instant follows that Ω will stay identically zero for every future time instant. In this case the set of equations (24) and (25) reduces to the equation

$$\rho \frac{D}{Dt} \langle v \rangle = -\nabla p + \mu \Delta \langle v \rangle + \rho \langle f \rangle \quad (38)$$

and Q in energy balance equation (27) reads as

$$Q = \mu (\nabla \langle v \rangle)^2. \quad (39)$$

Let us note that the RAT theory gives no reason to identify μ and k^{turb} as it is assumed in Classical Semi-Empirical Theory of Turbulence. The connection between μ and k^{turb} can be established for a special case accepting an additional assumption of dependence of μ on the energy of small-scale turbulence (like the coefficient of molecular viscosity depends on the temperature), i.e. assuming that

$$\mu = \mu(K'_0). \quad (40)$$

If the condition (40) takes place, instead of the equation (38), we have

$$\rho \frac{D}{Dt} \langle v \rangle = -\nabla p + \nabla \cdot (\mu \nabla \langle v \rangle) + \rho \langle f \rangle, \quad (41)$$

while the descriptions of transport and energy processes remain the same as in the case "a". The model describing resuspension in bottom layer, based on the described situation and complemented with the assumption (40), is in work.

c) The third situation is determined by the assumption (35) and the assumptions

$$\Theta_1 = J\mu \text{ and } \kappa \equiv 0. \quad (42)$$

The second assumption in (37) claims that the decay of internal moment of momentum due to the cascade process is excluded. In this case the condition

$$\Omega = \frac{1}{2} \nabla \times \langle v \rangle, \quad (43)$$

assumed to be valid at an initial time instant, expands to all future time instants. Unlike the previous case the equation (25) does not vanish and returns to the equation equivalent to the equation (38).

For a more detailed analyses of the situation let us inspect the simplest case, if

$$\langle v \rangle = (0, 0, \langle v \rangle(x)), \quad C = C(x), \quad K'_0 = K'_0(x), \quad (44)$$

then

$$|\Omega| = \frac{1}{2} \left| \frac{\partial \langle v \rangle}{\partial x} \right|, \quad (45)$$

$$\nabla \cdot (\tilde{k}^{turb} \cdot \nabla K_o^t) = \frac{\partial}{\partial x} \cdot \left(\tilde{k}^{turb} \frac{\partial}{\partial x} K_o^t \right) \text{ and } \nabla \cdot (k^{turb} \cdot \nabla C) = \frac{\partial}{\partial x} \cdot \left(\tilde{k}^{turb} \frac{\partial}{\partial x} C \right), \quad (46)$$

where

$$\tilde{k}^{turb} = k_0 K_o^t + k_2 |\Omega|^2. \quad (47)$$

Let us define, similar to l in (35), ℓ_Ω as

$$\ell_\Omega = \frac{1}{|\Omega|} \sqrt{K^\Omega}, \quad (48)$$

where

$$K^\Omega = \frac{1}{2} J \Omega^2, \quad (49)$$

and $|\Omega|^{-1}$ plays the role of internal time scale of large-scale turbulence. From (48) and (49) we get

$$\ell_\Omega = \frac{l}{\sqrt{2}}, \quad (50)$$

where $l = \sqrt{J}$. Let's note that l and ℓ_Ω are related like the Prandtl's and Taylor's mixing lengths of the semi-empirical theory.

Using turbulent diffusion coefficient \tilde{k}_Ω describing turbulent transport process caused by Ω , the semi-empirical formula

$$\tilde{k}_\Omega^{turb} \sim l \sqrt{K^\Omega} \quad (50)$$

and the definition of ℓ_Ω (48), we obtain

$$\tilde{k}_\Omega^{turb} \sim l \ell_\Omega \left| \frac{\partial \langle v \rangle}{\partial x} \right|. \quad (51)$$

After defining the effective mixing length \hat{l} ,

$$\hat{l} = \sqrt{l \ell_\Omega}, \quad (52)$$

the relation (51) obtains a well-known form, usual for semi-empirical theory of turbulence:

$$\tilde{k}_\Omega^{turb} \sim \hat{l}^2 \left| \frac{\partial \langle v \rangle}{\partial x} \right|. \quad (53)$$

Supposing that $J = const.$ and equalizing τ_Ω in the expression $k_2 = c_2 \tau_\Omega J$ with $|\Omega|^{-1}$, the expression for \tilde{k}_Ω^{turb} (53) becomes equivalent to the term $k_2 |\Omega|^2$ in (47).

Let us recall that all what was said about the accordance of the RAT theory and the Classical Semi-Empirical theory of turbulence holds in the case of absence external body forces and body

moments. If the external body forces and body moments exist, the situation can be different. For example, the latter discussed situation does not work for turbulent flows of stratified mediums.

The aim of showing links between the RAT theory and classical semi-empirical theories of turbulence in some specific situations is not the full rehabilitation of the methods of semi-empirical theories but just demonstrating how limited is the area where they can be applied. There is no any physical argumentation supporting validity of the conditions (36) or (37). The situation (35), as a rule, always generates the Ω field, different from $\frac{1}{2}\nabla \times \langle v \rangle$, and the description has to be based on both equations (24) and (25). As an example of such description a model of the vertical structure of the sea (*Ü. Võsumaa and J. Heinloo, JGR, v.101, No 11, 1996; J. Heinloo and Ü. Võsumaa, Annales Geophysicae, V.10, 1992*) can be mentioned.

Epilogue

The lecture started from a rather general philosophical treatment of the turbulence problem and finally reached concrete practical recommendations. Of course, one may find different reasons not to accept it. The traditions, the success of the classical turbulence treatment, personal habitudes are just some of them. But, if one wants to build up his scientific activity on scientific truth, he has to accept it first. I hope that the lecture at least stimulates your endeavors in this direction. Unfortunately, what was said is all I was able to address in this lecture. Those who can read Russian can find more detailed treatment in works [1-3]. Others have to wait until the English version of the book [1] will be published.

Recommended literature on the lecture topics:

1. J. Heinloo. Turbulence Mechanics. Introduction into the General Theory of Turbulence (in Russian), *Estonian Academy of Science, Tallinn, 1999*.
2. J. Heinloo. Phenomenological mechanics of turbulence (in Russian), *Valgus, Tallinn, 1984*
3. J. V. Nemirovski and J. Heinloo. Local-eddy theory of turbulence (in Russian), *Novosibirsk University, Novosibirsk, 1980*.

MODEL OF VERTICAL TRANSPORT IN STRATIFIED TURBULENT ENVIRONMENT, CONSIDERED AS ROTATIONALLY ISOTROPIC

Kalev Rannat and Jaak Heinloo

Estonian Marine Institute
Paldiski Road 1, 10137 Tallinn, Estonia

Introduction

Classical turbulence mechanics postulates an absence of internal rotational degrees of freedom of turbulent environments, independent from mean flow velocity. According to the theory of rotationally anisotropic turbulence of J. Heinloo [1-5] the mentioned property (called as rotational isotropy) is not universal. Application of more general theory will be unavoidable. The said does not exclude rotationally isotropic models but restricts their usability. The situation is discussed on the practical problem – the problem of vertical transport in stratified turbulent environments.

1. The theory

1.1. The definition

According to the theory of rotationally anisotropic turbulence (RAT theory) the rotational isotropy of turbulence is defined as a property of turbulence flow field with zero moment of momentum \mathbf{M} and internal rotation velocity $\boldsymbol{\Omega}$,

$$\mathbf{M} = \langle \mathbf{M}^* \rangle = 0, \quad \boldsymbol{\Omega} = \langle \boldsymbol{\Omega}^* \rangle = 0, \quad (1)$$

where

$$\mathbf{M}^* = \mathbf{v}' \times \mathbf{R} \quad \text{and} \quad \boldsymbol{\Omega}^* = \frac{\mathbf{M}^*}{R^2} \quad (2)$$

- instantaneous moment of momentum and internal rotation velocity of turbulent flow field. In (2) \mathbf{v}' - fluctuating component of flow velocity and \mathbf{R} - radius-vector of \mathbf{v}' field. In terms of $\boldsymbol{\Omega}^*$ and \mathbf{R} , \mathbf{v}' is represented as

$$\mathbf{v}' = \boldsymbol{\Omega}^* \times \mathbf{R} \quad (3)$$

and turbulence energy $K = \frac{1}{2} \langle v'^2 \rangle$ gets a form

$$K = \frac{1}{2} \left\langle R^2 \boldsymbol{\Omega}^{*2} \right\rangle. \quad (4)$$

1.2. The corollaries

From (3) and the condition $\langle \mathbf{v}' \rangle = 0$ follows that $\boldsymbol{\Omega}$ and \mathbf{R} are not correlated and the turbulent energy K in (4) is represented as

$$K = \frac{1}{2} \left\langle R^2 \right\rangle \left\langle \boldsymbol{\Omega}^{*2} \right\rangle. \quad (5)$$

Defining the characteristic length and time scales l and t_0 as

$$l = \sqrt{\langle R^2 \rangle}, \quad t_0 = \sqrt{\langle \Omega^2 \rangle^{-1}}, \quad (6)$$

we'll get

$$l = t_0 \sqrt{2K}. \quad (7)$$

1.3. The balance equations

Let q_i denote the set of scalar state parameters of environment and let $q_i = q_i(z, t)$ and $K = K(z, t)$. The equations for q_i and K , for the case of rotationally isotropic turbulent environments have the forms:

$$\frac{\partial q_i}{\partial z} - \xi \frac{\partial q_i}{\partial z} = \frac{\partial}{\partial z} \left[(k_i + k^{\text{turb}}) \frac{\partial q_i}{\partial z} \right], \quad (8)$$

$$\frac{\partial K}{\partial z} = \frac{\partial}{\partial z} \left[k^{\text{turb}} \frac{\partial K}{\partial z} \right] - \psi - \frac{g}{\rho_0} k^{\text{turb}} \frac{\partial \rho}{\partial z} + Q, \quad (9)$$

where ξ - the settling velocity; k_i and k^{turb} - coefficients of molecular and turbulent diffusion of q_i ; g - gravity acceleration;

$$Q = \frac{\mu}{\rho_0} \left(\frac{\partial v}{\partial z} \right)^2 \quad (10)$$

and ψ - turbulence energy generation and dissipation terms (μ - coefficient of turbulent shear viscosity and v - averaged flow velocity, assumed to be determined from any theory based on the assumption of rotational symmetry of turbulent flow field); ρ_0 and $\rho = \rho(q_i)$ - characteristic and actual density of environment; coordinate z is directed in the direction of gravity acceleration.

Using semi-empirical formulas for k^{turb} and ψ :

$$k^{\text{turb}} = c_1 l K^{1/2} \quad \text{and} \quad \psi = c_2 l^{-1} K^{3/2}, \quad (11)$$

and defining l according to (7) we'll get

$$k^{\text{turb}} = k K, \quad \psi = \frac{1}{t_K} K, \quad (12)$$

where $k = \sqrt{2} c_1 t_0 = c t_K$ and $t_K = \frac{1}{\sqrt{2} c_2} t_0$.

After substituting Q , k^{turb} and ψ in (8) and (9) by their expressions in (10) and (12), we'll get a set of equations for q_i and K :

$$\frac{\partial q_i}{\partial z} - \xi \frac{\partial q_i}{\partial z} = \frac{\partial}{\partial z} \left[(k_i + c t_K K) \frac{\partial q_i}{\partial z} \right] \quad (13)$$

$$\frac{\partial K}{\partial z} = c t_K \frac{\partial}{\partial z} \left[K \frac{\partial K}{\partial z} \right] - \left(\frac{1}{t_K} + \frac{g c t_K}{\rho_0} \frac{\partial \rho}{\partial z} \right) K + \frac{\mu}{\rho_0} \left(\frac{\partial v}{\partial z} \right)^2. \quad (14)$$

Within the linear state equation $\rho = \rho_0 + \sum_i \eta_i (q_i - q_{i0})$ the term $\frac{gct_K}{\rho_0} \frac{\partial p}{\partial z} K$ in (14) gets the form

$$\frac{gct_K}{\rho_0} \frac{\partial p}{\partial z} = \frac{gct_K}{\rho_0} \sum_i \eta_i \frac{\partial q_i}{\partial z}. \quad (15)$$

The equation (14) omits to t_K the sense of time extent in course of which turbulent energy K of homogeneous K , ρ and v fields decreases e times. Within a scope of RAT theory this time is assumed to be constant.

Let us note that there does not exist any reason, following from RAT theory, to equalize μ and k^{turb} . If we postulate this equality i.e. if

$$\mu = k^{\text{turb}}, \quad (16)$$

the equations (13) and (14) reduce to ones in classical semi-empirical theory with an additional assumption (7), expressing the mixing length through the turbulent energy K .

1.4. Admissibility of rotationally isotropic situation

According to the RAT theory the situation (1), (2) is unstable in general. It is stable only in case of absence of interaction between the mean flow, described by velocity field v and eddy rotation. In such a case the structure of turbulence becomes rotationally anisotropic (i.e. $M, \Omega \neq 0$), even if at the initial time instant the conditions (1) and (2) take place. In case of the description of dynamics of turbulent environment we need the simultaneous consideration of momentum and the moment of momentum balance, the turbulence generation term in (14) complicates, the turbulence energy divides into two interacting parts, interpreted as the energies of rotationally anisotropic and rotationally isotropic constituents of turbulence, and the turbulent diffusion coefficient depends on both of them.

2. Application of the theory. The model of vertical structure of a sea.

In a sea

$$q_i = \{T, S, C\}, \quad k_i = \{k_T, k_S, 0\}, \quad \eta_i = \{-\alpha, \beta, \eta\} \text{ and } \xi_i = \{0, 0, \xi\} \quad (16)$$

and the system of equations (12) and (13) reduces to the system of equations for T, S, C and K . Different restricted versions of the model (submodels) can be determined:

- the model of upper layer

$$k_S, k_T \ll ct_K K, \quad C \equiv 0; \quad (17)$$

- the model of medium layer [6]

$$C \equiv 0 \text{ and } v = 0; \quad (18)$$

- the model of bottom layer

$$T = \text{const}, \quad S = \text{const}. \quad (19)$$

References

1. J.Heinloo. Turbulence Mechanics. Introduction to the General Theory of Turbulence (in Russian), *Academy of Sciences of Estonia, Tallinn, 1999.*
2. J.Heinloo. Phenomenological Mechanics of Turbulence (in Russian), *Valgus, Tallinn, 1984.*
3. J.V.Nemirovski and J.Heinloo. Local-eddy Theory of Turbulent Flows (in Russian). *Novosibirsk University, Novosibirsk, 1980.*
4. J.Heinloo and Ü. Võsumaa. Rotationally anisotropic turbulence in a sea. *Ann.Geophysicae, 10, 1992.*
5. Ü. Võsumaa and J.Heinloo. The model of the vertical structure of the turbulent active layer of the sea. *JGR, vol.101. No.C10, 1996*
6. P.Miidla and K.Rannat , The dynamics of the intermediate layer of a sea (in Estonian). *Algebra ja analüüsmeetodid V, Tartu, 1998.*

A PRIORI ESTIMATES OF MIXING AND CIRCULATION IN THE HARD-TO-REACH WATER BODY OF LAKE VOSTOK

Alfred Wüest¹ and Eddy Carmack²

¹ Swiss Federal Institute of Environmental Science and Technology (EAWAG),
CH-8600 Dübendorf, Switzerland (wuest@eawag.ch)

² Institute of Ocean Sciences; 9860 West Saanich Road, Sidney, B.C. V8L 4B2, Canada
(carmacke@dfo-mpo.gc.ca)

Introduction

Of all lakes on Earth, Vostok reigns most mysterious. Located in East Antarctica (near 77°S; 105°E) this 10 to 20 million year-old freshwater body is covered by a 3.7 to 4.2 km thick layer of glacial ice. Lake Vostok is large: it has an area (~ 14,000 km²) near that of Lake Ladoga, a volume (~ 1,800 km³) near that of Lake Ontario, and a maximum depth (~510 m) near that of Lake Tahoe. Lake Vostok, has been probed by remote survey methods only (e.g. by airborne radio echo sounding, satellite altimetry, and seismic measurements) since its discovery in 1974 (Kapitsa et al., 1996), and no *in-situ* measurements have yet been made. There is evidence, however, that the lake is composed of fresh water, that up to 300 m thick sediments cover the lake floor, and that microorganisms that have been isolated from their surrounding for millions of years will be found in its waters and sediments (Kapitsa et al., 1996). The combination of extraordinarily thick ice cover and extreme isolation of its microorganisms makes Vostok an attractive analog for planetary exploration, as noted in the NASA Europa-Vostok Initiative.

2. Thermodynamic Factors Influencing Circulation in Lake Vostok

Due to the absence of wind and rivers, we suppose that density-driven flows will dominate water motion within sub-glacial lakes such as Vostok. Consideration must thus be given to (1) the effect of pressure on the temperature of maximum density; (2) the effect of pressure on the freezing temperature; (3) geothermal heating, (4) Coriolis effect and (5) potential particle and gas fluxes from the overlying ice and their related mineralization and dissolution within the lake's water. In turn, the inclined ice ceiling may modify these factors. The depression of the temperature of maximum density, T_{MD} [°C], with pressure p [dbar or 10⁴ Pa] is given in the "linearized-form" (Chen and Millero, 1986) by (cf. Figure)

$$T_{MD}(S,p) = T_{MD}(S, 0) - 0.00215 \cdot p, \quad [^{\circ}\text{C}] \quad (1)$$

where S is salinity. The depression of the freezing temperature, T_{FP}, with pressure is following (Figure)

$$T_{FP}(S,p) = T_{FP}(S,0) - 0.000753 \cdot p \quad [^{\circ}\text{C}] \quad (2)$$

(Fujino et al., 1974; UNESCO, 1978). Taking T_{MD}(0,0) ~ 3.984 °C and T_{FP}(0,0) ~ 0 °C, we see that the two lines cross at a critical pressure p_{Crit} ~ 2840 dbar {3.984/(0.00215 -

$0.000753\}$. This corresponds to an overlying ice cover of about 3170 m thickness (Figure) for an ice density of $\rho_{\text{Ice}} \sim 913 \text{ kg m}^{-3}$ (Kapitsa et al., 1996). Two cases are thus evident. First, for ice sheets thinner than this critical pressure p_{Crit} , we have $T_{\text{MD}} > T_{\text{FP}}$. We therefore have $T_{\text{MD}} > T$, which implies that the thermal expansivity $\alpha [\text{K}^{-1}] = -\rho^{-1} \partial \rho / \partial T < 0$. Hence, a stable density stratification occurs for geothermal heating from below (stability $N^2 [\text{s}^{-2}] = g \alpha \partial \theta / \partial z$; θ is potential temperature and z is vertical coordinate, positive upwards). This is the classical situation of stratified freshwater lakes in winter with an inverse temperature gradient, so we therefore refer to this as the "Lake case". Second, for ice sheets thicker than p_{Crit} , as it is the situation in Lake Vostok, the sign changes: $T_{\text{MD}} < T_{\text{FP}}$, and therefore $T_{\text{MD}} < T$. It implies $\alpha > 0$ and the stability $N^2 < 0$ will lead to unstable water columns for geothermal heating from below. In terms of convection, Lake Vostok behaves more like an ocean than a lake. We therefore refer to this ($\alpha > 0$) as the "Ocean case" (Figure).

Combined data from airborne radio echo sounding, ERS-1 satellite altimetry (Siegert and Ridley, 1998) and seismic measurements (Kapitsa et al., 1996) provide rough estimates of the lake's morphometry and ice cover (Table). The adjacent ice sheet flows onto the lake from the northwest and west at a speed of about 3 m a^{-1} (Kapitsa, et al., 1996; Siegert and Ridley, 1998). Over the lake, the ice sheet is significantly thicker towards the north: Being 4.2 and 3.7 km thick over the northern and southern ends of the lake, respectively, the ice cover is thinning towards south by $\sim 460 \text{ m}$. The ice surface has a north-south slope of $\sim 40 \text{ m}$ over the length of $L \sim 230 \text{ km}$ ($\sim 0.17 \text{ m km}^{-1}$). In order to balance hydrostatic pressure the ice sheet must thicken from the south to the north end of the lake by $\{1 + \rho_{\text{Ice}}/(\rho - \rho_{\text{Ice}})\} \cdot 40 \text{ m} \sim 460 \text{ m}$ (again $\rho_{\text{Ice}} \sim 913 \text{ kg m}^{-3}$ is assumed), in perfect agreement with soundings. For the presented calculations we choose the ice thickness difference as 460 m, which will lead to a temperature difference of $\Delta T_{\text{Ice}} = 0.31 \text{ K}$ along the 230 km north-south section. We expect the ice ceiling temperature $T_{\text{Ice}}(x)$ to be ΔT_{Ice} cooler at the north relative to the south end.

Two features of the ice sheet are important for our analysis. First, the ERS-1 satellite altimetry revealed an astonishing flat terrain over the lake's ice (Siegert and Ridley, 1998), indicating that the irregularities of the ice thickness flowing onto the lake are smoothed out by some processes (see below). Second, airborne ice penetrating radar and deep ice core drilling indicate the presence of a $\sim 150 \text{ m}$ thick "clear"-ice layer at the base of the ice over a $\sim 30 \text{ km}$ -long range at the southeast (down-flow) end of the lake (NSF, 1999). This is interpreted to be ice accreted from the lake's freshwater as the ice sheet flows over Lake Vostok towards the southwest. In addition there are signs that ice is melting at fast rates as inflowing ice encounters the lake water at the northwest end (NSF, 1999).

3. To be expected hydrodynamics in Lake Vostok

Four boundary conditions are crucial for the internal dynamics of the Lake Vostok water body:

- geothermal heat flux, F_{geo} ,
- Freezing and melting (or heat fluxes from/to the ice ceiling)
- absolute ice thickness, $H_{\text{Ice}}(x)$,

- tilt of the ice ceiling (temperature difference along the tilted ice ceiling, ΔT_{Ice})

In the presentation we will show how these four parameters govern the lake's internal dynamics by evaluating the vertical and horizontal convections. Information and assumptions on boundary conditions, lake morphometry and physical constants are listed in Table.

The time scale for ice to pass over the width of the lake (~60 km) is about $\tau_{\text{Ice-passage}} = 20,000$ years (60 km at 3 m a^{-1} , see NSF, 1999). On this time scale one can expect the lake volume and lower boundaries of the ice sheet to change substantially. Since we do not know those boundary conditions (including the conductive heat loss through the ice) well, we make the following rough assumptions: (1) The heat flux through the lake is equal to the geothermal heat flux $F_{\text{geo}} \sim 0.05 \text{ W m}^{-2}$ and is in steady-state, i.e. the heat entering from below leaves the lake water at the ice ceiling. This implies that there is no net heating or cooling of the lake water. (2) At the down-flow end of the ice-ceiling, re-freezing of ~150 m of ice takes place on the time scale of the ice passage over the lake (NSF, 1999). This corresponds to a freezing rate of $E \sim 7.5 \text{ mm a}^{-1}$. Taking $L_p = 334,000 \text{ J kg}^{-1}$ as the latent heat of freshwater ice, this is equivalent to a heat flux from the ceiling of $F_{\text{FM}} = E L_p \rho_{\text{Ice}} \sim 0.072 \text{ W m}^{-2}$ or $\sim 1.4 F_{\text{geo}}$. The second assumption expresses that the lake volume may behave quite intermittent on geological time scales, since the time needed for the equivalent volume of Lake Vostok to be melt is only $\rho H_{\text{avg}} L_p / F_{\text{geo}} \sim 27,000$ years (average lake water depth $H_{\text{avg}} = 130 \text{ m}$; Table), which is not significantly longer than the ice passage. Whereas the phenomenon of the subglacial lake may be old (millions of years), the actual water in the lake is most probably not (thousands of years).

Two types of internal motions can be expected: (a) convective vertical plumes with velocity scales of $\sim 0.3 \text{ mm s}^{-1}$ and (b) horizontal convection of the same magnitude driven by baroclinic pressure gradients, consistent with momentum and energy conservation. Whereas the vertical convection is mainly dependent of the geothermal heat flux, the key parameters for the horizontal circulation are the prescribed heat fluxes (melting, freezing), the tilting of the ice ceiling and the Coriolis force. Changes in the behavior of the circulation will occur over time scales of a few decades, defined by the time scales of temperature adjustment (< 1 decade), circulation time scale (several decades) and the time scale of removal of ice roughness elements (century). The horizontal convection will not stop, before the ice ceiling is leveled out. For sub-glacial lakes without a tilted ceiling, no horizontal motion can be expected.

Vertical mixing can be expected to be very fast, efficiently eliminating density differences in the vertical on a time scale of days. In the horizontal however there will remain a density difference, which is $\sim 1/3$ of the one imposed by the pressure-dependent freezing temperature $T_{\text{FP}}(p)$ along the tilted ice ceiling.

Coupled to the convection is a lake internal heat flux, which leads to melting at the "thick-ice" side (north) and freezing at the "thin-ice" side (south) of up to 150 m (NSF, 1999) as the ice sheet passes over the lake. These internal heat fluxes remove topographic irregularities on time scales much shorter than the ice passage time. This corroborates well with the observation that the ice surface is extraordinarily flat. The general shape of the ice sheet however (460 m thicker at the north end) reflects the N-S structure of the thickness of

the inflowing ice and is for sure not related to the internal ice pump, which tends to level the ice ceiling.

References

- Chen, C.T., and F.J. Millero, Precise thermodynamic properties for natural waters covering only the limnological range, *Limnol. Oceanogr.*, 31, 657-662, 1986.
- Fujino, K., E.L. Lewis, and R.G. Perkin, The Freezing point of sea water at pressure up to 100 bars. *J. Geophys. Res.*, 79, 1792-1797, 1974.
- Hinze, J. O., Turbulence, McGraw-Hill, New York, 618 pp., 1975.
- Kapitsa, A. P., J.K. Ridley, G de Q. Robin, M.J. Siegert and I. A. Zotikov, A large deep freshwater lake beneath the ice of central East Antarctica, *Nature* 381, 684-686, 1996.
- Lewis, E.L., and R.G. Perkin, Ice pumps and their rates, *J. Geophys. Res.*, 91, 11756-11762, 1986.
- NSF, Lake Vostok: A Curiosity or a focus for interdisciplinary study? Lake Vostok Workshop, Final Report, 7/8. November, NSF Washington DC, June 15, 1999, on web at <http://www.ldeo.columbia.edu/vostok/>.
- Siegert, M. J., J. A. Dowdeswell, M. R. Gorman, and N. F. McIntyre, An inventory of Antarctic sub-glacial lakes, *Antarctic Science* 8, 281-286, 1996.
- Siegert, M.J. and J. A. Dowdeswell, Spatial variations in heat at the base of the Antarctic ice sheet from analysis of the thermal regime above subglacial lakes, *J. Glac.* 42, 501-510, 1996.
- Siegert, M.J. and J. K. Ridley, An analysis of the surface and subsurface topography of the Vostok Station subglacial lake, central East Antarctica, *J. Geophys. Res.*, 103, 10,195-10,207, 1998.
- UNESCO, 1978, Eighth report on the joint panel on oceanographic tables and standards, Woods Hole, May, 23-25, 1977, UNESCO *Technical Papers in Marine Science* 28, 1978.

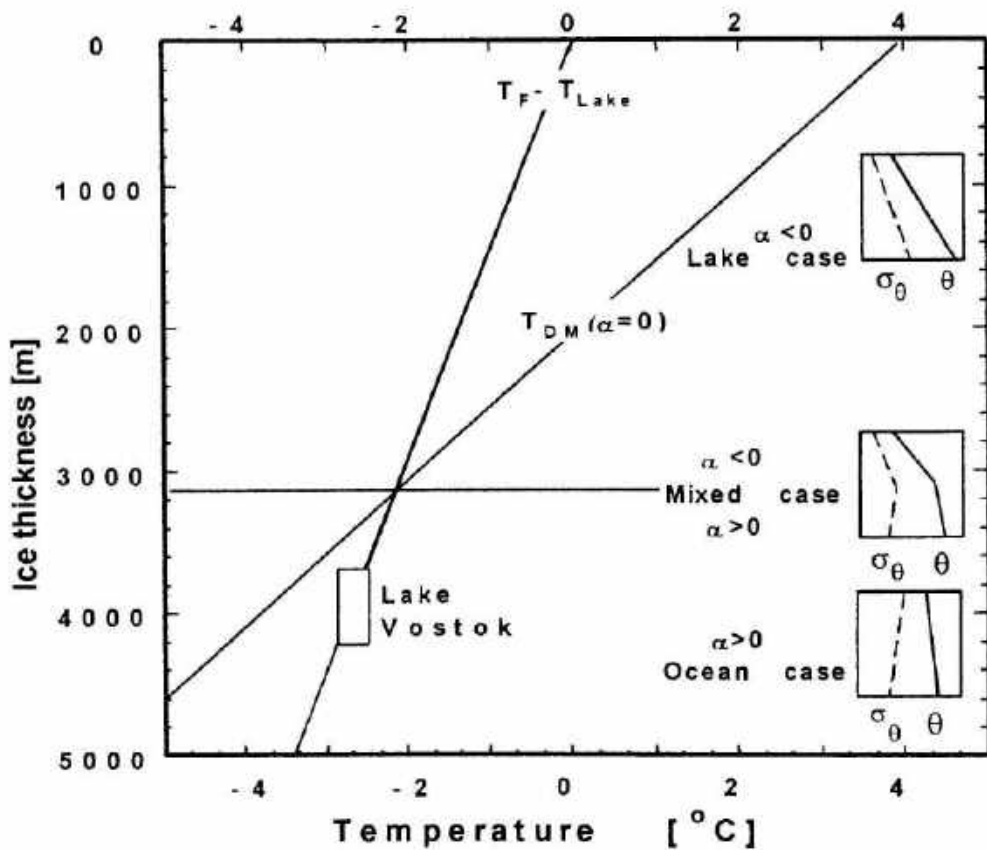
Table Lake Vostok morphometry, ice cover and physical constants

Quantity	Symbol	Value
Lake		
Volume	V	1,800 km ³
Area	A	14,000 km ²
Length	L	230 km
Horizontal coordinate	x	0 - 230 km
Average width		60 km
Depth	H(x)	0 - 510 m
Average depth	H _{avg}	130 m
Maximum depth	H _{max}	510 m
Geothermal heat flux ⁽¹⁾	F _{geo}	0.05 W m ⁻²
Ice cover		
Ice thickness	H _{Ice} (x)	~3750 - 4200 m
Ice thickness difference (N-S)	ΔH _{Ice}	460 m
Ice ceiling ⁽²⁾ temperature at N-end	T _{Ice} (x=0)	-2.83 °C
Ice ceiling ⁽²⁾ temperature at S-end	T _{Ice} (x=L)	-2.53 °C
Range of ice ceiling ⁽²⁾ temperature	ΔT _{Ice}	0.31 K
Constants		
Coriolis parameter (at 77 °S)	f	-1.4·10 ⁻⁴ s ⁻¹
Thermal expansivity ⁽³⁾	α	18·10 ⁻⁶ K ⁻¹
Heat capacity of water	C _{pρ}	4.2·10 ⁶ J K ⁻¹ m ⁻³
Thermal diffusivity	D _T	1.35·10 ⁻⁷ m ² s ⁻¹
Adiabatic gradient ⁽³⁾	Γ	1.1·10 ⁻⁵ K m ⁻¹
Latent heat of melting	L _p	334,000 J kg ⁻¹
kinematic viscosity	v	2.0·10 ⁻⁶ m ² s ⁻¹
Ice density	ρ _{Ice}	913 kg m ⁻³
Water density ⁽⁴⁾	ρ	1000 kg m ⁻³

⁽¹⁾ Assumption (world-wide average);⁽²⁾ Temperature of the ice-ceiling in contact with the lake water, using Eq. 2;⁽³⁾ Average value;⁽⁴⁾ Assumed salinity S~0 and compressibility neglected.

Figure

Plot of the freezing temperature (T_{FP}) and the temperature of maximum density (T_{MD}) as a function of ice thickness. Three types of lakes under ice can be expected in Antarctica, depending on whether the ice thickness is larger, less or about equal the critical depth (~ 3170 m depth for $\rho_{Ice} \sim 913 \text{ kg m}^{-3}$), at which T_{FP} and T_{MD} are identical. In Lake Vostok (lake temperature $\sim -2.7^\circ\text{C}$) T_{FP} is warmer than T_{MD} ($\sim -4^\circ\text{C}$) and the thermal expansivity α is positive ("Ocean case"); subsequently potential density σ_0 decreases as the potential temperature increases with depth (convectively unstable). In the "Lake case" σ_0 is stably stratified.



IS THE SURFACE BOUNDARY LAYER IN LAKES LAMINAR AT LOW WIND SPEEDS?

Alfred Wüest and André Simon

Swiss Federal Institute of Environmental Science and Technology (EAWAG),
Dübendorf, Switzerland (wuest@eawag.ch).

1. Introduction

Although for many locations on Earth and for most of the time wind speeds over oceans and inland waters are generally low (especially in the tropics), the momentum and energy coupling from the wind to the underlying water has been mainly investigated for relatively high winds (Garratt, 1977; Smith, 1980; Wu, 1980; and many others). For high winds ($> 7 \text{ m s}^{-1}$) the sea surface is generally considered to be aerodynamically rough. In that regime, the roughness – parameterized by the length z_0 – increases, as the significant wave height increases with wind speed. Below that high wind regime, it has been assumed for long, that the boundary layers of both the atmosphere as well as the water becomes increasingly smooth for decreasing wind.

Only recently, measurements by Bradley *et al.*, (1991) have demonstrated that the wind-stress coefficient C_{10} [-] increases as the wind decreases for very low wind speeds. C_{10} is defined empirically through the bulk aerodynamic flux formula:

$$\tau = \rho_{\text{Air}} C_{10} W_{10}^2 \quad [\text{N m}^{-2}] \quad (1)$$

(where ρ_{Air} [kg m^{-3}] is density of air, W_{10} [m s^{-1}] is wind speed measured at the reference height of 10 m above the water surface, and τ [N m^{-2}] is the atmospheric surface stress). This rather surprising observation was explained by Wu (1994), who claimed, that the roughness at low wind speeds is determined by surface tension, which increasingly dominates the force balance as winds approach zero speed. Intuitively one may sketch it the following way: The smoothing effect of the wind-induced surface stress τ disappears as wind decreases and subsequently the surface tension gains increasingly influence on the roughness. Wu (1994) concluded that the sea surface is aerodynamically rough even under very light winds (say $W_{10} < 3 \text{ m s}^{-1}$) and that consequently a range of wind speeds exist ($W_{10} \sim 3$ to 5 m s^{-1}), where roughness has a minimum.

The subject of this contribution is to give further evidence, that the water surface is rough for very low wind speeds and that the wind dependence of the drag coefficient is in such a way, as it would be expected for laminar flow. The reported data is based on the simultaneous observation of wind and turbulent kinetic energy (TKE) dissipation in a medium-sized lake.

2. The Lake Neuchâtel Experiment

In March 1996, during 13 days, a concentrated effort has been made to observe the surface boundary layer (SBL) turbulence by two microstructure techniques (Simon, 1997; Simon *et al.*, 1999). The experiment took place off the coast of Lake Neuchâtel. This site was chosen, since it sees strong and variable wind forcing. In addition, the lake is wide and deep enough to ensure, that the influence of the lake boundaries on the physics of the SBL of the open water is negligible and that the fetch is long enough to allow waves to become fully developed. The particular location for the experiment was selected for its wind exposure, the absence of a major river inlet and its steep shore line, which allowed a mooring depth of ~40 m within close reach to the shore.

Microstructure profiles were collected by using two completely different probes sensing small-scale temperature and shear. This allowed to infer dissipation $\varepsilon(z)$ [W kg^{-1}] of TKE from two independent microstructure profilers at ~ 300 m off-shore (Kocsis *et al.*, 1999). In order to measure the atmospheric forcing and wave heights we operated a meteorological station on a buoy (~ 2 km off-shore) and a moored pressure gauge, respectively. Wind (and other parameters) were measured by an AMS 2700 at 2.8 m above the lake surface every 10 minutes and wind speed was rescaled to the standard height of 10 m (W_{10}). During microstructure data collection, mean wind speed was 3.2 m s^{-1} . This rather low level was interrupted on two occasions, lasting for approximately one and two days, when wind speed exceeded 6 m s^{-1} (11% of the time of observation). The first occasion was on March 10/11 and the second occasion on March 12/13, when the maximum wind gusts, reached 14.6 m s^{-1} . During these two main events, wind blew almost parallel to the longside of the lake and had subsequently a long fetch. After March 14, winds exceeding 4 m s^{-1} occurred as short pulses of less than one hour duration and their directions indicated short fetches.

3. Observed wind-drag coefficient

The atmospheric stress τ splits into two momentum fluxes upon entering the water interface: (a) the SBL stress, τ_{SBL} , which is due to the turbulent transfer of momentum into the water SBL and (b) the wave-induced stress, τ_{wave} , which is due to acceleration of the surface gravity waves. We assume here - and many arguments support this assumption (Simon *et al.*, 1999) - that the wave-induced stress for very low wind ($W_{10} < \sim 3 \text{ m s}^{-1}$) is negligible (Janssen, 1989). The justification for this assumption stems from the fact that waves under very low winds reach saturation after short temporal and spatial scales. Therefore, we can estimate the drag coefficient C_{10} , from simultaneous measurements of wind W_{10} and dissipation $\varepsilon(z)$ at different depth levels in the water SBL. Assuming *Law-of-the-wall*, as evident from these and other observations (Simon *et al.*, 1999), allows to express C_{10} as a function of $\varepsilon(z)$ and W_{10} :

$$C_{10} = \overline{\left(\frac{\rho}{\rho_{\text{air}}} \right)^{2/3} \frac{1}{W_{10}^2}}^{(-15 \text{ m} \leq z \leq -3 \text{ m})} \quad [-] \quad (2)$$

For each of the ~ 450 dissipation profiles, collected during purely non-convective conditions, the mean value of C_{10} was computed for the depth range of -3 m to -15 m. The restriction to this particular depth range has two reasons: Firstly dissipation determined very close to the surface may be influenced by the surface waves. Secondly, dissipation values estimated deeper in the water column may be influenced by large-scale shear (such as internal waves or modes). Indeed, dissipation between 20 and 30 m depth was about constant. This depth restriction was not critical, since the application of Equation 2 to the depth range of 5 to 10 m revealed nearly identical values for C_{10} . The drag coefficients, calculated by using Equation 2 were sorted as a function of wind speed and finally averaged in bins of wind speed.

In the enclosed Figure, our C_{10} estimates are compared to the function $C_{10}^{\text{GB}} = 4.34 \cdot 10^{-3} (W_{10})^{-0.87}$, which is an approximation to the composite estimates determined by Geernaert *et al.* (1988) and Bradley *et al.* (1991) under mostly light winds in the ocean. Their drag coefficient C_{10}^{GB} is related to the total (atmospheric) stress τ in Equation 1, whereas C_{10} refers only to τ_{SBL} . For small wind speeds ($W_{10} < \sim 3 \text{ m s}^{-1}$), the agreement between our C_{10} and their C_{10}^{GB} values is excellent and confirms the rather astonishing increase of the drag coefficient as the velocity decreases at low winds. For wind speeds $> \sim 3 \text{ m s}^{-1}$, our SBL stress estimates are systematically smaller than theirs. τ_{SBL} was found to be only about half of their

atmospheric stress τ (according to their C_{10}^{GB}). This discrepancy has to be expected due to the existence of the wave-induced stress τ_{wave} .

4. Conclusions

Under low wind conditions, identified by both low wind speeds as well as low wave excitation, we observed the following in respect to the momentum transfer from the wind field into the water column and in respect to the TKE balance:

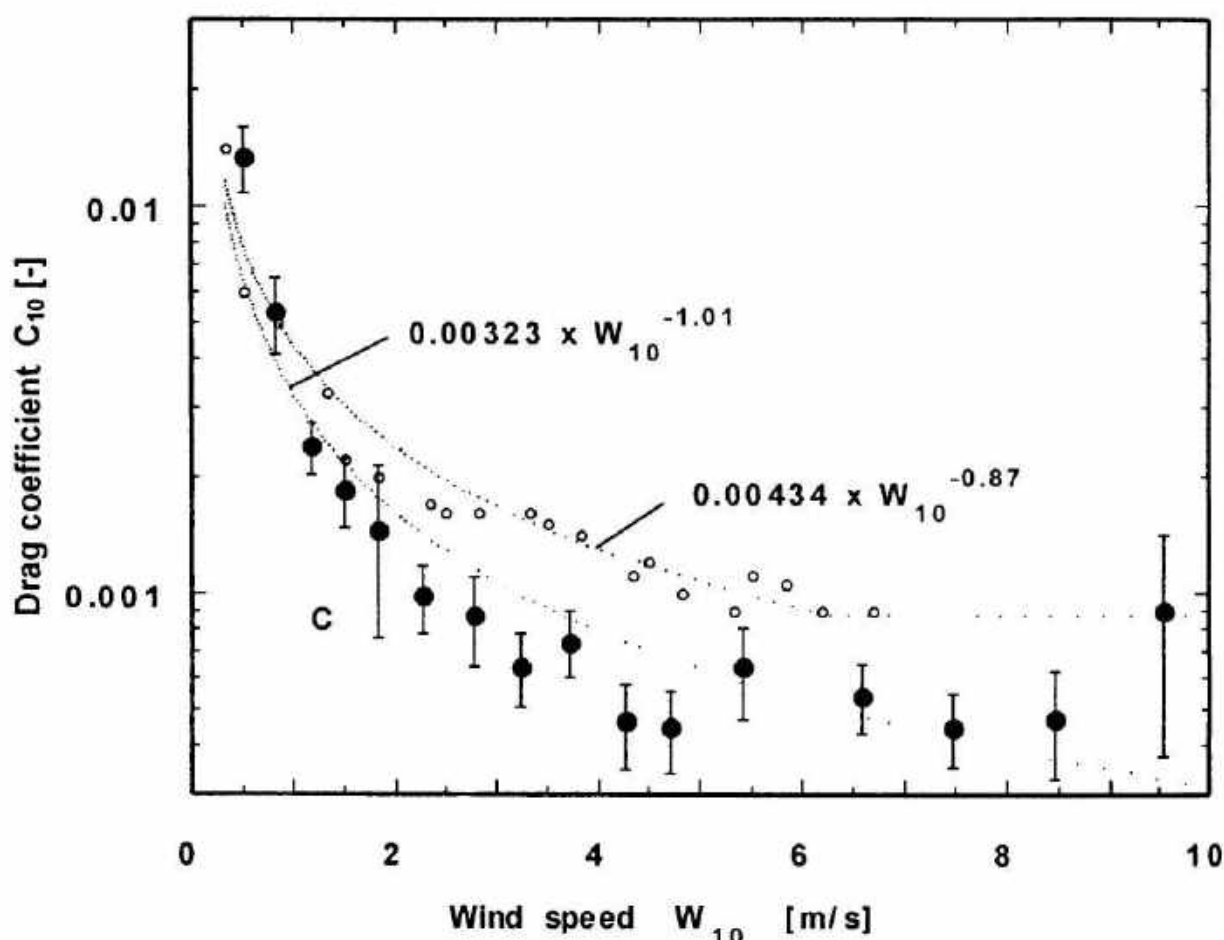
- (1) For wind speeds $W_{10} < \sim 2.5 \text{ m s}^{-1}$, the wave age parameter ($c_p/W_{10} < 1.2$) indicates developed but very small waves (c_p is group wave velocity at the peak frequency).
- (2) Below the wave-affected surface layer the vertical profiles of TKE dissipation $\varepsilon(z)$ follows *Law-of-the-wall* scaling to $\sim 20 \text{ m}$ depth. The 95% confidence interval determined from the bootstrap method was typically about 50% of the average dissipation within 0.5 m long vertical bins.
- (3) The stress balance at the air-water interface implies, that a significant fraction of the momentum flux into the water first takes the form of wave momentum. At medium to high wind speeds ($> 3-4 \text{ m s}^{-1}$), the SBL stress τ_{SBL} in the water column below the waves is therefore up to 50% smaller than its atmospheric counterpart τ . As a consequence, for fetch-limited cases, as was the situation in Lake Neuchâtel, a significant amount of the wave energy is transported horizontally to the shore. The turbulence in the SBL is reduced (by up to 50%) relative to fully-developed wave conditions.
- (4) For winds with speed $W_{10} < \sim 2.5 \text{ m s}^{-1}$, the waves became fully developed and the atmospheric drag coefficient C_{10}^{GB} (Bradley *et al.*, 1991; Geernaert *et al.*, 1988), matched closely with our C_{10} estimates, representing the SBL stress. At low winds the stress coefficient C_{10} consistently increased for decreasing winds approximately inverse proportional to the speed (i.e. $C_{10} \sim W_{10}^{-1}$). Consequently, the τ_{SBL} stress depends linear on wind speed, as typical for laminar flows. Evidently, the drag coefficient decreases inverse proportional to the Reynolds number (which is proportional to speed) as is the case for laminar particle settling or laminar pipe flow.

REFERENCES

- Bradley, E., P. Coppin, and J. Godfrey, Measurements of sensible and latent heat flux in the western equatorial pacific ocean, *J. Geophys. Res.*, 96, 3375-3389, 1991.
- Geernaert, G. L., K. Davidson, S. Larsen, and T. Mikkelsen, Wind stress measurements during the tower ocean wave and radar dependence experiment, *J. Geophys. Res.*, 93, 13913-13923, 1988.
- Janssen, P. E., G.J. Komen and W.J. de Voogt, 1984, An operational coupled hybrid wave prediction model, *J. Geophys. Res.*, 89, 3635-3654, 1984.
- Janssen, P. E., Wave-induced stress and the drag of air flow over sea waves, *J. Phys. Oceanogr.*, 19, 745-754, 1989.
- Simon, A., Turbulent mixing in the surface boundary layer of lakes. *Diss. ETH No 12272*, 100, 1997.
- Simon, A. et. al (1999) in preparation.

- Kocsis, O., H. Prandke, A. Stips, A. Simon and A. Wüest, Comparison of dissipation of turbulent kinetic energy determined from shear and temperature microstructure. *J. Mar. Systems*; 21, 67-84, 1999.
Wu, J., The sea surface is aerodynamically rough even under light winds, *Boundary-Layer Meteorol.*, 69, 149-158, 1994.
Prandke, H., and A. Stips, Test measurements with an operational microstructure-turbulence profiler: Detection limit of dissipation rates, *Aquatic Sciences* 60, 191 - 209, 1998.

Figure: Drag coefficients C_{10} , (determined by using Equation 2) from measured dissipation for different bins of wind speed (black dots) are compared to C_{10}^{GB} , the values observed by Geernaert *et al.* (1988) and Bradley *et al.* (1991) (open symbols indicate their median values). The lines represent power-law fits to the data, as indicated by the equations. The error bars represent the 95% bootstrap confidence intervals.



MODELLING VERTICAL TURBULENT MIXING IN THE HYPOLIMNION OF A LAKE

Juhani Virta and Kari Pulkkinen

Department of Geophysics, University of Helsinki
P.o.Box 4 (Fabianinkatu 24 A)FIN-00014

INTRODUCTION

There are several mechanisms influencing on the vertical mixing of the hypolimnion of lakes, which are difficult to parameterise in the one dimensional temperature models. Important feature is that the mixing is dependent on dimensions of the lake as has been experimentally shown in several studies.

The aim of this paper is to study a model for vertical mixing which is specially suited for lakes having limited deep part surrounded by shallow areas. Very many lakes in Finland have this property. In this kind of lakes internal oscillations may be so high that the hypolimnetic water may penetrate shallow parts to form a incoming and out going river like near bottom current. Vertical mixing in this kind of currents is believed to be the important mechanism in hypolimnetic mixing.

The model is planned to be used as part of one dimensional temperature model. For this reason there are several simplifying assumption in the formulation. The model was first presented in 1990 (Virta and Pulkkinen, 1990).

FORMULATION OF ONE DIMENSIONAL MODEL

Basic assumptions which make one dimensional computations possible are following:

1. Form of the lake is longish.
2. The whole water mass can be treated as two layered
3. The form of the oscillating thermocline is plane.
4. Prandtl's mixing length theory is valid for describing turbulent mixing in the hypolimnion.
5. The slope of the surface of the lake is always corresponding to the equilibrium wind inclination.
6. Period of thermocline oscillation is long so that steady state solutions can be applied.

Instead of real form for the cross section an equivalent rectangle with the surface area BD was used. In this case the continuity equation for the average current velocity in a vertical cross section may be computed in the form

$$V_m(x) = \frac{1}{B(x)D(x)} \frac{dS}{dt} \int B(s)(s - L_g) ds \quad (1)$$

where

- x is a coordinate along thermocline in the direction of the longitudinal axis of the lake
- V_m is the cross sectional average current velocity
- B is the breadth of the basin at the depth of the thermocline
- $D(x)$ is the average depth of the basin bellow the thermocline at point x
- S is the slope of the thermocline
- L is the length of the basin
- L_g is the x -coordinate of the gravity point of the thermocline surface

The average cross sectional velocity in a logarithmic profile is

$$V_m(x) = \frac{V^*(x)}{k} \left(\ln \frac{D(x)}{y_0} - 1 \right) \quad (2)$$

Where

- k is von Kármán constant
- V^* is the friction velocity
- y_0 is the roughness parameter

By eliminating the average velocity and solving friction velocity it is possible to compute from logarithmic profile the derivative of $\frac{dV}{dy}$ for each vertical. y is the local distance from the bottom. After this the average derivative over horizontal planes can be computed.

In this study direct solution of mixing processes is needed. For this reason the mixing length theory is used for the eddy viscosity and eddy conductivity in the form

$$K = \alpha_1 l^2 \left| \frac{dV}{dy} \right| (1 + \alpha_2 N^2)^\gamma \quad (3)$$

N is the Väistä-frequency and α_1 , α_2 and γ are constants. An experimental value -1.5 can be substituted for γ (Rodi, 1984). The approximate value of α_1 for eddy viscosity is 1 and for eddy conductivity it is less than 1. In the case under consideration when the flow has both upper and lower boundaries, the mixing length may be approximated according to Henderson (1966, p. 425) as

$$l = k(D - z) \sqrt{\frac{z}{D}} \quad (4)$$

Where $z = D - y$ of depth from thermocline.

Earlier analysis for different lakes (Virta and Elo, 1994) show that the long period oscillation of the hypolimnetic current may be modelled with a linear transfer function model with the second power of wind as input and the transfer function corresponding to that of damping oscillating system. From this it follows that the theory of damping oscillator may be used also for modelling of S and dS/dt .

The differential equation of a damping oscillator is

$$\frac{d^2S}{dt^2} + 2b \frac{dS}{dt} + \omega_n^2 [S - F(t)] = 0 \quad (5)$$

Where input function F is

$$F(t) = \frac{C \rho_s W^2(t)}{g \Delta \rho H_{\text{ref}}}$$

The symbols have the following meaning

- b is damping coefficient
- ω_n is the natural angular velocity corresponding to the internal seiche period
- C is the drag coefficient
- ρ_a is the air density
- W is the wind velocity
- $\Delta\rho$ is the density difference between hypolimnion and epilimnion
- H_t is the depth of the thermocline

The reason for equation 5 is that it is modelling a system with a natural angular velocity ω_n and correct theoretical slope of the thermocline under condition of a constant wind.

It is possible to determine time series of eddy diffusivity K from equations (1)-(5) with the aid of time series of wind velocity. In this presentation a trial was made to compare different lakes without any special observation of wind velocity in each lake. Because mixing in the hypolimnion is relatively slow, it is possible to use a rather long averaging period, one or two months, and average eddy diffusivity can be computed instead of momentary eddy diffusivity. For this purposes the model uses one single characteristic thermocline term, and this is defined as

$$S_e = \sqrt{\text{var}\left(\frac{dS}{dt}\right)} \quad (6)$$

The variance of dS/dt can be determined with the transfer function of the system and spectral function of input function. As the time dependent variable in the input function F (Eq 5) is W^2 the spectral function of which can be expressed experimentally as

$$G_F = \text{var}(W^2) \frac{4a}{a^2 + \omega^2} \quad (7)$$

α is a constant to be estimated from wind velocity data.

Now the average eddy diffusivity over a horizontal surface with the area of $A(z)$ may be obtained from the equation

$$K(z) = \alpha_1 M(z) \dot{S}_e (1 + \alpha_2 N^2)^{-1.5}$$
$$\dot{S}_e = \sqrt{\text{var}(W^2)} \frac{\rho_a}{g \Delta \rho H_i} \left(\frac{\alpha}{T_*} \right)^{1/2} \sqrt{\frac{\pi}{\alpha^2 + \alpha p + 1} \left(\frac{1+\alpha}{4\xi} - \frac{\sqrt{\alpha}}{2} \right)}$$
$$M(z) = \frac{1}{A(z)} \int_0^L z [D(x) - z] D^{-2}(x) \left[\ln \frac{D(x)}{y_0} - 1 \right]^{-1} \int_x^L B(s)(s - L_s) ds dx \quad (8)$$

Where $\alpha = (a/\omega_n)^2$, $T_n = 2\pi/\omega_n$, $p = 2 - 4\xi^2$, $D \gg y_0$

ξ is the damping ratio. α_1 and α_2 are constants to be determined by calibration. α_1 includes parameter Ck^2 as well as the scale factor due to the selection of characteristic slope term presented in Eq 6. α_2 corresponds to the parameter α_2 in Eq 3.

APPLICATION OF THE MODEL

Calibration of the model for four lakes has been presented earlier in (Virta and Pulkkinen, 1990). Some new results with new observation data will be presented.

REFERENCES

- Henderson, F. M., 1966: Open channel flow. 522 p., McMillan.
- Rodi, W. R., 1984: Turbulence models and their application in hydraulics. State-of-the-art-paper of IAHR, 104 p., Delft.
- Virta, J. and A.-R. Elo, 1994: Transfer function model for current to wind. Water Poll. Res. J. Canada, Vol 29, Nos 2/3, 281-291.
- Virta, J. and K. Pulkkinen, 1990: Vertical mixing in the hypolimnion. Test of the model. Nordisk Hydrologisk Konferens 1990. Kalmar, Sverige 29 juli- 1 augusti 1990, Redigerad av Gun Sigurdsson, Nordisk NHP-rapport nr 26, pp 394-399.

THE USE OF A PHYSICALLY BASED LAKE MODEL

Aija-Riitta Elo

Department of Geophysics, University of Helsinki
P.o.Box 4 (Fabianinkatu 24 A) FIN-00014

In a lake, water temperature is the most important physical factor, which can be determined according to calculations and measurements. At the surface, temperature can be used in describing all the connections with atmosphere. Of course, there are also other climatic factors affecting. These vary mostly according to the location of the lake. Globally, solar radiation is naturally very important, while it is responsible for the heating of the whole system. It is also forming the wind field, together with the forms and heterogeneity of the surface. Because of the nature of the atmosphere, it has to be treated as a separate variable, when actual lakes are modeled.

Wind affects causing drag, which creates mixing and downwelling of heat in the lake. The process of returning to stable temperature distribution can be seen as convection. It is often significant and needs to be described separately. The liquid state of water causes differences compared to solid earth. This affects most clearly in autumn, when the water at the surface of deep lakes cools later due to heat stored in the water mass. This may cause differences in freezing times of lakes close to each other. For three Alpine lakes this is described by Livingstone (1997a). It can be seen also in other phenomena, especially Lake Districts have a mesoscale influence on climate. Over the oceans the climate is obviously much more clearly affected by the water and the heat stored. Along a heterogenous surface the variations are naturally also heterogenous, but again, due to viscosity differences, changes inside the water mass are slower. This might induce currents. Also wind and pressure differences may create wave motion in the water body.

These interactions need to be studied in detail, when physical models of the energy exchange are used. Commonly there are problems in describing particular lakes and some corrections are needed to take into account the lack of data to describe the lake as an entity, or even small sections. These may be treated using various correction or calibration factors, using different theoretical approaches. Heterogenities of air over Lakes Tämnaren and Råksjö have been studied by Venäläinen (1998). Naturally, it is not often possible to describe all components of

the heat balance at the same time. Therefore some feature is often selected for more accurate inspection and very good results may be obtained with these case studies. Difficulties of the modeling schemes benefit design of measuring, modeling and testing strategies and systems. Also the questions with increasing importance, like climate change and other environmental problems challenge old ways of thinking and increase also the need of better models e.g. for assessment purposes.

The effects considered are based on assuming that the lakes remain relatively unchanged. If this is not the case, the whole question gets new dimensions and different kind of models may be needed. This can be the case during natural evolution over longer time periods. Humans may also change the system in a short period e.g. by constructing different structures. There are also natural catastrophic events like flooding, although often these might be affected by human action. These kinds of phenomena can be considered as special cases. One more interesting special case is rivers, in which flow obviously is important. However, in many aspects they can be rather similar to lakes and the difference of a lake and a river may need to be specified.

There are also other factors, which have turned out to be important in former lake studies including physical aspects. Very often limnologists, who naturally are interested about the biology in the lakes, have conducted these studies. Then of course there are other factors, which are important, too, in addition to physical factors. The composition of the water can be changed. This is related to exchange of water, which in the hydrological sense can be considered as water flow in the catchment and through the lake. The different substances flowing with water and the biological and chemical processes affect the composition of water in a lake. This affects in principle physical properties e.g. the stability through the equation of state. Also optical properties and absorption of heat in water can be changed, so that different amounts of heat are absorbed in different depths. These changes can be important when changes are relatively large.

Modeling of Lake Pääjärvi was studied especially when analyzing the effects of climate change (Elo et al. 1998). It was found to be important to have long series of data, and period 1961-1990 was studied as a reference. Measurements from the lake were used and all the components of the heat balance could be simulated and estimates of the accuracy could be given. Several other Finnish lakes were also simulated in the same study using data from land

area. A k-epsilon model, based on Svensson's lake model (Svensson 1978), was used. Also two other shallow lakes from Northern Europe, Lakes Tämnaren and Råksjö, have been studied and some results have been presented already. In Northern Europe ice cover is an important part of the yearly cycle in lakes. It can also tell about the suitability of modeling. In addition to temperature profile in water the model should also be able to describe ice cover. When the temperature profile is suitable, ice cover may exist over it. In addition to strong effect of climate from above, temperature profile under ice is important, when the ice cover is not thick. Also partial ice cover may exist. The modeling of such special cases demands more details, if suitable criteria are not found or more detailed information is needed.

A series of simulations was made to find the effects of varying absorption of heat using different extinction coefficients representing Finnish conditions. The data were from land area. Considerable effects were seen e.g. in depths of thermocline and its formation time in spring. Short time periods were analyzed also using data measured over lakes and making simulations taking into account also the division of light absorbed in various wavelengths (Lakes Tämnaren and Råksjö). Very important effects could be seen from these simulations.

In order to gain more information, more lakes from different climatic regions have been studied. Also the variety of shapes and sizes has thus increased. The Finnish lakes, like many other small lakes are not very steep and they have typically large shallow parts. Actually most very steep and deep natural lakes are situated somewhere in a mountainous area, due to formation of the Earth's surface. This also affects local climate. When larger lakes are considered, the rotation of the Earth is more important. It is usually included in the equations used, but its effects may be relatively more important when dynamics is analyzed in more details.

Lake Mendota in Wisconsin, North America, has also long series of data and it could be compared with modeling of Lake Pääjärvi, paying initially highest interest on ice cover (Elo and Vavrus 1999). A two-layer model called LIMNOS was used together with the k- ϵ model. The LIMNOS-model can further be used. It may assist e.g. in determining the depth of the thermocline, which may be complicated from the vertical profiles. For many purposes the profiles are anyway needed. Good results were obtained from the comparison study. More studies concerning water temperatures are going to be made in modeling of Lake Mendota,

temperature at surface layers and under the ice were too high to be taken quite realistically. These kinds of problems can be found easily from other studies, too.

Lake Constance in Central Europe has been studied e.g. by Gaedke et al. (1998) especially considering biological aspects and by Bäuerle et al. (1998) mainly from the geophysical point of view. Ollinger and Bäuerle (1998) have applied another version of Svensson's model and studied effects of weather on plankton development. There are also long data series from this lake, concerning the same period as Lakes Pääjärvi and Mendota. The treatment of the data is only partly done. The period includes also one very interesting year, 1963, when the lake had a complete ice cover (Dobras 1992). In assisting this study there are also long series of data from Swiss lakes. These may also give valuable information for modeling. They have been studied by Livingstone (1993 and 1997b). Some preliminary calculations using Svensson's $k\cdot\epsilon$ model have been applied in modeling Lake Constance in order to estimate effects of changes in the environment. Very strong effects in the temperature profiles are seen, when optical properties of the water have been changed. The effects are strong also during mild winters in that area. Usually there is no protecting icecover. Rather small changes in the value of extinction coefficient can change ice formation. The area is also usually not very windy. Possible changes in the wind conditions can also be expected to have important effects.

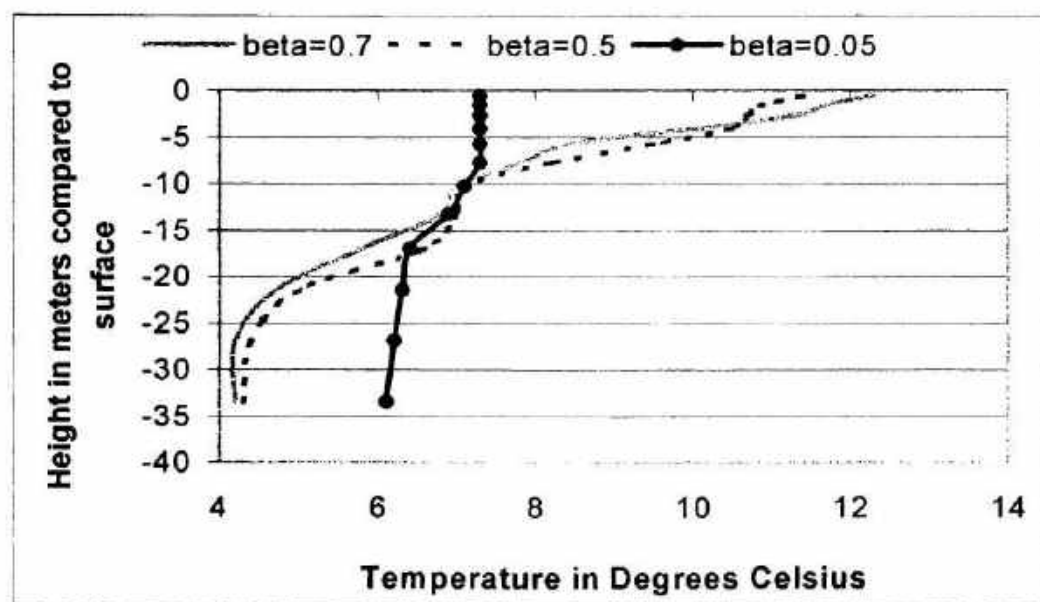


Figure 1. Temperature profiles 13.5.1997 with different values of beta, the extinction coefficient.

References

- Elo A.-R., Huttula T., Peltonen A. and Virta J. 1998. The effects of climate change on the temperature conditions of lakes. *Boreal Env. Res.* 3: pp. 137-150.
- Elo A.-R. and Vavrus S. 1999. Ice modelling calculations, comparision of models PROBE and LIMNOS. To be pressed by Verh. Internat. Verein. Limnol., SIL Congress, Dublin, 14.8.1998.
- Bäuerle E. Ollinger D. and Ilmberger J. 1998. Some meteorological , hydrological, and hydrodynamical aspects of Upper lake Constance. In: Bäuerle E. and Gaedke U. eds. Lake Constance characterization of an ecosystem in transition. *Arch. Hydrobiol. Spec. Issues Advanc. Limnol.* 53, pp. 31-83.
- Dobras W. 1992. Seegfrörne. Die spannende Geschichte der Seegfrörnen von 875 bis heute. Verlag Stadler, Konstanz, 124 p.
- Gaedke U., Ollinger D., Bäuerle E. and Streile D. 1998. The impact of the interannual variability in hydrodynamic conditions on the plankton developement in Lake Constance in spring and summer. In: Bäuerle E. and Gaedke U. eds. Lake Constance characterization of an ecosystem in transition. *Arch. Hydrobiol. Spec. Issues Advanc. Limnol.* 53, pp. 565-585.
- Livingstone D. M. 1993. Temporal structure in the deep-water temperature of four Swiss lakes: A short-term climatic change indicator? *Verh. Internat. Verein. Limnol.* 25, Stuttgart, September 1993, pp. 822-828.
- Livingstone D. M. 1997a. Break-up dates of Alpine lakes as proxy data for local and regional mean surface air temperatures. *Climatic Change* 37: pp. 407-439.
- Livingstone D. M. 1997b. An example of the simultaneous occurance of climate-driven "sawtooth"deep-water warming/cooling episodes in several Swiss lakes. *Verh. Internat. Verein. Limnol.* 26, Stuttgart, Dezember 1997, pp. 822-828.
- Ollinger Dieter and Bäuerle Erich 1998: The influence of weather conditions on the seasonal plankton development in a large and deep lake (L. Constance). In: Management of Lakes and Reservoirs during Global Climate Change, ed. D. Glen George, J. Gwunfryn Jones, Pavel Puncochar, Colin S. Reynolds and David W. Sutcliffe, 1998, pp. 57- 70.
- Svensson U. 1978. A mathematical model of the seasonal thermocline, Report No 1002. Dep. of Resources Eng. Univ. of Lund. Lund, Sweden, 187 p.
- Venäläinen A. 1998. Aspects of the surface energy balance in the boreal zone. Finnish Meteorological Institute Contributions 25, 114 p.

APPLICATION OF INVERSE MODELING TO LAKE STUDIES

Elena A. Tsvetova

Institute of Computational Mathematics & Mathematical Geophysics
Novosibirsk, 630090, Russia, e-mail: Tsvet@OMMFAO.sccc.ru

Inverse modeling is a comparatively new approach in limnology. It can be applied for studying the hydro-physical and transport processes in reservoirs. Diagnosis, prognosis, monitoring and water quality control are some examples of a variety of inverse modeling applications. Unlike direct modeling, inverse procedure allows an immediate feedback from the solution to input data to be established. It provides the finding of the key model parameters which are responsible for the adequate description of the processes under investigation. Moreover, inverse modeling enables the following problems to be solved: data assimilation; reconstruction of the state function in the case of data lack and estimation of model quality with respect to measurements, identification of parameters; control of anthropogenic sources at given criteria and constraints and so on.

The solution of an adjoint problem is the basic procedure of inverse modeling algorithm. The statement of the adjoint problem is formulated for given objective functional with the use of the direct problem as a constraint connecting the state function and model parameters. After the solutions of direct and adjoint problems have been obtained, the calculation of sensitivity functions and realization of optimization procedures for the construction of direct and back relations between the models and quality functionals are produced. The essence of the approach as a whole is in the construction of discrete approximations with the help of variational formulation of the model in the form of integral identity as well as the use of variational principles in the combination with splitting, decomposition, and optimization techniques. Such conglomerate ensures coordination of all the stages of technology and efficiency of their realization.

Let us write an operator form of a mathematical model:

$$\mathbf{B} \frac{\partial \phi}{\partial t} + \mathbf{G}(\phi, \mathbf{Y}) - \mathbf{f}(\mathbf{x}, t) = \mathbf{r}(\mathbf{x}, t). \quad (1)$$

The following notations are used here: ϕ is a state vector, \mathbf{Y} is a parameter vector, \mathbf{B} is a diagonal matrix, some diagonal elements of which can be zero, $\mathbf{G}(\phi, \mathbf{Y})$ is a non-linear matrix operator depending on the state functions and parameters, \mathbf{f} is a function of sources, \mathbf{r} is a function of model errors, $D_t = D \times [0, t]$, D is a domain of spatial variables \mathbf{x} , $[0, t]$ is the time

interval, $Q(D_i)$ is the space of state functions satisfying the boundary conditions, $R(D_i)$ is the range of admissible parameter values. For the considered class of problems the operator $\mathbf{G}(\phi, \mathbf{Y})$ is defined by hydrothermodynamic equations, transport and transformation of pollutants. It includes all the terms of equations except the time derivatives. With respect to the components of the state function ϕ , this is a non-linear matrix operator with partial derivatives. In the stationary case, \mathbf{B} -matrix is zero. The initial conditions at $t=0$ and the model parameters can be written in the form

$$\phi^0 = \phi_a^0 + \xi(x), \quad \mathbf{Y} = \mathbf{Y}_a + \zeta(x, t). \quad (2)$$

Here, ϕ_a^0 and \mathbf{Y}_a are the given a priori estimates of the initial fields ϕ^0 and the parameters' vector \mathbf{Y} ; $\xi(x)$ and $\zeta(x, t)$ are the errors of the initial state and parameters. If it is supposed that the model and input data are exact, the error terms in (1)-(2) should be omitted. The boundary conditions for the closure of the model are the consequences of the physical content of the problem under investigation. It is worth mentioning that the problem (1),(2) may be formulated for separate parts of the complex model, for example, for transport of pollutants, hydrodynamics, etc.

Variational form of the model (1)-(2) can be given by integral identity [1,2,5]

$$\mathbf{I}(\phi, \mathbf{Y}, \phi^*) = (\mathbf{B} \frac{\partial \phi}{\partial t} + \mathbf{G}(\phi, \mathbf{Y}) - \mathbf{f} - \mathbf{r}, \phi^*) = 0, \quad (3)$$

$$\phi \in Q(D_i), \quad \phi^* \in Q^*(D_i), \quad \mathbf{Y} \in R(D_i).$$

Here, ϕ^* is an arbitrary sufficiently smooth function, $Q^*(D_i)$ is the adjoint space of sufficiently smooth functions defined in D_i . The functional $\mathbf{I}(\phi, \mathbf{Y}, \phi^*)$ in (3) is formed in such a way that all the equations of model (1), initial and boundary conditions, and external sources are included in it. Besides, the functional and scalar product (3) are chosen so that $\mathbf{I}(\phi, \mathbf{Y}, \phi) = 0$ is the equation of total energy balance for the model (1),(2).

The integral identity for 3D hydrodynamics and transport of pollutants model has the form [2,5]

$$\begin{aligned} \mathbf{I}(\phi, \phi^*, \mathbf{Y}) = & \int_{D_i} \left\{ \sum_{i=1}^{4+mw} \left(\frac{\partial \phi_i}{\partial t} + \Lambda \phi_i - F_{\phi_i} - Q_{\phi_i} \right) \phi_i^* e_i + l(u^* v - v^* u) + g p w + \right. \\ & \left. \left(\frac{u^*}{\rho_0} \operatorname{grad} p - u \operatorname{grad} p^* \right) \rho_0 dD dt + \int_{\Omega_L} u_n p * \rho_0 d\Omega dt - \int_{\Omega_S} \left(\frac{\partial \zeta}{\partial t} p^* \rho_0 \right) |_{z=\zeta} d\Omega dt \right\} = 0 \end{aligned} \quad (4)$$

Here $\{\phi_i\} = \{u, v, T, S, c_n, n=1, \dots, nw\}$ is the part of the state vector, u, v, w are the components of u ; $p, T, S, \zeta, \rho, \rho_0$ are pressure, temperature, salinity, free surface, density and reference density, c_n are pollutant concentrations; Λ, F_φ are transport, diffusion operators; Q_φ are the source terms; e_i are the scale parameters; Ω_L, Ω_S are lateral and surface boundaries of D_t .

The problems of monitoring, forecast and control require to introduce **generalized characteristics of the processes** as functionals of the form

$$\Phi_k(\varphi) = \int_{D_t} F_k(\varphi) X_k(x, t) dDdt, \quad k = \overline{0, K}, \quad K \geq 1 \quad (5)$$

Here $F_k(\varphi)$ are some given functions, $X_k(x, t) \geq 0$ are weight functions, and $X_k dDdt$ are the corresponding Radon's or Dirac's measures. The functionals of five main types should be outlined: (a) functionals of generalized description of the system behavior; (b) quality functionals which evaluate deviations between measured and calculated values, (c) measurements functional; (d) restrictions functionals, (e) objective or cost functionals for control and design. As for (c)-type functionals, we need the definition of the model of measurements and given corresponding attributes.

The construction of discrete analogs of the models, adjoint problems and sensitivity functions is built with the help of a sum analog of identity (3) or (4) $I^h(\varphi, Y, \varphi^*) = 0$. The upper index h denotes discrete analog. With this end in view decomposition of the domain D to subdomains $D = \bigcup_{n=1}^N D_n$, $N \geq 1$ may be carried out and a grid domain D_t^h is introduced. The method of weak approximation with fractional steps (splitting technique) is applied for time discretization [1]. The discrete form of the governing equations (1) is obtained from the stationarity conditions for the sum functional $I^h(\varphi, Y, \varphi^*)$ with respect to the variations of the grid components of the function φ^* on D_t^h . The adjoint system is derived from the stationarity conditions for the extended functionals $\Phi_k^h(\varphi) + I^h(\varphi, Y, \varphi^*)$ with respect to the variations of the grid components of the state function φ on D_t^h . As a result, the systems of governing and adjoint equations look like numerical splitting schemes that are mutually coordinated by means of the sum functional. To solve the inverse problems and investigate sensitivity, the source terms for the adjoint system should be prescribed. To meet our goals, we choose them as $\partial \Phi_k^h(\varphi) / \partial \varphi$. As a consequence, the **sensitivity functions** for the functionals (5) can be

calculated by the formula $\partial I^h(\varphi, Y, \varphi_k^*) / \partial Y_i$, where φ is the solution of the direct problem, φ_k^* is the solution of the adjoint problem for the functional with the number k , Y_i are the components of parameter vector in $R^h(D_i^h)$. The following set of formulas gives both the definition of sensitivity relations and algorithm for their calculation for the model (4) and functional (5)

$$\delta\Phi_k^h(\varphi) = (\text{grad}_Y \Phi_k^h(\varphi), \delta Y) = \frac{\partial}{\partial \alpha} I^h(\varphi, Y + \alpha \delta Y, \varphi_k^*)|_{\alpha=0} = \\ \left(\sum_{i=1}^{4+nw} \left\{ \int_{D_i} [\delta \mu_{\varphi_i} \text{grad } \varphi_i \text{ grad } \varphi_k^* - \delta Q_{\varphi_i} \varphi_k^*] \rho_0 dD dt - \int_{\Omega_i} \delta q_{\varphi_i} \varphi_k^* \rho_0 d\Omega dt + \right. \right. \\ \left. \left. \int_{\Omega_L} \delta(\varphi, u_n) \varphi_k^* \rho_0 d\Omega dt - \int_D (\delta \varphi_i \varphi_k^*)|_{t=0} \rho_0 dD \right\} + \int_{\Omega_s} (\delta \zeta p_k^*)|_{t=0} \rho_0 dS \right\}^h, \quad k = 1, \dots, K. \quad (6)$$

Symbol δ denotes the operation of input parameters variation, α is a parameter, μ_{φ_i} are the turbulent coefficients, q_{φ_i} are the fluxes across the boundary Ω_i of D_i , u_n is the normal component of the velocity vector. By the definition, the sensitivity functions are the expressions at variations.

Numerical algorithms of the direct and inverse modeling. The generalized quality functional is introduced in the form

$$\tilde{\Phi}^h(\varphi) = \Phi_k^h(\varphi) + 0.5 \left\{ (\mathbf{r}^T M_0 \mathbf{r})_{D_i^h} + (\xi^T M_1 \xi)_{D_i^h} + (\zeta^T M_2 \zeta)_{R^h(D_i^h)} \right\}^h + [I^h(\varphi, Y, \varphi^*)]_{D_i^h}, \quad (7)$$

where M_i , ($i = \overline{0, 2}$) are weight matrices, index T denotes the operations of transposition. A minimization functional problem with respect to the components of the vectors \mathbf{r}, φ^0, Y is formulated. The set of computational algorithms for direct and inverse modeling is obtained from the stationarity conditions for $\tilde{\Phi}^h$ to variations of the components of vectors $\varphi^*, \varphi, \mathbf{r}, \varphi^0, Y$ on D_i^h . Being the result of the problem's solution, functions φ^0, φ describe the space-time system behavior, function \mathbf{r} shows the model errors estimated with respect to measured data. Simultaneously, the solutions of adjoint problems and the set of sensitivity functions for the quality functionals presented by the first term in (6) are obtained. They are used for the solution of inverse and optimization problems.

Some applications to lake problems. Applications of the methodology were made to the solution of the problems of hydrodynamics and transport of pollutants both for deep [2-5] and shallow reservoirs. Examples of the two cases are discussed. The first one was intended for

the estimation of "danger" function for Lake Baikal to be polluted from the sources placed in the Northern hemisphere. To that end, the sensitivity functions with respect to variations of the sources' powers were calculated. Configuration and values of sensitivity functions were used for estimations of "danger" level of sources distribution in space and time. As for ecology the reveal of the domains which are of a high danger for the protected region is one of the most important problems.

The second case study was made for Mueggelsee. As in the previous example, the direct and inverse scenarios were considered. With the help of the inverse modeling for tracer transport problem, the sensitivity functions for different objective functionals were calculated. The results of this and the other numerical experiments with the developed models will be presented. Some of them are the computer movies.

The research reported in the paper is supported by Russian Foundation of Basic Research, Grants 97-05-96511, 98-05-65318 ; by Integrating Grant SD RAS (IG SD RAS -97 N30); by the Advance Information Technology Program of the Russian Ministry of Science and Technology.

References

1. Penenko V.V. 1981. Methods of numerical simulation of atmospheric processes. Gidrometeoizdat, Leningrad, 351p.
2. Penenko V.V., Tsvetova E.A. 1998. Structure of a complex of models for investigation of the interactions in the "Lake Baikal - regional atmosphere" system. Atmospheric and Oceanic Optics, v.11, N 6, P.507-513.
3. Tsvetova E.A. Numerical Studies of Lake Baikal hydrodynamics. Third Workshop on Physical Processes in Natural Waters. UFZ-Bericht. Nr.23/1998. pp.42-45 .
4. Tsvetova E.A. 1999. Direct and Inverse Modeling: Some aspects of a Modern Methodology for Lake Investigation. Lake 99, Copenhagen . V.1. S4A-10
5. Penenko V.V., Tsvetova E.A. Mathematical models for studying of interactions in the regional atmosphere-Lake Baikal system. Applied Mechanics & Technical Physics. 1999, V.40. N2, 137-147.

INTERNAL SEICE CLIMATE IN THE LAKE OF GENEVA (LAC LEMAN)

U. Lemmin¹, C.H. Mortimer²

¹LHR-DGC, EPFL, CH-1015 Lausanne, Switzerland

²Center for Great Lakes Research, University of Wisconsin Milwaukee,
Milwaukee, Wisc., 53201, USA

Introduction

Long internal waves in lakes commonly take the form of standing waves (seiches) whose frequency and form is determined by basin shape and density (temperature) stratification in the water column. In large lakes, the Coriolis force transforms the end-to-end motion into rotating (amphidromic) wave patterns (Mortimer 1993). The first horizontal mode resembles a shore-hugging Kelvin wave traveling counter-clockwise (cyclonically) around the lake basin in northern hemisphere lakes, as was first demonstrated in the Lake of Geneva (Mortimer 1963).

For higher horizontal modes, the resulting rotating wave patterns in large lakes depend on the basin shape and size and become more complicated. The spatial structure of higher modes can only be visualized through numerical modeling compared with observations. Those observations, in thermally stratified lakes, are predominantly of vertical oscillations of near thermocline isotherms and/or current measurements. However, the thermocline oscillations are accompanied by proportional, but much smaller amplitude (ca 1/1000) out-of-phase oscillations of the water surface. It is therefore possible to use numerically filtered deviations of surface level from equilibrium to detect the presence and progress of internal motions. This possibility arose for the Lake of Geneva, because the Swiss Service Fédérale des Eaux, (SFE), (1954) published tables of water levels measured in 1950 by 13 high-precision water level recorders spaced around the lake shore.

The Lake of Geneva environment

The Lake of Geneva (Fig. 1) is curved in shape and is composed of two main basins: a deep central eastern basin (310 m maximum depth, 157 m mean depth) called Grand Lac ("big lake") and a relatively small and narrow section in the west called Petit Lac ("small lake," maximum depth 70m; typical width about 4 km). The lake has a total length of 70.2 km and a width of 13.8 km in the central part. The eastern part of the lake is surrounded by high mountains sheltering it from most strong winds. The central and western part of the lake form part of the Swiss central plateau. The windfield over the lake is affected by the plateau. It is consequently dominated by events of strong winds from the NE and SW which may last from several hours to several days (Lemmin and D'Adamo 1996).

Analysis of the SFE water level records

Water levels were recorded from 4 June to 3 November 1950 with high-precision recorders. From the strip chart records, 6h mean levels were tabulated at 3 h intervals. By this averaging, level fluctuation with periods of 3h or less (i.e. surface seiches with periods of 73 min.) were smoothed out. The smoothed data points were brought to a common "hydrostatic" reference level by taking the mean of the water levels of each gauge during 693 selected nearly undisturbed periods of calm weather, uniform barometric pressure and no obvious disturbance (for details see SFE 1954). The date were divided into a summer period from 4 June to 24 August and a fall period from 28 August to 30 November.

A systematic out-of-phase behaviour of the large amplitude excursions is found for stations at the E and W ends of the basin. Thus, even though strong wind forcing typically only acts over the western and central part of the lake, the eastern end still responds as though forcing had occurred along the lake axis.

Plotting the distribution of the surface excursions around the basin during a typical forcing event (Fig. 1), three observations can be made:

1. As soon as a strong and steady wind from the SW sets in the whole lake responds by a depression at the W end (stations 1, 13, 12) and a rise at the E end (stations 5, 6, 7). The rise at station 6 was always found to be significantly higher than at 5 or 7. This may be attributed to the inflow effect of the Rhone river ($\pm 200 \text{ m}^3 \text{s}^{-1}$) which enters the lake close to station 6. In the

case of forcing from the opposite direction, the depression at 6 is comparable to those at 5, 7 and 8. In this case, the elevation at 1 and 13 at the W end is the very pronounced being about four times as high as the depression at the E end.

2. During the initial phase of the forcing, geostrophic adjustment can be seen by a rise of the surface at stations 2 and 3 when comparing with the surface elevations at stations 12 and 9/11 respectively on the opposite shore. This behaviour was also found in all other events investigated and clearly shows the significance of the Coriolis effect in this lake.

3. During the first half of day 37, the wind event dies down rapidly. It can be seen (Fig. 1) that the corresponding lake level changes occur at a much slower rate. Furthermore, a cyclonic pattern is set in motion at the E end of the lake. The appearance of the peak of maximum elevation in the records of stations 7 to 11 is systematically shifted in time and occurs at 11, a full day after station 7. This pattern cannot be followed further into the Petit Lac because of the surface rise setting in from the W end of the lake at the same time. The same pattern was also observed during other events. Surface elevations correspond to thermocline depressions. Documentation of Kelvin seiches in current and temperature measurements in the water column are always related to thermocline depressions. It can thus be seen from the surface elevation data in this figure that Kelvin seiches are set in motion at the E end of the lake in the case of wind forcing from the SW even though this end is not under the direct influence of the wind. This is different from the situation of the forcing from the NE when the W end is directly under the wind. The high elevations observed in this case will cause a strong depression of the thermocline at the W end.

The spectral analysis of such records was carried out for all stations for the summer period and the fall period separately.

Modes detected

Modes were identified by comparing the periods corresponding to prominent spectral peaks with those predicted for a two-layered approximation fitted to the lake dimensions and density distribution (Merian formula). Observations and predictions are close. Independent of season and station location, only certain modes are excited.

The most prominent is the first mode (Fig. 2). Its period is near 83 h in summer. Spectra from the narrow western end of the lake always show the first mode response most clearly. A weak second mode signal could be detected in the spectra of the stations in the central part of the Grand Lac (stations 3, 9, 10, 11), but not at other stations. The third mode with periods of 33.49 h was found at all stations around the lake. In the eastern part of the lake basin the pattern strongly changes with season. During the summer the shape of the spectra at station 7 resembles that of the station 2 at the W end with the highest energy in the first mode. During the fall period, the third mode becomes the dominant period in the spectra. Mode four is found in some summer spectra but not in those for the fall. Modes five to nine have not been observed in any spectra. Mode ten is the first cross basin mode, with a summer period of 11.1 hours. It is seen most clearly in the spectra in the central part of the lake basin and is often found in the eastern part. Modes higher than ten cannot be detected with certainty because of the cut-off imposed by the SFE filter.

Cross spectral analysis reveals the wave propagation pattern. In each case, coherence and phase were determined between pairs of stations. In most cases, coherence was well above the 95% confidence limit. This is illustrated for the first mode at end-basin stations 1 and 7 in Fig. 2. For the tenth mode, the amphidromic pattern displayed coherence between stations which are part of the same amphidromic cell, but no coherence between stations in different cells.

With station 2 as reference station and progressing cyclonically around the lake, coherence is found to decrease slightly from W to E along the southern shore. For the stations along the northern shore, coherence increases again from E to W and becomes high for those stations in the narrow Petit Lac. From the phase angles calculated from the data, cyclonic progression is clearly established indicating that the first mode seiche travels a full cycle around the lake.

Discussion

Evidence for "Kelvin-seiche" responses to wind forcing

Initial analysis of these water level data had already shown that a periodicity in the surface elevation signals corresponded to the first mode "Kelvin seiche" (Mortimer 1963). This signal was visually correlated with the thermocline oscillation at Geneva. The surface elevation signal

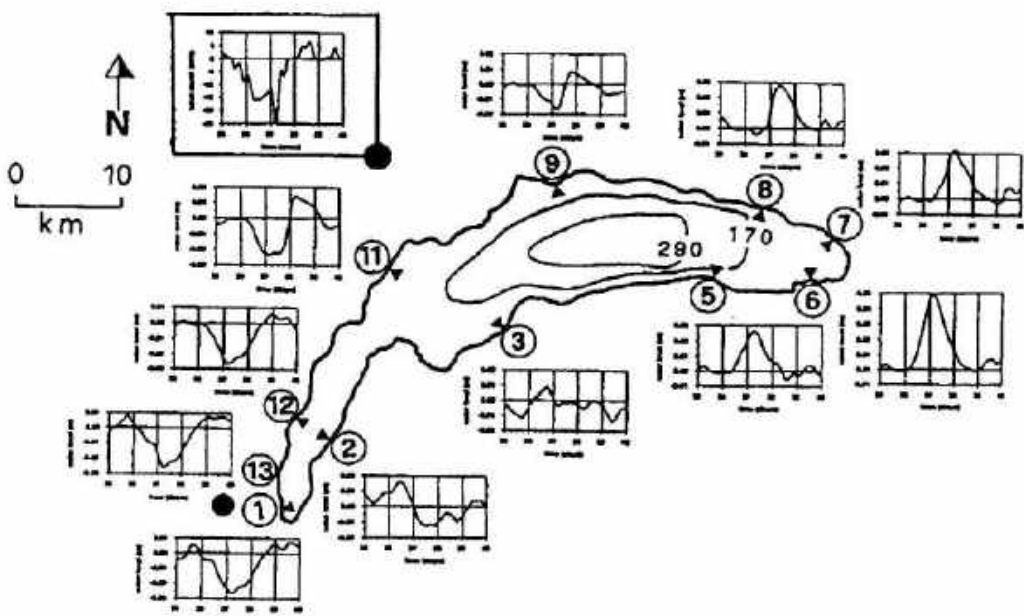


Fig. 1: Time series of surface denivelations at several stations during a wind event with winds from the SW. The black dot indicates the position of the wind measuring station. The record of the squared wind component in the direction of the steady wind (from 220°) is given on the top.

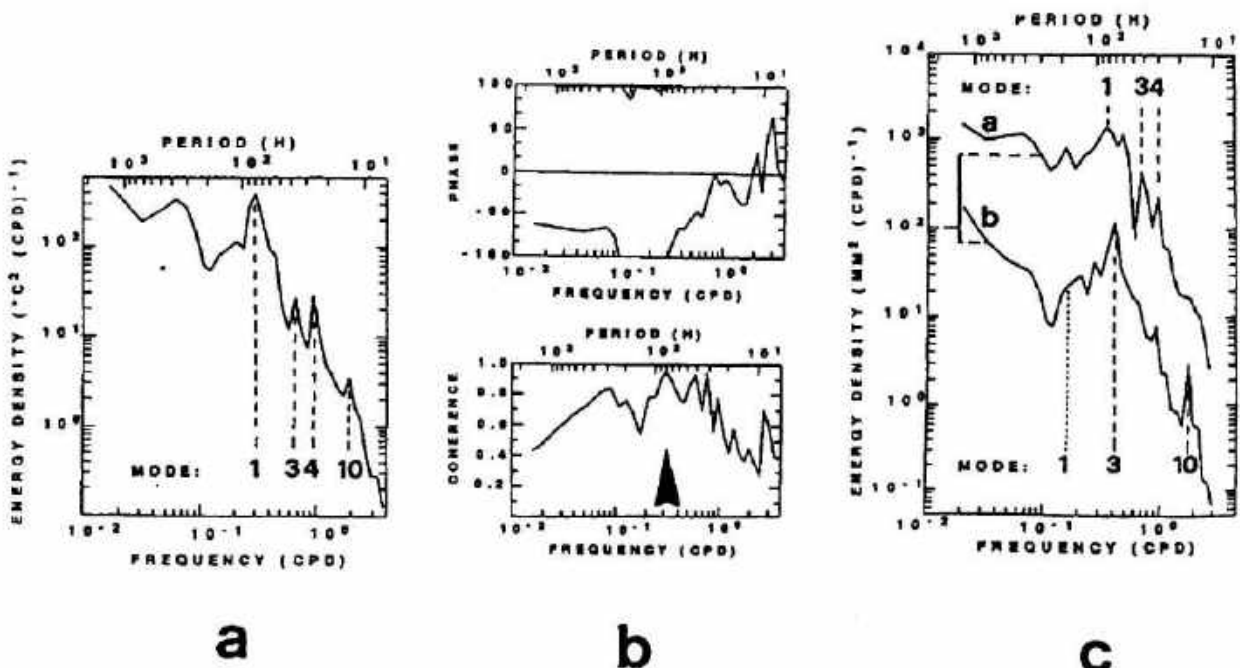


Fig. 2: a. Spectrum at station 2 during summer period. Arrows indicate internal wave periods calculated from the numerical model; labels give the mode number. b. Coherence and phase between stations 2 and 7. Note that at the first mode (arrow) coherence is limited to a narrow band around that period. c. Spectrum at station 7; curve a: during summer, curve b: during fall.

progressed around the lake perimeter at a nearly constant speed corresponding to a first mode internal seiche.

The results of the present statistical analysis show that, for the first mode, coherence is high in the summer. In the fall, it is falling off toward the eastern end of the lake where, at station 6 it even fell below the confidence limit.

Analysis of lake temperature and current data has previously shown (Bohle-Carbonell 1986) that typically one or two whole-basin circuits are completed if post-storm calm persisted long enough. However, Bohle-Carbonell and van Senden (1990) suggested that basin-mode models are inappropriate interpreters. They concluded that currents in large lakes, at least those in this lake, may be best described as transient in time and only locally organized in space.

Coherence and phase angle patterns, evident in the present study, demonstrate that basinwide modes do occur. This is further supported by an analysis of more recent water level data series from the permanent stations in Chillon, St. Prex and Secheron on the north shore. The first, third and tenth mode were the only ones excited and cyclonic progression was established for the first and third mode. Evidence for the Kelvin wave character of the first mode wave comes also from the analysis of current and temperature recordings carried out in the lake (Mortimer et al. 1983).

Recognition of basin-mode responses occurring in large lakes depends to some extent on how those responses are defined. If, with Bohle-Carbonell and van Senden (1990), one regards a basin mode oscillation as one which persists for more than five crossing periods (2.5 cycles) then frictional dissipation dictates that few internal basin modes are caught in their statistical net.

Non-linear fronts and pulses

A major complication in the generation of basin mode internal seiches is the strong non-uniformity of the wind stress imposed on the Grand Lac by topographic sheltering (Lemmin and D'Adamo 1996). Other complicating factors, to which Bohle-Carbonell and van Senden (1990) drew attention, are: differential warming which gives rise to local winds and local current fields; the effect of shore topography; and nonlinear interactions which exchange energy between motions of different time and space scales (Bohle-Carbonell and Lemmin 1988). Nonlinear interactions are strongest during late fall, when internal wave speed falls to the level of ambient current speeds.

The net result of these complications is the production of seiches with initially steep fronts indicating the importance of non-linear effects. Such frontal steepness is often observed after strong wind pulses have generated internal seiches in lakes of all sizes (Mortimer 1955; Lemmin 1987). The fronts evolve into regular seiches as times passes.

The local depression of the thermocline caused by a local wind pulse may still move at the same wave speed around the basin as a pulse rather than as a seiche. It is possible that some of these pulses are missed in the present analysis because of the SFE filter. However, it is obvious from the peaks in the spectra that a significant number of basinwide seiches which make more than one turn around the lake is generated.

Coupling with higher modes

The passage of the steep front of the first mode Kelvin wave seen at all stations is often followed by a train of tenth mode waves. The link between the first mode and the tenth mode is thus evident in the observations.

Is this mode a cross basin seiche or is it a Poincaré wave? The fact that a wave of near 11 h period has been detected in the shore-based water level records would favour interpretation as a standing cross-basin wave in the central part of the lake. But since the same periodicity appears in all parts of the basin, independent of local topography, a Poincaré wave interpretation may be more likely. Progressive vector diagrams disclose circular patterns characteristic for Poincaré waves. Further support for the Poincaré wave concept comes from spectra calculated by Mortimer et al. (1983) for current and temperature data at different stations in the lake.

Energy dissipation

The passage of the large-amplitude "Kelvin seiche" produces thermocline displacements over bottom slopes, sometimes extending laterally 100 m or more (Thorpe et al. 1996). This produces strong bottom shear associated with high turbulent energy dissipation rates and the potential for sediment resuspension. Recently, other processes, in addition to bottom friction, have been revealed which point to the importance of internal seiches in lake dynamics, i.e. the generation of short progressive internal wave during the passage of an internal seiche (Thorpe et

al. 1996). A direct correlation between Kelvin seiches and progressive internal waves has been demonstrated experimentally in the Lake of Geneva (Thorpe and Jiang, 1998). The above recent findings show the cascade from internal seiches to short internal waves and energy dissipation and demonstrate the importance of internal seiches in lake dynamics.

Conclusions

The present study of internal lake dynamics by mean surface water level records has confirmed its potential which was initially demonstrated by Mortimer (1963). Easily installed and maintained, these instruments allow measurements year-round without interference with other activities on the lake, such as commercial drift netting which precludes the use of mid-water moorings.

In addition to the dominant first and tenth mode internal wave dynamics, third mode seiches have been shown to exist in the lake. They have not been previously seen in current data, while numerical models always have predicted them. Their basinwide motions are important in the water mass circulation. Their excitation can be attributed to inhomogeneity of the wind field.

An important aspect of internal seiche dynamics is the generation of short progressive internal waves (Thorpe et al., 1996). Interaction of the seiches and those waves with the lateral bottom slope creates a turbulent boundary layer and high dissipation (Thorpe and Jiang, 1998). Recently, Imberger (1998) has noted the importance of this wave-slope interaction in the determination of the particle flux path.

References

- Anonymous, Service fédéral des eaux; SFE (1954). Les dénivellations du lac Léman. Département fédéral des postes et des chemins de fer.
- Bohle-Carbonell, M. (1986) Hydrodynamic des Genfer Sees, Gleichgewichte und charakterisierende Größen. Doctoral Thesis No 611, EPFL, Lausanne, Switzerland.
- Bohle-Carbonell, M., and U. Lemmin (1988) Observations on non-linear current fields in the Lake of Geneva. *Ann. Geophysicae* **6**: 89-100.
- Bohle-Carbonell, M., and D. v. Senden (1990) On internal seiches and noisy current fields-theoretical concepts versus observations. Large Lakes Ed. M. T. a. C. Seruya. Springer. 81-105.
- Imberger, J. (1998) Flux paths in a stratified lake: a review. Physical processes in lakes and oceans Ed. J. Imberger. Washington, DC, AGU. 1-17.
- Lemmin, U. (1987) The structure and dynamics of internal waves in Baldeggersee. *Limnol. Oceanogr.* **32**: 43-61.
- Lemmin, U., and N. D'Adamo (1996) Summertime winds and direct cyclonic circulation: observations from Lake Geneva. *Ann. Geophysicae* **14**: 1207-1220.
- Mortimer, C. H. (1955) Some effects of earth rotation on water movements in stratified lakes. *Verh. Int. Ver. Limnol.* **12**: 66-77.
- Mortimer, C. H. (1963) Frontiers in physical limnology with particular reference to long waves in rotating basins. *Publ. Great Lakes Res. Div., Univ. Mich.* 9-42.
- Mortimer, C. H., C. Perrinjaquet, and M. Bohle-Carbonell (1983). Internal oscillatory responses of Lac Léman to wind impulses during 1977/1978 compared with waves in rotating channel models. Communication No. 50. LHYDREP, EPFL Lausanne, Switzerland.
- Mortimer, C. H. (1993). Long internal waves in lakes: review of a century of research. Center for Great Lakes Studies; University of Wisconsin-Milwaukee, Special report No 42.
- Thorpe, S. A., K. J. Keen, R. Jiang, and U. Lemmin (1996) High frequency internal waves in Lake Geneva. *Phil. Trans. Roy. Soc. London A* **354**: 237-257.
- Thorpe, S.A. and R. Jiang. 1998. Estimating internal waves and diapycnal mixing from conventional mooring data in a lake. *Limnol. Oceanogr.* **43**: 936-945.

INTERNAL WAVES IN LAKE BAIKAL

Sergei V.Semovski¹, Michail N.Shimarev¹, Werner Alpers², Corinna Schrum²

¹Limnological Institute SB RAS, P.O.Box 4199, Irkutsk 664033 Russia,
Phone: +7-3952-460768, Fax: +7-3952-466933, E-mail: semovsky@lin.irk.ru

²Institute fuer Meerskunde, Hamburg University, Germany

1. Introduction

The existence of internal waves (IW) in Lake Baikal is known from observations of V.B.Shostakovich and L.L.Rossolimo made in 1930's. Estimations of amplitude and spectrum were derived using observations of moored temperature recorders. Long series of acoustic observations realised on the underwater neutrino telescope give the possibility to detect long nonlinear IW of high intensity. New remote sensing tools, such as Radar with Synthetic Aperture (SAR), produce high-resolution imagery of the lake surface. Numerous surface manifestations of IW can be observed and many parameters can be estimated. However, numerous problems are still open and between them is IW formation, movement, interaction with frontal structures, their role in mixing processes.

2. Statistical characteristics of internal waves

Spectra of Baikal gravitational IW were calculated by V.I.Verbolov et al. (1986). It was shown that level of energy density spectrum is lower in comparison with model spectrum of Garret & Munk (1972) (Fig.1). Lowest energy of IW is typical for March (period of ice-cover, when effect of wind driven forcing is minimal). It was shown as well that maxims of spectra for temperature and currents are often close to those of internal seiches. Positions of maxims for statistical cepstrum correspond to two-, thri-, tetra-undulatory interaction of internal oscillations (8 hours, 330-350 min, 190-215 min, 105-115 min, 40-45 min).

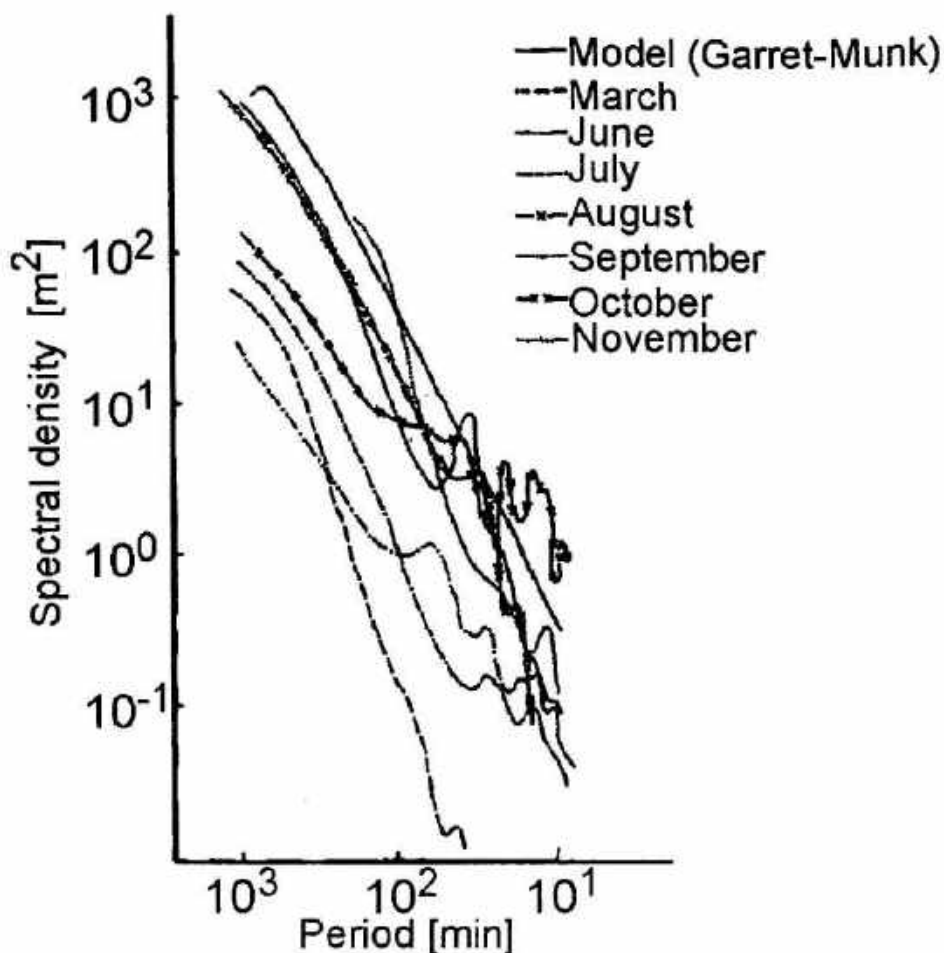


Fig.1. Annual variability of internal wave spectra for the South Baikal
(from Shimaraev et al., 1994).

3. Long internal waves

The presence of long internal waves of high intensity with period of few days and weeks can be traced on continuous records of temperature profiles. Figure 2 presents temperature records carried out in South Baikal during early spring of 1970. Observed oscillations in thermocline have period 7-15 days. Note, that wave of 28.02 has sharp front, and its nonlinear structure looks similar to so called "internal surge", which existence is known for some lakes and for Gibraltar straight (Pharmer, 1978).

High-resolution acoustical observations of nonlinear long internal waves have been made on the underwater neutrino telescope site (South Baikal, see Chensky et al., 1998). Quasi-regular variations in temperature were measured in 50-120 m layer under ice cover during early spring of 1991-1997. The period of oscillations is close to three weeks and

greatly surpassed period of inertial fluctuations. The factors forming such internal features in absence of wind stress (see Fig. 1) are still unknown.

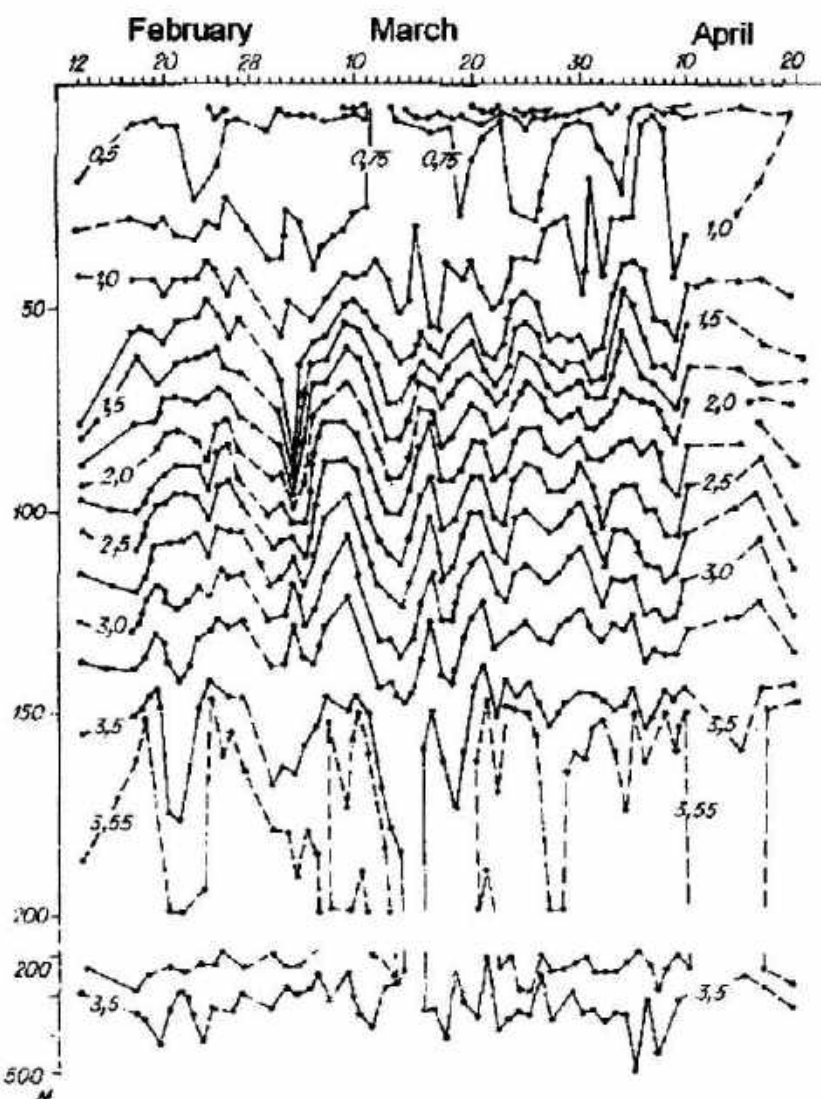


Fig.2. Spring 1970 temperature records for South Baikal,
station location is 7 km offshore Angara source.

4. Internal waves high-frequency detected on SAR imagery

New knowledge on short internal waves occurrence, distributions and statistical characteristics can be derived from satellite imagery. High-resolution passive remote sensing in infrared band can show surface manifestations of internal waves. For Baikal, unfortunately, such data is unavailable. Synthetic Aperture Radar (SAR), that produce images of surface roughness with high resolution (25 m for ERS satellites) can be used for detection of different events on the surface of water objects, including internal waves (Ivanov et al., 1997).

Courtesy to European Space Agency announcement of opportunity, ERS SAR images of the lake Baikal collected using ESA mobile receiving station during autumn 1997 and summer 1998 was given in our disposition. Numerous structures can be detected on ERS images of the lake surface.

— internal seiches, surges and baroclinic internal waves of different intensity.

High-frequency seiches (tetra-undulatory with period of 40–45 min), probably, are detectable on SAR images during period of homothermy (June), when stratification is very low (Fig.3).

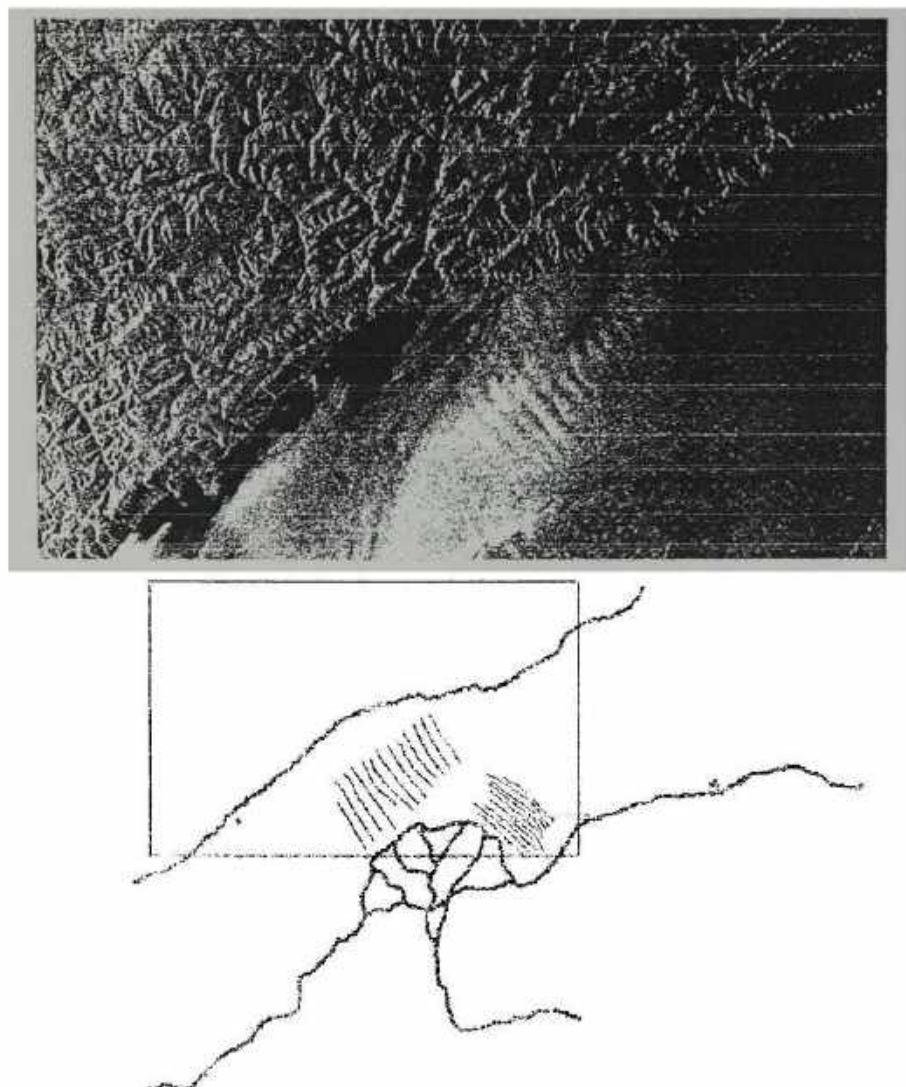


Fig.3.ERS SAR image of Selenga mouth region, 3.06.1997
and internal waves manifestation.

Baroclinic internal waves, forming during period of stratification are generated due to seiches interaction with bottom orography and coast and due to wind forcing. Figure 4 presents numerous trains of internal waves in South Baikal detectable on the areas of developed surface wind waves (grey areas). Two days before the image strong wind was

observed in the lake area (up to 17 m/sec), it can be the factor affecting on internal waves generation.

Note the transformation of internal waves train on shallow Murino Bank presented in the southern part of the lake.

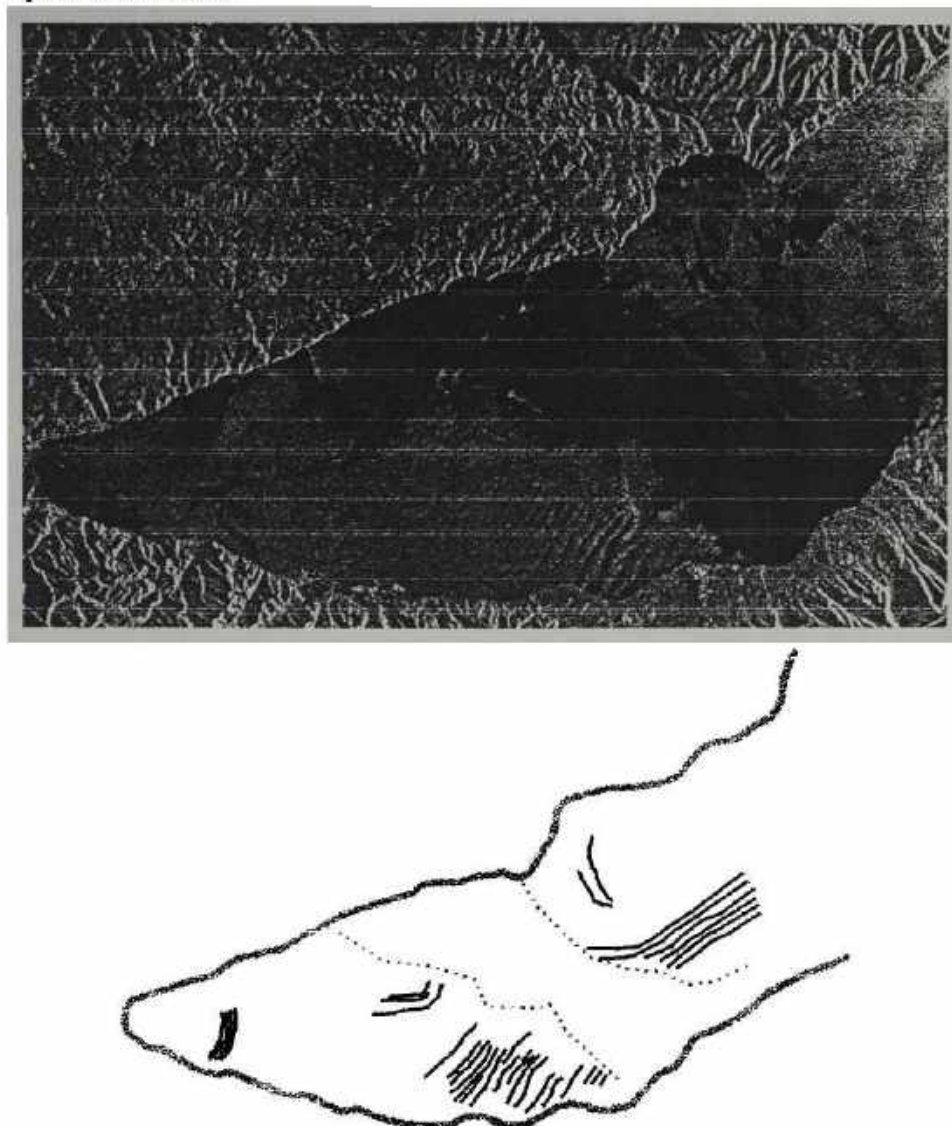


Fig.4. ERS SAR image of South Baikal, 26.07.1997 and internal waves manifestation.

5. Role in mixing processes

One of the peculiar feature of lake Baikal hydrophysics is the process of deep mixing. Ventilation of bottom layer is realised due to this and functioning of deep ecosystem became available. The role of different physical mechanisms responsible for events of direct surface water penetration into the bottom layer is still under discussion. One of the possibilities is surface water patterns deep penetration along the thermal bar, firstly observed by

M.N.Shimaraev et al. (1993). However, for surface water volumes transport into the deep layer the mesothermal maximum of temperature influence should be neglected. It was shown that IW are abundant in the lake during all the year. There are sufficient reasons to believe that IW interaction with thermal bar and following disintegration of mesothermal maximum can be the necessary condition for deep mixing event.

REFERENCES

- Chensky A.G., Lovtsov S.V., Parfenov Yu.V., Rastjogin, V.Yu.Rubtsov, On the coastal-trapped waves in the southern area of lake Baikal, Oceanic Fronts and Related Fenomena, Konstantin Fedorov memorial symposium, Sankt-Petersburg, 18-22 May 1998, pp.29-30.
- Garret C., Munk W., 1972, Spatial and temporal scale of internal waves, *Geophys. Fluid Dynamics*, v.3(3), pp.225-264.
- Ivanov A.Yu., Alpers W., Naumenko M.A. and Karetnikov S.G., Lake Ladoga surface features on the ERS-1 SAR imagery, in: Proceedings of 3rd ERS Symposium on Space at the service of our Environment, Florence, Italy, 17-21 March 1997 [ESA SP-414, May 1997], pp.1035-1040, 1997.
- Pharmer D., 1978, Observations of long nonlinear internal waves in a lake, *J.of Phys.Ocenogr.*, vol.8, pp.63-73.
- Shimaraev M.N., Elements of the heat regime of Lake Baikal. "Nauka", Novosibirsk, 1977, 149 p. (in Russian).
- Shimaraev M.N., Granin N.G., Zhdanov A.A., 1993, The role of spring thermal bar in the deep ventilation of Lake Baikal water. *Limnology and Oceanogr.* v.38(5), P.1068-1072.
- Shimaraev M.N., Verbolov V.I., Granin N.G. and Sherstyankin P.P., Physical limnology of Lake Baikal: a review, Baikal International Center for Ecological Research, preprint No.2, Irkutsk-Okayama, Russia-Japan, 1994.
- Verbolov V.I., Pokatilova T.N., Shimaraev M.N., Fedorov V.N., Granin N.G., Zhdanov A.A., Formation and dynamics of lake Baikal water. "Nauka", Novosibirsk, 1986, 118 p. (in Russian).

A STOCHASTIC MODEL FOR THE SEA LEVEL DATA ANALYSIS

Aleksander Toompuu and Urmas Raudsepp,

Estonian Marine Institute
Paldiski Road 1, 10137 Tallinn, Estonia

The Baltic Sea water level varies over a wide range of temporal and spatial scales. The spectra of the sea levels recorded at different locations of the Baltic Sea gives dominant peak at the annual period. Still, there is no clear physical explanation what forces this periodic process in the Baltic Sea. Vermeer *et al.* (1988) suggests the main cause to be the east-west directed wind forcing over the Danish Sounds pumping water into and out from the Baltic Sea. The statistical analyses by Lass and Matthäus (1996) on the seasonal cycle of the winds and sea level in the Baltic Sea support the above argumentation. Inspection of the time series of the monthly average river inflow values to the Baltic Sea and its sub-basins shows a clear annual variability (Bergström and Carlsson, 1994). According to simple model calculations by Samuelsson and Stigebrandt (1996), 50-80% of the annual sea level variations is imported into the Baltic Sea from the North Sea. In the short-term sea level spectra domain (up to several month) no significant peaks have been

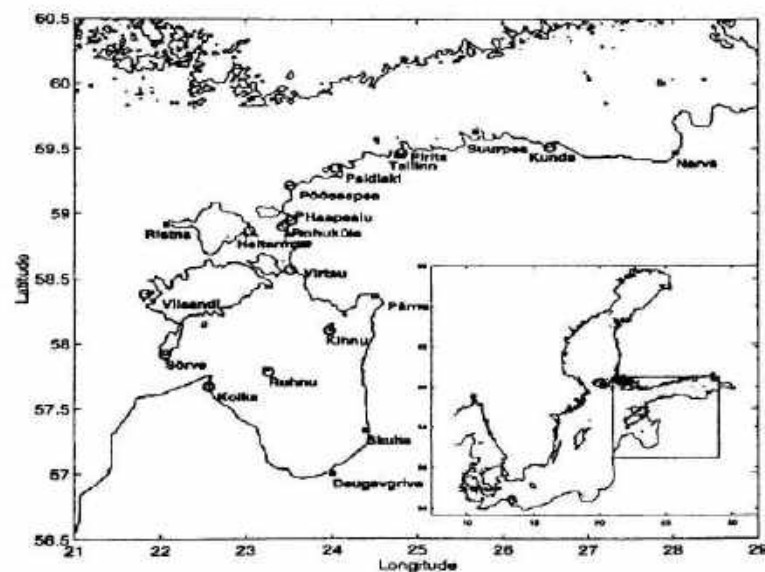


Figure. The location of sea level stations around Estonian coast and in the Gulf of Riga. The stations are equipped with either mareographs (■) or bench sticks (○).

found and the spectrum of the daily mean values is rather white (Vermeer *et al.*, 1988). Most of the high frequency changes are governed by the short-term winds, air pressure changes and currents variability (Samuelsson and Stigebrandt, 1996).

The main objective of the present work is to

develop a stochastic model for reconstruction of the Baltic Sea level field in a particular coastal sub-basin. The knowledge of the detailed sea level field variations in coastal region could be utilized for estimation of the coastal up- and downwelling, of the along-shore and off-shore volume and mass transport as well as the water and matter exchange balances between semi-enclosed marginal sub-basins and the open sea (Võsumaa *et al.*, 1995; Lilover *et al.*, 1995). Besides, the sea level fields are required for verification and/or forcing of numerical water circulation models. In the Baltic Sea, the diversity of the factors of nearly equal weight forcing simultaneously the short-term and small-scale sea surface topography variations does not allow a set-up of any simple dynamical model. Therefore, it seems reasonable to use the stochastic modeling approach. Thus, a statistical model for the sea level reconstruction is developed following the principles of optimal analysis (Gandin, 1965; Cressie, 1991). The formulation of the method for oceanographic applications is thoroughly discussed by Bretherton *et al.* (1976) and Toompuu and Wulff (1995; 1996), therefore for the method basics we refer to the listed papers. The first step of the model building is specification of the mean and random fluctuation fields. The second step is estimation and approximation of the fluctuation field correlation function, including evaluation of the noise-to-signal ratio of the available data. The third step is quantification of the data quality and reconstruction of the sea level field values at space-time points where and when the measurements are missing. In this paper, a stochastic model is developed for the Estonian (and partly Latvian) coastal sea. The sea level records spanning over a five-year period, 1978-1982, in three topographically defined areas - the Gulf of Finland, the Gulf of Riga and Väinameri, have been used.

Twenty sea level series recorded along a part of the Latvian coast surrounding the Gulf of Riga and at the Estonian coast are picked out (see Figure). The used sea level series consist of either mareograph hourly or bench stick (two or four times a day) readings. The five-year long time series (from 1978 to 1982), comprising the most regular observations, are used in the analysis. The entire model domain was divided into three sub-domains (including the stations): the Gulf of Finland (Narva, Kunda, Piritu, Tallinn, Paldiski and Põõsaspea), Väinameri basin (Haapsalu, Rohuküla, Heltermaa, Virtsu and Ristna) and the Gulf of Riga (Pärnu, Kihnu, Skulte, Daugavgriva, Ruhnu, Kolka, Sõrve and Vilsandi). The data statistics was estimated for each basin independently.

From the optimum analysis approach it follows that the least squares optimum linear estimator for the random field fluctuation value $\tilde{\psi}_k \equiv \tilde{\psi}(\mathbf{r}_k)$ at an arbitrary location with a point vector \mathbf{r}_k has the form

$$\tilde{\psi}_k = \frac{1}{1 + \eta^2} \sum_{i=1}^n T_{ki} \sum_{j=1}^n M_{ij}^{-1} \psi_j^o , \quad (1)$$

where M_{ij}^{-1} is the inverse of the measured data correlation matrix M_{ij} , T_{ki} is the correlation matrix of true values, η^2 is the data noise-to-signal ratio and ψ_j^o is an observed fluctuation at location \mathbf{r}_j with $i,j = 1, 2, \dots, n$. The most powerful tool of the approach, the variance of the relative error of the estimate (1),

$$E_k^2 \equiv \frac{\langle (\psi_k - \tilde{\psi}_k)^2 \rangle}{\sigma^2} = 1 - \frac{1}{1 + \eta^2} \sum_{i,j=1}^n T_{kj} M_{ji}^{-1} T_{ik} , \quad (2)$$

depends only on the noise-to-signal ratio and the correlation of the fluctuation field. The maximum possible value of the relative error variance is 1. The optimum estimate of the fluctuation field $\tilde{\psi}_i$ at a data point \mathbf{r}_i does not coincide with the observed value ψ_i^o ,

$$\tilde{\psi}_i = \psi_i^o - \frac{\eta^2}{1 + \eta^2} \sum_{j=1}^n M_{ij}^{-1} \psi_j^o . \quad (3)$$

The standard deviation of the difference is

$$\langle (\tilde{\psi}_i - \psi_i^o)^2 \rangle^{\frac{1}{2}} = \left\langle \left(\frac{\eta^2}{1 + \eta^2} \sum_{j=1}^n M_{ij}^{-1} \psi_j^o \right)^2 \right\rangle^{\frac{1}{2}} = \frac{\eta^2}{1 + \eta^2} (M_{ii}^{-1})^{\frac{1}{2}} \quad (4)$$

and the ratio of the difference to its standard deviation (relative error) is

$$\vartheta_i = \frac{\tilde{\psi}_i - \psi_i^o}{\langle (\tilde{\psi}_i - \psi_i^o)^2 \rangle^{\frac{1}{2}}} = \frac{\sum_{j=1}^n M_{ij}^{-1} \psi_j^o}{\left(M_{ii}^{-1} \right)^{\frac{1}{2}}} . \quad (5)$$

The absolute value of ratio ϑ_i can be considered as a measure of correctness of data ψ_i^o at the point \mathbf{r}_i in relation to all other data and to the second order statistical characteristics of the fluctuation field. Let $C(\mathbf{r})$ be the sea level at a point $\mathbf{r} = (x, t)$, where x is space- and t -is time co-ordinate. Considering the sea level fluctuation field $\psi(x, t)$ homogenous, isotropic and stationary, the correlations in (1) to (5) depend on the space and time lags Δx and Δt . There are two main problems to solve in order to apply the described

approach to the real data. Firstly, the random field is to be determined and the observations, interpreted as samples out of realisations of the random field, are to be divided into the mean and fluctuational parts. Secondly, the second-order two-point statistics or correlations of the fluctuation field and the noise-to-signal ratio of the data are to be estimated.

In the present approach the mean field is interpreted as having basically a deterministic nature forced by a few either known or unknown factors. If the major forcing factors and their relation to the sea level variation are well known, the mean could be determined via a deterministic dynamical model. On the other hand, if some of the important forces are still unknown or if the way of the direct causal influence is indistinct or even if the direct deterministic modeling appears much too resource demanding, an alternative way of the mean determination, based on the qualitative argumentation, is still available. In the latter case the mean should be expressed in a simple way with the least number of parameters.

The data show a distinct seasonal cycle with the low water in March-May and high water in October-November. The mean sea level at each station is approximated by the sum of a linear trend and a harmonic of the annual period,

$$\langle C(t) \rangle = a + bt + A \sin(2\pi t / T + \varphi), \quad (6)$$

where t is the time and T is the annual period (365.25 days). The approximation coefficients a , b , A and φ are calculated by the least squares from the original data series.

The calculated sea level data quality (5) appears to be rather uniform. The data quality estimates (errors) have single-mode histograms with different widths. Suppose the errors of the regular data are formed as a sum of influence of a number of independent random factors of nearly equal weight and resemble, according to the central limit theorem, a normal distribution. Suppose also that the errors of the outliers include the influence of some factors of extraordinary high weight (e.g. complete misreading, data coding failure or irregular natural phenomena). Then the estimated outlier errors deviate the error histograms from the normal distribution. Following these assumptions, the normalized empirical error frequency distributions were checked against the normal probability density. It appeared that according to the chi-square (χ^2) goodness of fit test all empirical error frequency distributions were quite far from the normal, but approached the normal distribution if a certain amount of largest errors were removed from the original sample. So, an increasing fraction of the most erroneous data was gradually removed from the original sample of data errors. It is

remarkable that the calculated χ^2 -values versus the cut-off error display for all stations a general minimum, where the distribution is the closest to the normal. The data with errors exceeding the cut-off error for the minimum χ^2 -value were considered outliers. The fraction of outliers appeared to be rather small (less than 10%) in all tested data samples.

The sea level field in the Estonian coast for the period 1978-1982 was reconstructed by the optimum analysis approach (1) utilizing the suggested statistical model, the available sea level data, the estimated field statistics and the data noise-to-signal ratio. The most erroneous data (less than 10%) were excluded from the reconstruction procedure. As an example, the sea level fluctuation reconstruction outcome (1) at Põõsaspea and Suurpea stations in 1979 is compared with the actual (twice a day) measured values. Põõsaspea is located in the marginal area of the selected Gulf of Finland sub-basin, therefore the reconstruction error should be the largest. Suurpea, on the contrary, is situated in the middle of the sub-basin. All data measured at Põõsaspea station were excluded from the original data set for the example calculation and the reconstruction estimates were obtained on the basis of the rest of the data in the sub-basin. Suurpea station data were not included even into the field statistics estimate. The average standard deviation (9) of all 712 reconstructed values at Põõsaspea was 3.2 cm, while at Suurpea it was expectedly smaller, 2.2 cm. The coefficients of the fitted regression line $y = ax + b$ at Põõsaspea have values $a = 1.016$, $b = -0.209$ with 95% confidence intervals (0.997, 1.037) and (-0.575, 0.157), respectively. At Suurpea the corresponding coefficient values are $a = 0.938$, $b = 1.013$ with 95% confidence intervals (0.924, 0.951) and (0.822, 1.204).

A stochastic model for reconstruction of the sea level fluctuations on the meso- and synoptic space-time scales in the Estonian coastal area, based on the optimal interpolation method was developed. The five-year (1978-1982) sea level records at twenty locations covering three different sub-basins were analyzed to determine the mean and fluctuation fields and to estimate the spatial and temporal second-order statistics. The mean field was defined to comprise the overall time average, linear trend and seasonal cycle. The time average sea level was higher in the river mouth area and expectedly followed the general mean sea level topography of the Baltic Sea. The extracted positive sea level trends from 1.3 to 3.2 mm/year reflect the large-scale inter-annual sea level variability. The seasonal signal had amplitudes between 17 and 23 cm with high water in October and low water in April. The factors forcing the mean sea level field are not uniquely determined so far and fall outside of the scope of the present paper. The solution of the

problem is relaxed due to the high spatial coherence of the mean field variability in the Baltic Sea. Gaussian function was chosen to approximate the estimated spatial and temporal correlation components of the fluctuation field. The temporal correlation radius (e-folding scale) of about 8-10 days and spatial correlation radius 200-400 were obtained from the approximations. The data noise-to-signal ratio was estimated to be 0.2-0.6.

Based on a suggested stochastic model the sea level data quality was quantified. It is evident that the most erroneous data or outliers originate not only from the data mistreatment events, but also from the natural irregularities. Though the sea level data quality estimate is rather important because of the different observation methods and time intervals used at the sea level stations around the Estonian coast, it should be realized that the approach fails to reconstruct the extreme or irregular sea level variations of natural causes. According to the criterion, developed on the basis of the suggested stochastic model, at least 90% of the sea level data from the Estonian coastal area should be considered as meeting the quality requirements. There was no significant difference in the quality of the data measured either continuously by mareographs or observed by reading the bench sticks.

After removal of the most erroneous data, the approach was utilized to reconstruct the sea level field in around the Estonian coastal sea with a satisfactorily low reconstruction error. The described reconstruction procedure can be equally well applied to fill out data gaps in the sea level data series and to estimate the reconstruction uncertainty, if required.

The work was supported by the Estonian Science Foundation.

References

- Bergström, S. and Carlsson, B., 1994. River runoff to the Baltic Sea: 1950-1990. *Ambio*, 23: 280-287.
- Bretherton, F. P., Davis, R. E. and Fandry, C. B., 1976. A technique for objective analysis and design of oceanographic experiments applied to MODE-73. *Deep-Sea Res.*, 23: 559 - 582.
- Cressie, N., 1991. Statistics for spatial data. John Wiley and Sons Inc.
- Gandin, L. S. 1965. Objective analysis of meteorological fields. Jerusalem.
- Lass, H.U. and Matthäus, W., 1996. On temporal wind variations forcing salt water inflows into the Baltic Sea. *Tellus*, 48A: 663-671.
- Lilover, M.-J., Raudsepp, U. and Kõuts, T., 1995. Variability of the velocity field and its relation to the external forcing in the Gulf of Riga. In: J. Elken and A. Toompuu (Editors), Hydrographic studies within the Gulf of Riga Project, 1993-1994. EMI Report Series, No. 1., Tallinn, Estonia, pp. 35-82.

- Samuelsson, M. and Stigebrandt, A., 1996. Main characteristics of the long-term sea level variability in the Baltic Sea. *Tellus*, 48A: 672-683.
- Toompuu, A. and Wulff, F., 1995. Spatial large-scale correlations for optimal interpolation of temperature, salinity and nutrient concentrations in the Gulf of Finland. *Environmetrics*, 6: 55 - 72.
- Toompuu, A. and Wulff, F., 1996. Optimum analysis of monitoring data on temperature, salinity and nutrient concentrations in the Baltic Proper. *Environmental Monitoring and Assessment*, 43: 283 - 308.
- Vermeer, M., Kakkuri, J., Mälkki, P., Boman, H., Kahma, K. K. and Leppäranta, M., 1988. Land uplift and sea level variability spectrum using fully measured monthly means of tide gauge readings. *Finnish Marine Research*, 256: pp. 3-75.
- Võsumaa, Ü., Eilola, K. and Stigebrandt, A., 1995. Application of an enhanced one-dimensional model to the Gulf of Riga. In: J. Elken and A. Toompuu (Editors), *Hydrographic studies within the Gulf of Riga Project, 1993-1994*. EMI Report Series, No. 1., Tallinn, Estonia, pp. 121-142.

INSTABILITIES AND ALONG-SHORE VARIABILITY IN THE FINNISH COASTAL CURRENT

Tapani Stipa

Department of Geophysics, University of Helsinki
P.o.Box 4 (Fabianinkatu 24 A) FIN-00014

Abstract

Both measurements and model results are used to show that there exists a meandering, sharply defined coastal current along the northern coast of the Gulf of Finland. This current, which is formed by freshwater runoff and intermittent coastal processes, may exhibit large-amplitude isopycnal displacements. We present results from recent measurements of along-coast variability in the Gulf, use an idealized 3d process model to show how hydrodynamic instabilities are trapped into this current, and discuss the possible importance of this process in the nutrient supply to the cyanobacterial blooms in the summer of 1997. It turns out that no wind is needed to create a violent coastal current system.

Linear theory

The dynamics of the entrance of river plumes is well documented by e.g. *Chao and Boicourt* [1986]; *Yankovsky and Chapman* [1997]; at the river entrance, a bulge is formed, from which a geostrophically balanced current leaks along the coast. The largest river of the Baltic Sea, Neva, discharges at the eastern end of the Gulf of Finland (GoF), which means one can expect to find the discharge water to flow along the northern coast of GoF.

There is available potential energy in the coastal current, however. The setup is unstable to baroclinic instability (see e.g. *Pedlosky* [1987]) which tends to release the potential energy as wave-like instabilities growing with a rate of approximately $(5d)^{-1}$.

The time scale of advection of a parcel from the Neva entrance to the Baltic Proper is about three weeks, i.e. by this time the river plume has, according to linear theory, disintegrated by baroclinic instability.

Field experiments

In contrast to the theoretical prediction, the presence of a narrow coastal current all the way to the Northern Baltic Sea has been found earlier and described [Stipa *et al.*, 1995; Stipa, 1997]; see also Palmén [1930]. It is found in its most clear form during relatively calm periods of a week or more, typically in late spring or early summer, when it has been observed for several weeks in essentially the same form, with its position slightly altering. Figure 1 shows a series of observations from May 1993.

An example of the results, shown in Figure 1, indicate the presence of an offshore deflecting meander in the middle of the transect.

Numerical experiments

Retaining the essential features of the Gulf of Finland, we simplify the system as a periodic channel in the east-west direction that has a linear bottom sloping up towards north. The channel is 30 km in N-S and 100 km in E-W directions and is resolved with a grid size of 1 km. The depth varies from 20 m in the north to 100 m in the south.

The coastal current is conceptualized in the feature model

$$s(y, z) = \frac{s_2(0) - s_1}{2} \left(\tanh \left(\sqrt{\left(\frac{z}{h_0} \right)^2 + \left(\frac{y - y_0}{l_0} \right)^2} - a \right) - 1 \right) + s_2(z) \quad (1)$$

with the depth scale $h_0 = 6$ m, horizontal position $y_0 = 30$ km and horizontal scale $l_0 = 900$ m. $a = 6$ is a scaling factor setting the position of the front.

The time evolution of this feature is evaluated with the MIT GCM [Marshall *et al.*, 1997b, a]. The model is started from rest with a density structure prescribed by the feature model, and run in a closed, adiabatic mode with no momentum forcing, i.e. the dynamics in the results are solely due to internal release of potential energy.

A baroclinic instability sets in, but its growth is arrested by the topographic potential vorticity gradient (e.g. Rhines [1977]) and the result is a meandering current along the coast which resembles closely what can be inferred from the observations (Fig. 2).

In the vertical, the current has also a wave-like structure (shown in Fig. 5), where the isopycnals at the wave crests are raised to the surface, bringing with them nutrients from the deeper layers to the euphotic zone. The frequency of these waves is of the order of 2 days.

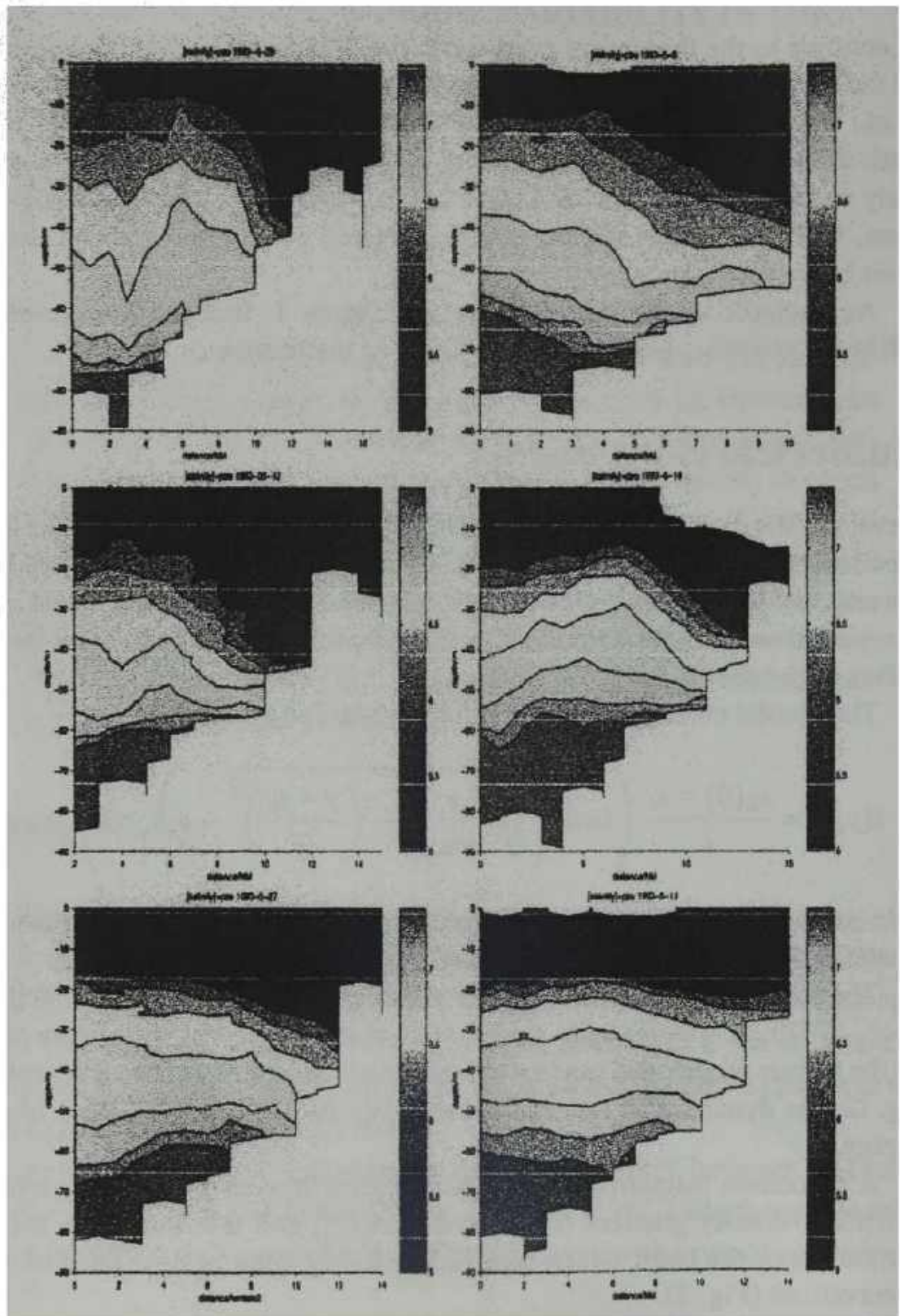


Figure 1: A repeated north-south section near Hanko Peninsula. The coastal current is visible for more than one month (Stipa, Tamminen and Seppälä, *in prep.*).

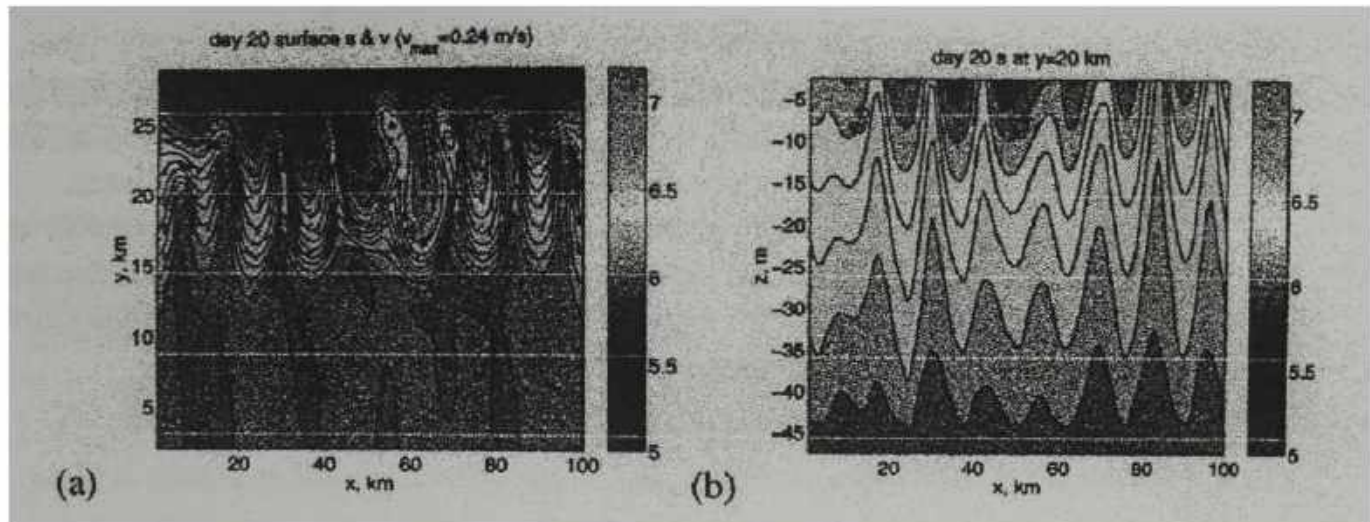


Figure 2: (a) Surface salinity and currents after 20 days of integration of the feature model in Equation (1). Maximum current vector = 0.24 m/s. (b) Vertical section along $y = 20 \text{ km}$ in (a). The initially deep isopycnals outcrop to the surface.

Topographic potential vorticity gradient in general has been shown to reduce the linear growth rate of baroclinic instabilities dramatically, which is also seen in the model results. The eddies are formed in the very nonlinear limit of breaking waves and the process has been shown to be sensitive to e.g. horizontal diffusivity, frontal strength and bottom depth [Sloan III, 1996], therefore the parameter space needs some further explorations before final conclusions of e.g. mixing efficiency across the front can be made.

Conclusions and impacts

The measurements indicate an unstable, meandering coastal current that nevertheless retains its form for the length of GoF, certainly longer than expected from the linear baroclinic growth rate. This discrepancy is nicely reconciled by the model results, which show how the growth of the instability is slowed down or arrested into this meandering current. The internal potential energy in the density field is a sufficient source for the kinetic energy of this current.

This current shows isopycnal displacements with a large amplitude (Fig. 2). The ideas of recent studies on eddy supported primary production (e.g. McGillicuddy Jr. et al. [1998]) apply to the coastal case as well, although they are not the whole story.

The summer 1997 was characterized by a long, calm and warm period from the end of June until the beginning of August, providing not only ideal conditions for massive cyanobacterial blooms but also for the free development of the

coastal current system here depicted. Isopycnal displacements whose amplitude and frequency are in accord with this study have indeed been observed in 1997 (K. Kononen, pers. comm.; data by J. Pavelson, Estonian Marine Institute).

Therefore it is possible to hypothesize that the current system we depict here has played a role in the maintenance of nutrient supply to the cyanobacterial blooms. Direct evidence for this hypothesis and an evaluation of its importance, however, call for further field studies and model experiments.

Acknowledgements

TS has been funded by Maj and Tor Nessling foundation. The numerical experiments were begun during a visit to MIT by TS.

References

- Chao, S.-Y., and W. Boicourt, Onset of estuarine plumes, *J. Phys. Oceanography*, 16, 2137–2149, 1986.
- Marshall, J., A. Adcroft, C. Hill, L. Perelman, and C. Heisey, A finite-volume, incompressible Navier Stokes model for studies of the ocean on parallel computers, *Journal of Geophysical Research*, 102, 5753–5766, 1997a.
- Marshall, J., C. Hill, L. Perelman, and A. Adcroft, Hydrostatic, quasi-hydrostatic, and non-hydrostatic ocean modeling, *Journal of Geophysical Research*, 102, 5733–5752, 1997b.
- McGillicuddy Jr., D., A. Robinson, D. Siegel, H. Jannasch, R. Johnson, T. Dickey, J. McNeil, A. Michaels, and A. H. Knap, Influence of mesoscale eddies on new production in the Sargasso Sea, *Nature*, 394, 263–266, 1998.
- Palmén, E., Untersuchungen über die Strömmungen in den Finnland umgebenden Meeren, *Commentationes Physico-Mathematicae*, 12, 45–94, 1930.
- Pedlosky, J., *Geophysical Fluid Dynamics*, 2nd ed., Springer Verlag, 1987.
- Rhines, P., The dynamics of unsteady currents, in *The Sea*, vol. VI, pp. 189–318, Wiley, 1977.
- Sloan III, N. Q., Dynamics of a shelf slope front: Process studies and data-driven simulations in the Middle Atlantic Bight, Ph.D. thesis, Harvard University, Cambridge, Massachusetts, 1996.
- Stipa, T., Resolving the Finnish coastal current, vol. 15 of *Annales Geophysicae*, European Geophysical Society, 1997, (poster in the 22nd EGS general assembly).
- Stipa, T., J. Seppälä, and T. Tamminen, Material fluxes across the entrance to the Gulf of Finland, (oral presentation in the 1st Nordic Marine Sciences Meeting, Göteborg).
- Yankovsky, A. E., and D. C. Chapman, A simple theory for the fate of buoyant coastal discharges, *Journal of Physical Oceanography*, 27, 1386–1401, 1997.

ON THE HYDRAULICALLY CONTROLLED FLOW WITH ZERO POTENTIAL VORTICITY THROUGH THE DEEP PASSAGE OF THE IRBE STRAIT

Janek Laanearu and Madis-Jaak Lilover

Estonian Marine Institute
Paldiski Road 1, 10137 Tallinn, Estonia

The Gulf of Riga is one of the semi-enclosed sub-basins of the Baltic Sea. The sea water is diluted in the gulf by the river-water runoff as well as precipitation and has two outlets: the Irbe Strait, being a direct gap into the Baltic Proper, and the Suur Strait, leading to the open sea via a shallow area of straits, cf. Fig. 1. The density difference between the open sea and the diluted gulf waters provides a thermohaline circulation through the Irbe Strait, while the flow through the area of straits is mainly sea-level driven. The water column in the Baltic Proper is vertically strongly stratified, the brackish surface waters are superimposed upon a high-saline deep-water. Since the threshold of the Irbe Strait is rather high (sill depth is less than 25 meters), only the open sea upper layer water originating from above the Baltic main halocline (at depth of 60 ~ 70 meters) can penetrate through this passage into the gulf.

In the calm summer of 1995 the large-scale study IRBEX-95 in the region of the Irbe Strait was undertaken. Within 10 days CTD surveys were supported by *Eulerian* current measurements using AANDERAA instruments. A low-frequency bottom jet near the southern coast of the strait, transporting the open sea water into the gulf, was detected. The baroclinic flow through the Irbe Strait provides the largest contribution to the transport of sea water from the open Baltic into the Gulf of Riga. According to the Knudsen formula the mean volume flux of salt water into the gulf should be around $3300 \text{ m}^3 \text{ s}^{-1}$. The observations revealed that the cross-strait halocline was quasi-geostrophically balanced and corresponding average of the bottom-water fluxes (with salinity's higher than 6.2 PSU) was estimated to be around $5200 \text{ m}^3 \text{ s}^{-1}$ (Laanearu, 1996). The cross-channel width of the Irbe Strait (~ 30 km) is sufficiently large compared to the internal Rossby radius of deformation (~ 3 km), therefore the principles of rotating sill flow could be applied to description of dynamics in this area. During the observation period in the summer 1995 the horizontal salinity field at 15 meters depth revealed a typical "S"-like pattern (Lilover et al., 1998). The pattern is similar to the flow structure which a Kelvin wave originating from a "dam break" causes in a channel wide

compared to the Rossby radius of deformation. It was found from the observations that the upper-layer flow from the gulf into the open Baltic took place predominantly close to the northern boundary of the passage. This made it possible to consider the upper layer superimposed over the deep water as more or less passive. The aim of the present work is to solve the hydraulic problem for the stationary inviscid baroclinic discharge from the Baltic Proper taking into account the bathymetric peculiarities of the Irbe Strait. We assume that the flow is principally directed along the channel, the upper layer is inactive and the upstream basin is infinitely deep. Thus, Bernoulli and potential vorticity equations, describing the deep-flow in a channel, are simplified.

Following the mathematical notation from Borenäs and Lundberg (1988) we use the right-hand Cartesian co-ordinate system. Rotation axis and vertical axis in z direction are parallel, along-channel axis y is directed downstream, and the left- and right-bank intersection points between the parabolic channel boundary and the interface are given by $x = -a$ and $x = b$, respectively. The flow is assumed to vary slowly in the downstream direction and in that case it may be shown that the along-channel velocity is thus geostrophically balanced

$$fv = g' \frac{\partial \eta}{\partial x} \quad (1)$$

and potential vorticity of the flow is described by

$$\frac{f + \partial v / \partial x}{D} = \frac{f}{D_\infty}. \quad (2)$$

Here v is the velocity component in the downstream direction, f - the Coriolis parameter and g' - the reduced gravity for the two-layer system. The reference level $z = 0$ is taken to be the sill elevation at the topographically determined "control section" and η - the interface elevation above this level. The parameter D represents the thickness of the moving layer and D_∞ the "potential depth" (i.e. the fluid depth in the upstream basin, where the strait flow velocity and relative vorticity must vanish). Equations (1) & (2) are difficult to handle in general because of their non-linear form, but in a special case, if the potential vorticity is zero, an analytical solution is obtained. The assumption about the infinitely deep upstream basin (i.e. $D_\infty \rightarrow \infty$) allows demonstration of a simple relationship between the relative vorticity and the planetary vorticity terms in equation (2): $\partial v / \partial x = -f$. Substitution into the

geostrophic statement (1) leads to a second-order ordinary differential equation for the cross-channel flow field:

$$\frac{\partial^2 \eta}{\partial x^2} + \frac{f^2}{g'} = 0, \quad (3)$$

which can be solved for the interface elevation η at the boundary conditions $\eta(-a) = \alpha a^2$ & $\eta(b) = \alpha b^2$. Here α represents a quadratic term constant for the equation of parabola (inversely proportional to the channel width). Henceforth parameter η_∞ defines the elevation of the interface in the upstream basin, where the velocity of strait flow is equal to zero. Thus, the solution for (3) at the described boundary conditions is given by

$$\eta(x) = (f^2/2g') \left\{ -x^2 + ((2+r)/r)[x(b-a) + ab] \right\}. \quad (4)$$

Here $r = f^2/g' \alpha$ is a dimensionless combined parameter governing the degree of rotation in the f -plain, the fluid stratification and the channel width. (Note, that in our calculations $f = 1.23 \times 10^{-4}$ s⁻¹ and $g' = 0.012$ m s⁻².) The along-channel velocity component yields from (1). In accordance with the classical hydraulic procedure, an extremum of the volume flux $Q = \int_{-a}^b v(x) D(x) dx$ with respect to the flow width ($a + b$) is now sought by using the

function differentiation theorem. Borenäs and Lundberg (1988) demonstrated that the volume flux has a proper maximum:

$$Q_{\max} = \eta_\infty^2 \left(\frac{3g'}{2\alpha} \right)^{1/2} \frac{1}{(2+r)}. \quad (5)$$

The solution yielding Q_{\max} represents a controlled flow situation corresponding to a non-standard Froude number ($F = \bar{v}/|\bar{v} - c|$, based on the over cross-section averaged along-channel velocity: $\bar{v} = \frac{1}{(a+b)} \int_{-a}^b v(x) dx$, and the non-linear Kelvin wave phase-speed c

relative to the flow) equal to 1 for these particular values of a and b . In the classical case, however, the concept of hydraulic control is applicable only for such values of the topographical parameter r which yields unidirectional flow at the most pronounced constriction of the channel, i.e., the control section. The limiting value of r , below which the cross-channel sheared along-channel velocity component stay unidirectional over the entire

control section, is found by prescribing $v(b) = 0$ in the mathematical analysis. It can be shown algebraically that the class of solutions for which the concept of a controlled flow holds is characterised by $r \leq 2/3$.

In principle, given continuous and moderately smooth bathymetric data, application of the hydraulic theory principles should pose no problems but from a practical standpoint this task proves to be somewhat less straightforward. Looking at the bathymetric map of the Irbe Strait in Fig. 1, it can be recognised how poorly the deep passage conforms an idealized image of topographical control, i.e. for if the threshold summit coincides with the most horizontally pronounced cross-section. In fact, the Irbe Strait has only one well-defined passage below the 10-meter isobath and the deep-water flow from the Baltic Proper into the Gulf of Riga is restricted mainly by the most pronounced "throats" of the connecting channel. Taking into account the water layer below the 10-meter isobath (which represents also the "bifurcation" depth of the open-sea and the gulf water masses here, cf. Whitehead, 1998), the deep passage has two distinct geometrical "threshold summit-horizontal constriction" extremum cross-sections: gaps of S1 and S2 in Fig. 1. The precise orientation of the cross-sections relative to the main axis of the channel has been chosen so as to maximize the "symmetry" of the bottom profiles in the least-squares sense. Note here, that the channel width for both of these sections exceeds the internal Rossby radius of deformation.

In the present limiting case of zero potential vorticity flow the upstream basin is assumed to be infinitely deep and the theory yields an analytical solution for the controlled flux, expressed by formula (5). A corresponding volume transport, based on the bifurcation depth of 10 meters and the topographic parameters associated with the most pronounced cross-section at S1 (described by $\eta_\infty = 14.5$ meters and $r = 0.6$), would be around $8000 \text{ m}^3 \text{ s}^{-1}$ (unidirectional flow). The second constriction at the cross-section at S2 (with $\eta_\infty = 13.5$ meters and $r = 2.0$) yields an integrated volume-flux approximately equal to $8500 \text{ m}^3 \text{ s}^{-1}$ (the flow structure in this case is bi-directional, with a reversed flow of approximately $300 \text{ m}^3 \text{ s}^{-1}$ adjacent to the right-bank). The latter situation is not compatible with the accepted image of a controlled flow being one where no signals emanating downstream can propagate across the critical section. However, the volume-transport estimates presented here must be regarded as fairly satisfactory in view of how sensitive this transport is to the choice of upstream interface

level (where a one-meter shift of the bifurcation depth yields a change of approximately 10 % in the controlled transport).

In general a three-layer density structure during the field study IRBEX-95 was observed in the Irbe Strait area; below the seasonal thermocline a two-layer contra-directional flow was found, which in turn was modulated by sub-inertial fluctuations. The average density difference between the Gulf of Riga water and the Baltic Proper water above the main halocline slightly exceeds 1 kg m^{-3} and the mean sea level difference between these sub-basins (with a higher level in the gulf) is around 0.02 meters. These values indicate that the magnitudes of baroclinic and barotropic forcings are approximately equal (cf. Lilover et al., 1998). The observed circulation scheme suggests, that the water exchange through the Irbe Strait was consistent with the estuarine circulation on average. Time-dependent effects (mainly due to 2-day variations of the air pressure and the 24-hour seiche in the gulf during the experiment) modified the water exchange through the Irbe Strait, but these oscillations had too short wave-periods to carry the sea water directly through the strait and so did not contribute much to the "real water exchange" between the sub-basins. At low frequency the barotropic flow (at the circular frequency below f) the sea level across-strait tilt can be "geostrophically controlled". The estimate of external Rossby radius of deformation (based on the sill depth of the Irbe Strait) is about 130 kilometers, indicating that the effects of the Earth's rotation for the barotropic flow are less important than for the baroclinic flow in the passage. Thus, the modulating effect for the cross-strait halocline tilt can be ignored in the sense of the lowest order approximation of the deep-water flow investigated here.

In case of hydraulic models the potential depth is usually identified with the depth of the discharging upstream fluid layer at a location where both flow velocity and relative vorticity vanish. During the experimental period in June 1995 in the Gulf of Riga and in the open sea (in vicinity to the Irbe Strait) the seasonal thermocline laid at the depth of around 10 meters. The lower boundary of the open-sea intermediate layer was more or less permanently determined by the main halocline of the Baltic Proper. Hence, it appears reasonable to define the potential depth on the basis of the upstream intermediate layer thickness. As recognized from the map of the Irbe Strait, instead of one well-defined topographical control, we have two throats at S1 & S2, pertaining to the "narrow and deep" and "broad and shallow" sections of the passage, respectively. Thus, according to the current understanding of the non-

zero potential vorticity flow (i.e. in the case when the potential depth is finite), the control-section is flow-dependent and must be exerted somewhere in between the combination of a sill and horizontal contraction. Summing up the present work, in view of the general difficulty of establishing a definite measure of the potential depth, the lowest-order approximation of the rotating channel flow represents the maximal unidirectional flow-rate, which is determined mainly by topographic characteristics of the upstream cross-section.

References

- Borenäs, K.M. and Lundberg, P.A., 1988. On the Deep-Water Flow Through the Faroe Bank Channel. *J. Geophys. Res.*, 93: 1281-1292.
- Laanearu, J., 1996. Sill flow observations between sub-basins and analytical description of frictionless strait flow (The Gulf of Riga and the Baltic proper). *Thesis for Master of Science*, Tartu University, Faculty of Physics and Chemistry, Department of Applied Physics, pp. 62. Supervisors Dr. Urmas Lips (MEI) and Dr. Olev Saks (Tartu University).
- Lilover, M.J., Lips, U., Laanearu, J. and Liljebladh, B., 1998. Flow regime in the Irbe Strait. *Aquatic Sciences*, 60(3): 253-265.
- Whitehead, J.A., 1998. Topographic control of oceanic flows in deep passages and straits. *Review of Geophysics*, 36(3): 423-440.

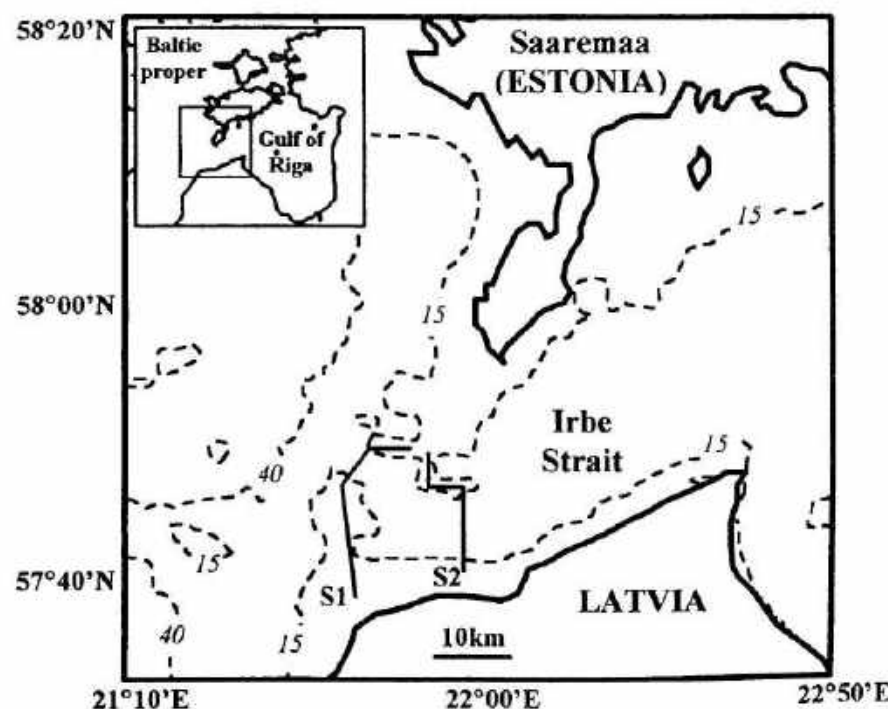


Figure 1. Map of the Irbe Strait area. Sections S1 and S2 (gaps, which were used to determine the controlled volume fluxes) are shown as solid lines.

PREDICTING THE STRATIFICATION OF FUTURE MINING LAKES

Bertram Boehrer¹, Andreas Matzinger² and Michael Schimmele³

¹ UFZ-Gewässerforschung, Brückstr. 3a, D-39114 Magdeburg

² ETH-Zürich Abt. Umweltwissenschaften, Buchenstr. 2, CH-4118 Rodersdorf

³ UFZ-Gewässerforschung, Brückstr.3a, D-39114 Magdeburg; presently: VESGO

Moislingen 4, D-21369 Nahrendorf

Introduction

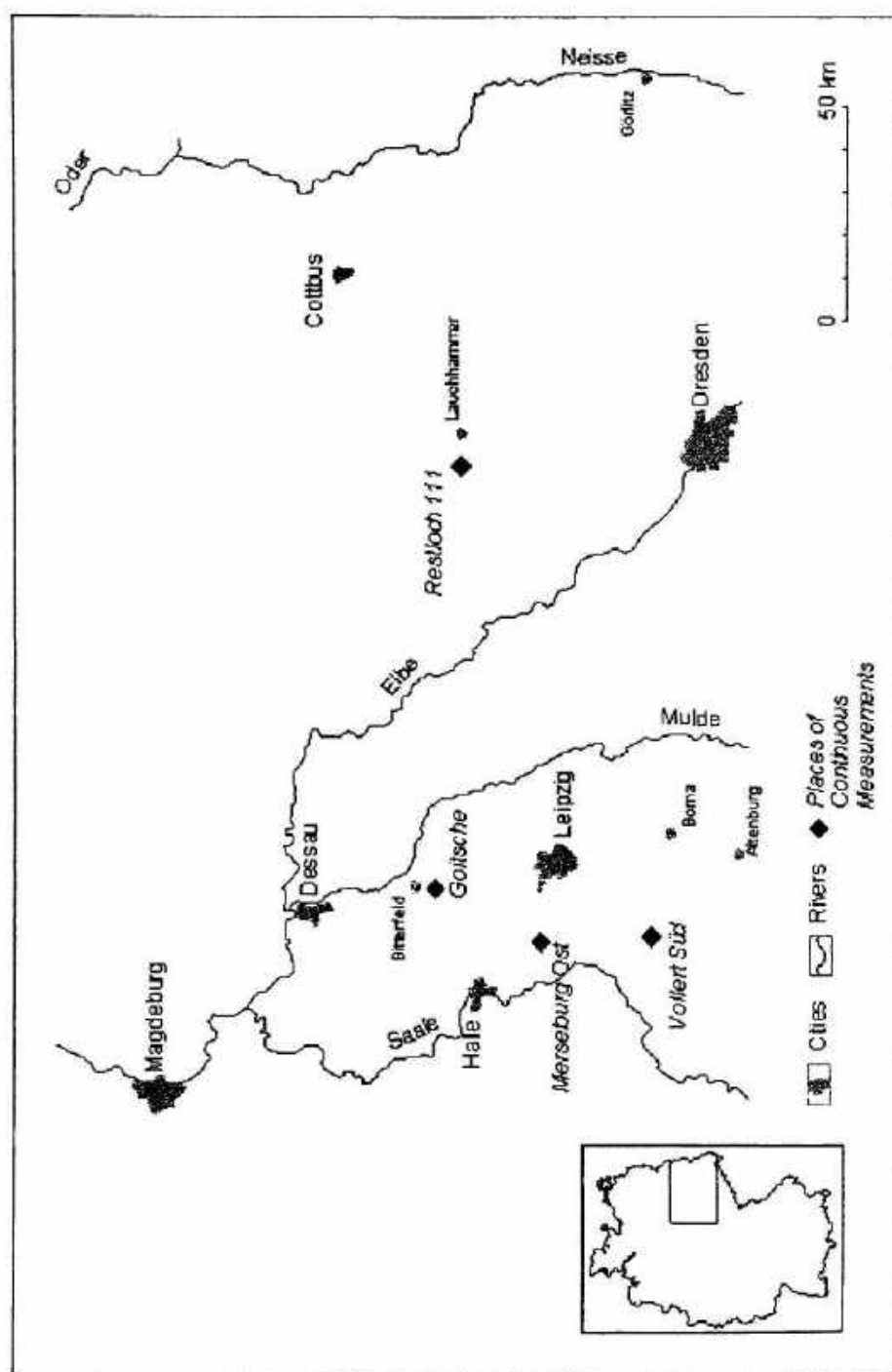
With more than 100 mid size mining lakes currently coming into existence in Germany, the question poses, how to predict the future stratification of those lakes (Schultze and Klapper 1997, Stevens and Lawrence 1997, 1998, Boehrer et al 1998, Heidenreich et al 1999) with respect to the special features concerning the stratification of many of those lakes (Schimmele 1994, 1997). From groundwater sources traversing the tailings, many of the lakes have received and in future will receive inflows of high mineral concentration. Hence a number of the lakes tends to be meromictic. For the prediction of water quality of the future lakes or a reasonable estimate of gross content of acidity or dissolved substances a prediction of the future stratification is inevitable.

Measurements of weather conditions on the lake surface are difficult as the lakes might not yet exist, or do at least not exist in their final configuration. In many cases, we now find a relatively small water body in a deep depression. The question arises which input parameters can be used to predict the stratification in the future. This includes the annual temperature cycle on one hand, but at least as important on the other hand the prediction of the possible meromixis.

Within this contribution, we argue that the surface temperature of the lakes does not depend strongly on the mixing dynamics and thus is well suited for an input parameter. Today's measurements might be transferable to the future lakes, under some additional considerations. For more detailed information and further references on the topic see Boehrer et al 2000.

Observation Programme

Figure 1: Location of the surveyed lakes within the mining areas Central Germany and Lusatia (from Boehrer et al. 2000)



Data were acquired from five lakes (Table 1), out of which 4 were located in the Central German mining area (around Leipzig), and one in the Lusatian (in the North of Dresden) mining area (see Fig. 1). In each lake, we deployed a meteorological station and a thermistor chain or a multiparameter probe with a jo-jo drive. Measurements were done in the years 1997 (Merseburg-Ost 1a, Restloch 111 (=void 111=mining pit 111) and Vollert-Süd) and 1998 (Merseburg-Ost 1a, Merseburg-Ost 1b, Restloch 111, Vollert-Süd and Niemegk).

The lakes of our intensive measuring program were selected because of one special feature / environmental hazard. All of them are - or tend to be - meromictic. The location of the lakes as well as their variability in size covers the range of lakes we have to deal with. The lakes differ remarkably as far as wind speed (Table 1) and size is concerned. As a consequence, the temperature profiles of the lakes (Fig. 2) show differences in the stratification. Merseburg-Ost 1b for example shows the obvious temperature increase in the monimolimnion, as it is found below strongly stratified chemoclines of meromictic lakes. In addition the thickness of the epilimnion is remarkably smaller for the smaller lakes with less wind (RL 111 and Vollert-Süd) compared to the Merseburg-Ost 1a, Merseburg-Ost 1b or Niemegk.

Table 1 (after Boehrer et al 2000):

Lake	area /10 ⁶ m ²	volume /10 ⁶ m ³	max. depth /m	distance /km to Merseburg-Ost 1a	wind speed cubic mean /(m/s) in 1998 $\langle v^3 \rangle^{(1/3)}$
Merseburg-Ost 1a	2.07	14.7	20	0	4.75
Merseburg-Ost 1b	1.84	21.7	20	3	4.95
Restloch 111	0.11	0.5	10	110	2.60
Vollert-Süd	0.15	1.8	30	25	2.14
Niemegk (Goitsche)	0.70	4.0	15	25	4.19

Figure 2: Temperature profiles of the five respective lakes in mid summer 1998 (from Boehrer et al. 2000)

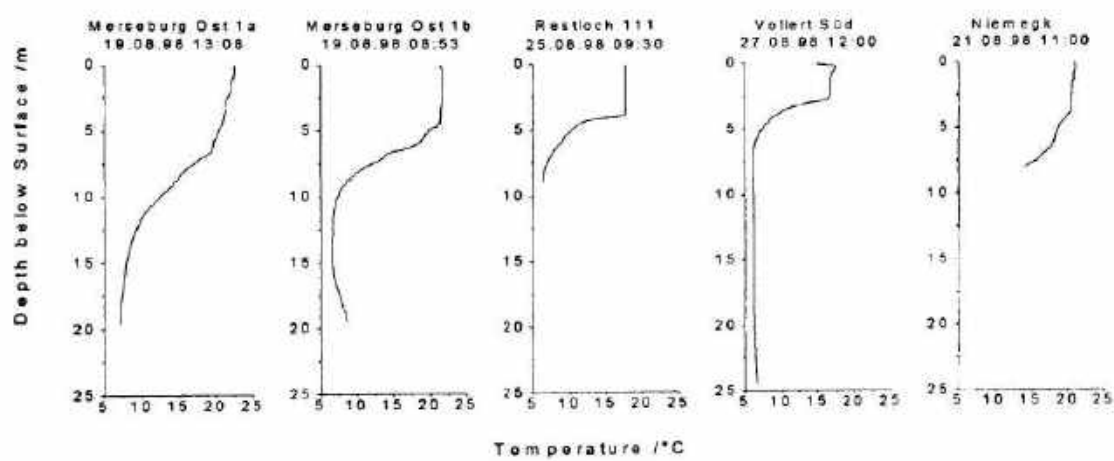
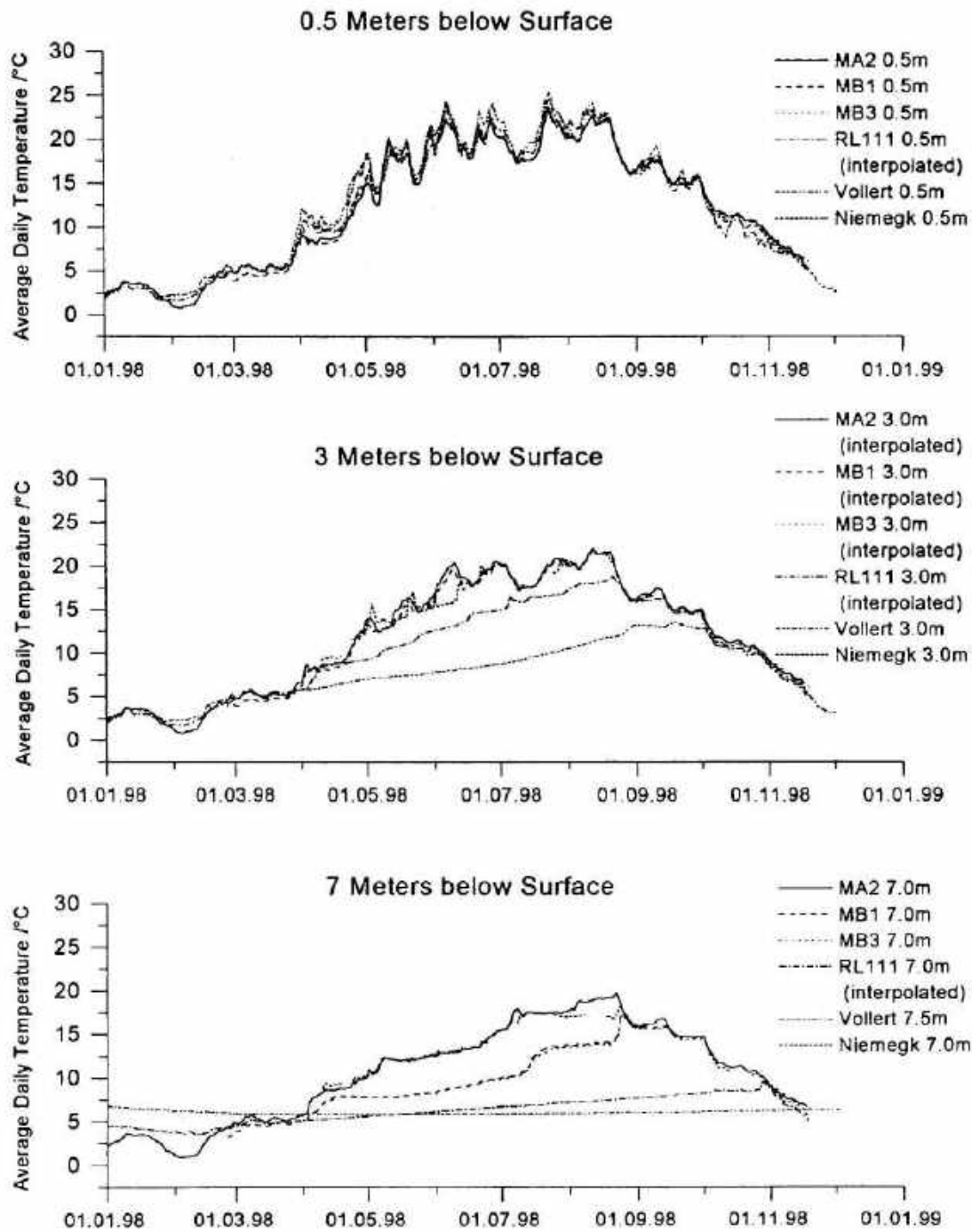


Figure 3: Daily mean temperature traces of five lakes at various depth in the year 1998 (from Boehrer et al. 2000)



Intercomparison between lakes

From all five lakes, we compare the daily mean temperatures at depths (0.5m, 3m and 7m) (Fig. 3). At 0.5m depth, the temperature traces run very much in parallel. The temperature pattern as well as the absolute value is nearly the same for all lakes. Only a very close look reveals that the smaller lakes (RL 111 and Völlert-Süd) with less strong winds are heated

faster in spring time and the absolute maxima in summer are slightly higher. At greater depth (3m and 7m), a different picture emerges: The temperature traces can be clearly distinguished between various lakes.

As differences in the daily means of surface temperature between the lakes are small it can be assumed that this physical magnitude does not strongly depend on the mixing dynamics of the lake, and thus contemporary measurements can, under additional considerations, be used for predictions of future lakes. The temperature traces at greater depth however differ widely between the lakes and thus, for a proper prediction of the stratification with the depth, some kind of modelling the lake seems inevitable.

Acknowledgements

Many thanks to our technicians Karsten Rahn, Uwe Kiwel, Kerstin Lerche and Siegfried Frimel for their excellent field work. Thanks to the UFZ-Sanierungsforschung who owned the meteorological station and the thermistor chain in Vollert-Süd.

References

- Böhrer B., Heidenreich H., Schimmele M. and Schultze M., 1998. Numerical Prognosis for salinity profiles of future lakes in the opencast mine of Merseburg-Ost, Int. J. Salt Lake Res. 7: pp 235-260
- Boehrer B., Matzinger A., Schimmele M., 2000. Similarities and differences in the annual temperature cycles of East German mining lakes, Limnologica (submitted)
- Heidenreich, H., Boehrer, B., Hennig, G. and Kater, R., 1999. Gekoppelte Modellierung geohydraulischer und limnophysikalischer Vorgänge in Tagebaurestseen und ihrer Umgebung. Grundwasser, 2/99, pp 49-54.
- Schimmele, M., 1994. Zur Schichtungsproblematik in Bergbaurestseen. DGL Deutsche Gesellschaft für Limnologie, e.V., Erweiterte Zusammenfassungen der Jahrestagung 1994, Hamburg, Vol. II 2, pp 749 – 753.
- Schimmele, M., 1997. Influence of dissolved substances on the physical properties of lignite mining lakes. 2nd Workshop on "Physical Processes in Natural Waters", 3 - 5 Nov 1997, Joint Research Centre, I-21020 Ispra, Italy.
- Schultze, M. and Klapper, H., 1997. Möglichkeiten der Beeinflussung der Seewassergüte bei der Fremdflutung von Tagebaurestseen. in Jahrbuch BergbauFolgeLandschaft 1997, ed. Dachverband Bergbaufolgelandschaft e.V., ISBN 3-9805368-4-X.
- Stevens, C.L. and Lawrence, G.A., 1997. The effect of sub-aqueous disposal in standing waters. Journal of Hydraulic Research, Vol 35, 1997, No 2.
- Stevens, C.L. and Lawrence, G.A., 1998. Stability and Meromixis in a Water-Filled Mine Pit. Limnology and Oceanography.

VERTICAL NUTRIENT FLUXES DURING SHARP DENSITY STRATIFICATION

Vladimir M. Kushnir¹, Boris S. Shtainman² and Irina A. Danilova¹

¹ Marine Hydrophysical Institute NAS Ukraine. Sevastopol. Ukraine

² Y. Allon Kinneret Limnological Laboratory IOLR. Tiberias. Israel

ABSTRACT

The data of fine-structural measurements of the current and density profiles in the Black Sea, Lake Kinneret and Loch Ness were used for the analysis of correlation between local estimations of the vertical currents shifts E and Brunt-Vaisala frequency N and also between normalized $\log N/N_{max}$ and depths $z=h/h_m$ meanings, $N(h_m) = N_{max}$. Statistical characteristics of the vertical fluxes of dissolved substances or passive impurity are determined on the base of this analysis. The estimations of average fluxes are received for the density jump layer at various N_{max} values.

Key words: Vertical diffusion fluxes, current shifts, Brunt-Vaisala frequency

1. INTRODUCTION

Sharp density gradients render strong influence to the vertical nutrients fluxes in the upper layer of the summer natural waters. It is connected with two opposite tendencies. On the first hand, the vertical movements are complicated by the Archimed's forces, on the second hand, concentration of the internal waves and eddy-wave energy is increased in the same layers and it results the increase of vertical current speed shifts and the probability of turbulence development. The local centers of hydrodynamical instability are formed irregularly, have the various sizes and intensity in zones of the large vertical shifts of current speed. These features of hydrodynamical processes become a basis of the Ozmidov's representations (1997) about the mechanism of a vertical turbulent diffusion in the sharp density layers by means of irregular "turbulent flares". Some data about the statistical characteristics of such turbulent structures and parameters of a vertical diffusion were received by Kushnir and Shtainmann (1998) for the Lake Kinneret and Kushnir (1998) for the Black Sea on the base of the fine-structural measurements of the current and density profiles. The technology of such measurements is rather complex and consequently the data of such synchronous fine-structural measurements are not concerning numerous. In this connection the present work is devoted to a problem of parameterization of the vertical nutrients fluxes on the base of the fine-structural measurements of the density profiles. The technology of such measurements is much more simple and appropriate data are more numerous. The basic opportunity of such approach is based on the mentioned above effect of concentration of the internal waves and eddy-wave energy in the layers of significant vertical density gradients.

2. NORMALIZATION AND ANALYSIS OF EXPERIMENTAL DATA

Series of the vertical profiles of temperature and current with vertical 1 cm resolution on depth in the central Lake Kinneret part (Kushnir and Shtainman, 1998) and series of the vertical profiles of density and currents with vertical 20 cm resolution on depth in the Northwestern part of the Black Sea (Kushnir, 1998) were used for calculations of the characteristics of density stratification and dynamic stability characteristics of the upper layer of these basins. These data were received in the period of the most significant summer heating when the sharp gradients of density are formed in the water column. The experimental data about current speed and density profiles in the Loch Ness published by Torpe (1977) also were used for the analysis. Common feature of the current and density profiles is the increase of the vertical current shifts at increase of density gradients. This effect is explained, as already it was marked, by concentration of the internal waves and eddy-wave energy in layers with the large density gradients.

Profiles of currents and density were used for calculations of the vertical distributions of estimations of the local Brunt-Vaisala frequency $N(z)$ and vertical currents shifts $E(z)$ sizes. The correlation dependences of these parameters for the Black Sea, Lake Kinneret and Loch Ness are submitted in Fig.1.

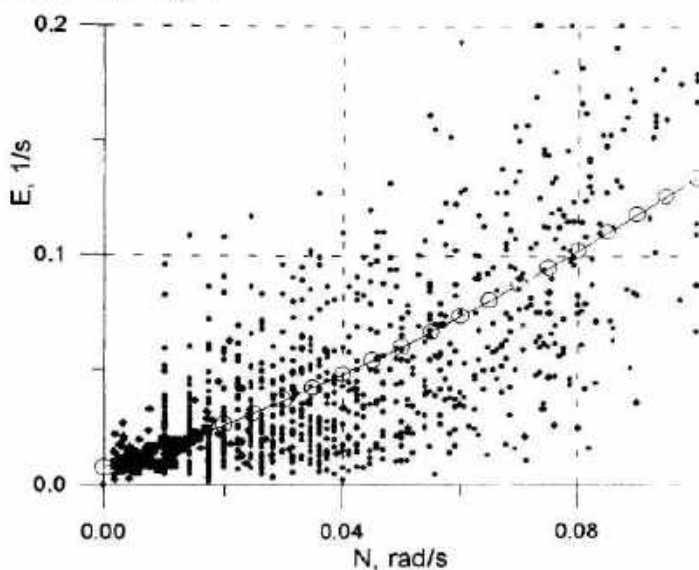


Fig.1. Correlation dependences between vertical current shifts E and Brunt-Vaisala frequency N for the Black Sea ($R = 0.704$), Lake Kinneret (0.642), Loch Ness ($R=0.820$) and average regression lines.

The average regressional curve of the kind $E = a_2N^2 + a_1N + a_0$ are shown there for these basins. It is necessary to note significant positive correlation between local E and N estimations and it allows calculate average Richardson numbers $\langle R_i \rangle$ values in the next form:

$$\langle R_i \rangle = (N/E)^2 = (a_2N^2 + a_1N + a_0/N)^{-2}.$$

(1)

It is expedient to calculate of the vertical Brunt-Vaisala frequency profiles $N(z)$ in the dimensionless form for exception of the vertical displacement effects and reception comparable characteristics of the density stratification. Such normalization is executed in the following kind: Brunt-Vaisala frequency $n = N/N_m$, N_m - its maximal value; depth $z = h/h_m$, $N_m = N(h_m)$. Logarithms of n -values are used owing to large range of its change.

The regression lines of the $\log n = f(z)$ dependences are submitted in Fig.2 for the Black Sea (B.S., $R= 0.707$), Lake Kinneret (L.K., $R= 0.643$) and Loch Ness (L.N., $R= 0.872$). The average regressional lines (A.L.) of the kind $\log n = b_3z^3 + b_2z^2 + b_1z + b_0$ for the specified basins are shown in this figure.

Received dependences are a basis for calculation of the vertical profiles of the average Richardson numbers using (1) and dependence $N = N_m 10^{\log n}$.

$$\langle R_i \rangle = f(N_m, h_m, z).$$

(2)

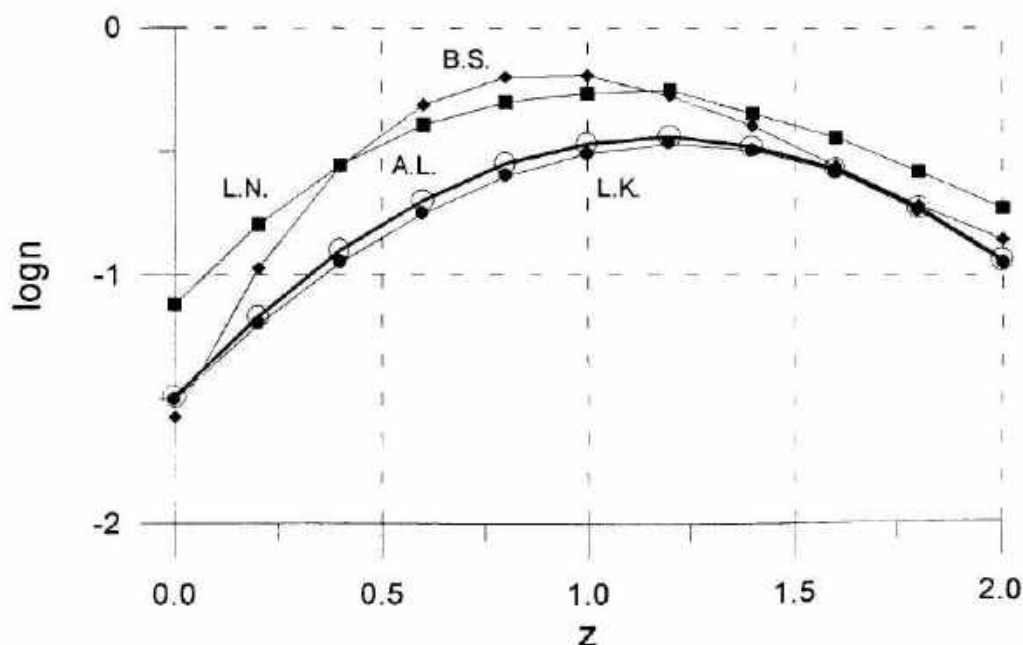


Fig.2. Regressional dependences between $\log n$ and z values.

3. STATISTICAL ESTIMATIONS OF THE VERTICAL DIFFUSION COEFFICIENTS

The dispersion $D(\log Ri) = \sigma_R^2$ of the $\log Ri$ local estimations is submitted in Fig.3 as the dependence of the logn meanings. The assymetry G_a and excess G_e coefficients for this dependence are shown in this figure.

Torpe (1977) has found that distributions of probability of the $\log Ri$ values are close to the normal (Gauss). Our calculation of the assymetry G_a and excess G_e coefficients (Fig.3) have shown that their sizes relatively small and so it is possible to use the near-normal distribution of probability in the next form:

$$W(X) = \frac{e^{-0.5X^2}}{\sqrt{2\pi}} [1 - \frac{G_a}{6} H_3(X) + \frac{G_e}{24} H_4(X)],$$

(3)

where $H_n(X)$ - Ermit's polynomus,

$$H_3(X) = X^3 - 3X, \quad H_4(X) = X^4 - 6X^2 + 3, \quad X = (\log Ri - \langle \log Ri \rangle).$$

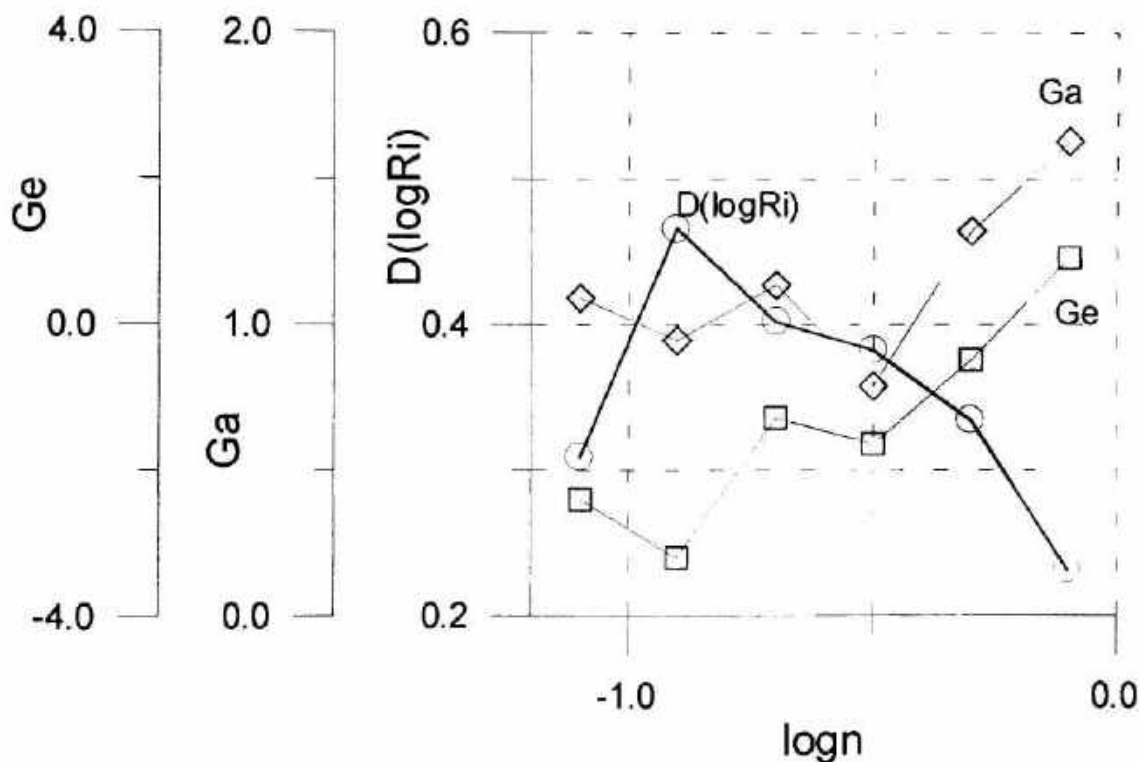


Fig.3. Dependences of the $D(\log Ri)$, G_a , G_e values from the logn size.

Coefficient of the vertical diffusion is calculated on the base of Ozmidov's model (1965) of the vertical exchange in stratified water column with use of estimations of the Richardson numbers (Kushnir 1998):

$$(4) \quad K_z = 0.75v/Ri,$$

where v - kinematic viscosity.

Minimal K_z meaning is equal to $0.1v$ and defined by the condition of equality of the Ozmidov's and Kolmogorov's scales.

Distribution of probability of the $K_z/v=Y$ value is determined on the base of the common rule of nonlinear transformation of a stochastic sizes:

$$(5) \quad W(Y) = \frac{\exp[-0.5(\log Y/L)^2 \sigma_R^{-2}]}{5.771Y\sigma_R} [1 - \frac{G_a}{6} H_3(-\frac{\log Y/L}{\sigma_R}) + \frac{G_e}{24} H_4(-\frac{\log Y/L}{\sigma_R})],$$

$$L = 0.75 \cdot 10^{<\log Ri>}.$$

Standard deviation of the $\log Ri$ sizes (σ_R) is equal to 0.4605 in the layer of density jump, $G_a = 0.301$, $G_e = 0.08$ (Fig.3) and at $z = 1$, $\log n = -0.312$, $n = 0.48$ Nm.

Distribution of probability $W(Y)$, value of the probability P of the turbulent flars development ensuring an effective vertical diffusion ($K_z = 0.1-1$ cm²/s) and the meanings of average fluxes $<F>$ of a dissolved substances or passive impurity with a gradient equal to Gr were calculated for the density jump layer by numerical methods at various N_m meanings. The results of these calculations are submitted below

N_m , rad/s	$<Ri>$	$<F>$	P, %
0.052	0.550	0.874vGr	0.95
0.100	0.967	1.540vGr	2.87
0.150	0.684	1.098vGr	1.51

4. CONCLUSIONS

1. Statistical analysis of the Brunt-Vaisala frequency N and current shifts E local estimations has shown a rather high positive correlation ($R = 0.704$ for the Black Sea, 0.642 for the Lake Kinneret and 0.820 for the Loch Ness) for a sharp density gradient in the natural water column. The high correlation is observed also between dimensionless dependences

$\log(N/N_m)$ and $z=h/h_m$ ($R = 0.707$ for the Black Sea, 0.643 for the Lake Kinneret and 0.872 for the Loch Ness). It allows to receive estimations of the average Richardson numbers Ri sizes in dependence of the maximal N_m size and h_m depth finding of this maximum.

2. The dispersion σ_R of local estimations of the $\log Ri$ values changes in limits from 0.3 to 0.47 at $\log n$ change between -0.3 to -1.1 . The σ_R size is equal to 0.4605 for the density jump layer.

3. The probability of hydrodynamical instability flares development with an effective vertical diffusion in the density jump layer ($K_z = 0.1-1 \text{ cm}^2/\text{s}$) is in limits from 0.95 to 2.87% at change of the maximal Brunt-Vaisala frequency size from 0.052 to 0.15 rad/s .

4. Estimations of the average vertical fluxes of the dissolved substance or passive impurity with the vertical gradient G_z are changed from $0.87vGr$ to $1.54vGr$ in the density jump layer at change of the maximal Brunt-Vaisala frequency from 0.052 to 0.15 rad/s . These values are closed to the similar data received by Kushir and Shteinman (1998) on the base of the fine-structural measurements of currents and densitu profiles in the summer Lake Kinneret ($\langle F \rangle = 2.96vGb$ at $N_m = 0.16 \text{ rad/s}$) and by Kushnir (1998) for the summer Black Sea ($\langle F \rangle = 0.77vGb$ at $N_m = 0.04 \text{ rad/s}$).

REFERENCES

- Kushnir V.M., Shteinman B.S. 1998. Turbulent diffusion in the Lake Kinneret by summer heating. Unpublished manuscript.
- Kushnir V.M. 1998. Turbulent fluxes parameterization in the upper Black Sea layer. UFZ-Bericht. Nr.23/1998. Third Workshop on Physical Processes in Natural Waters. 31.8-3.9.1998 in Magdeburg. P.22-27.
- Ozmidov R.V. 1965. Turbulent exchange in steady stratified Ocean. Izv.Acad. Sci. of the USSR. Physics of Atmosphere and Ocean. Vol.1. No.8.P.853-859 (in Russian)
- Ozmidov R.V. 1997. Vertical exchange through the layers with large vertical density gradients in Ocean. Oceanology. Vol.34.No.4.P.492-496. (in Russian).
- Thorpe S.A. 1977. Turbulence and mixing in a Scottish Loch. Phil. Transaction of Royal Soc. Of London. Vol.286. No.1334. P.125-181.

MODELLING THE OXYGEN STRATIFICATION OF LAKE AMMER

Lars Umlauf¹ and Klaus Jöhnk²

¹Institut für Mechanik AG 3, Fachbereich Mechanik, TU Darmstadt,
Hochschulstrasse 1, 64293 Darmstadt Germany

²Limnological Institute, University of Konstanz, Germany

1 Introduction

The precise prediction of water quality is based on a reliable thermo-mechanical model providing in particular an exact description of the distributions of temperature and diffusivities. Since in most lakes the major exchange of heat and tracers is known to be vertical one-dimensional models are frequently used in lake simulations. We also adopted this approach for our coupled physical-biological model of the vertical distribution of temperature and oxygen.

One-dimensional models can be formulated in two different ways: Using either an integral method or a differential method, which is based on a turbulent closure scheme. Many integral models used for the prediction of water quality (e.g. Imberger and Patterson [6], Riley and Stefan [18]) are extensions of the work of Kraus and Turner [26], [10]. These models describe very well the main features of the vertical turbulent processes in a stratified fluid and give a considerable insight in the physics accompanying them. However, the work of Franke [2] made clear that pure integral models exhibit a couple of undesirable features including a strong oscillation of the predicted thermocline depth and the lack of a detailed description of the epilimnic exchange coefficient restricting their applicability to physical-biological coupled systems. Because of the above shortcomings recent coupled models make use of differential methods and solve the one-dimensional diffusion equation for heat and tracers. However, most of these models implement only very primitive zeroth-order turbulent closures to describe the vertical distribution of the turbulent exchange coefficient. (see, e.g., Stefan and Fang [20].)

We decided to use a more advanced technique employing a $k-\epsilon$ turbulent closure as described, e.g., in Rodi [19] and in Mohammadi [16]. $k-\epsilon$ -models have been applied successfully to many areas of hydromechanics. Beyond the

capabilities of integral methods they provide a reliable tool for the description of a continuous temperature profile in situations where no pronounced thermocline has developed. In addition, k - ϵ -models intrinsically supply turbulent diffusivities for both temperature and momentum no matter if the turbulence is excited by shear or by density instabilities. In contrast to that, many algebraic formulae like the formula used by Stefan and Fang [21] depend only on the density gradient and thus provide undefined diffusivities when no stratification is present.

Since accurate descriptions of the temperature and the diffusivities are crucial for a biological sub-system we consider k - ϵ -models the best choice in one-dimensional lake modelling. Once the mathematical and numerical difficulties are mastered, a one-dimensional k - ϵ -model may simulate one year real-time in a few minutes on a present-day personal computer, still retaining timescales of less than one minute. This makes the model a useful, fast tool for a wide range of limnological problems between the simulation of short scale phenomena (e.g. a high resolution model of thermocline erosion) and the simulation of long-term climate response scenarios.

Our coupled oxygen model consists of a one-dimensional transport equation for oxygen employing the vertical diffusivities and the temperature profiles provided by the k - ϵ model. The mass of photosynthetic algae is represented by measured values of the chlorophyll-a concentration. Surface reeration is represented as a flux term and time and depth depending source and sink terms for photosynthetic production, respiration of algae, biochemical oxygen demand (BOD), and sedimentary oxygen demand (SOD) are included.

2 Model Formulation

We found evidence of a bottom boundary influence and a concise parameterization of the boundary fluxes as volume production terms only for the balance of heat

$$\frac{\partial T}{\partial t} = \frac{1}{A} \frac{\partial}{\partial z} \left(AD^{(T)} \frac{\partial T}{\partial z} \right) + P_T \quad (1)$$

and for the oxygen budget

$$\frac{\partial O}{\partial t} = \frac{1}{A} \frac{\partial}{\partial z} \left(AD^{(O)} \frac{\partial O}{\partial z} \right) + P_O, \quad (2)$$

which are thus formulated depending on the area $A(z)$ as shown above. $D^{(T)}$, $D^{(O)}$ and P_T , P_O are the effective diffusivities and the production terms for heat and oxygen, respectively. All other balance equations presented below are formulated in an area independent fashion that is strictly speaking valid only for the limit of an horizontally infinite lake.

In our model the turbulent diffusivity of momentum will be calculated from the values of the turbulent kinetic energy k and its viscous dissipation ϵ by

$$D = c_\mu \frac{k^2}{\epsilon}, \quad (3)$$

where k and ϵ are the solutions of

$$\begin{aligned}\frac{\partial k}{\partial t} &= \frac{\partial}{\partial z} \left(D^{(k)} \frac{\partial k}{\partial z} \right) + P + G + \epsilon, \\ \frac{\partial \epsilon}{\partial t} &= \frac{\partial}{\partial z} \left(D^{(\epsilon)} \frac{\partial \epsilon}{\partial z} \right) + \frac{\epsilon}{k} (c_1 P + c_3 G - c_2 \epsilon) .\end{aligned}\quad (4)$$

The production P of k by shear stress may take on only positive values, whereas the buoyancy production G of k can be either positive or negative depending on the stability of the water column. A detailed description of the formulae above is found in Rodi [19].

We adopted the standard values for the empirical turbulent parameters as suggested by Launder and Spalding [12] and Launder et al. [11]. All diffusivities are related to the diffusivity of momentum by constant Prandtl/Schmidt numbers. Only the sensitive Prandtl number for the temperature, σ_T , will be calculated in dependence of the velocity and the temperature gradient by a more enhanced algebraic stress relation as suggested by Svensson [22], who first formulated a k - ϵ model for a lake.

3 Physical Parameterizations

3.1 Production Terms

The incoming solar radiation has been calculated from astronomical and geographical data according to Kirk [9] and Forsythe et al. [1] and has been corrected by cloud shading and a wind dependend water surface reflectivity.

We described the decay of the short-wave radiation I according to Beer's law also including the effect of self-shading of phytoplankton. The extinction coefficient for clear water was determined proportional to the invers of the Secchi-Depth as suggested by Henderson-Sellers [5]. For the chlorophyll-a specific absorption coefficient we adopted the value $a_{Chla} = 0.02 \text{ m}^2 \text{ mgChla}^{-1}$ from the work of H  se [4], who determined this value in the very similar Lake Constance.

The production of heat due to the geothermal heat flux q_{geoth} was assumed to be neglectible. Thus the absorbtion of short-wave radiation I remains the only heat production term included in Eq. (1).

3.2 Boundary conditions

According to the law of Stefan-Boltzmann the long-wave radiative loss of the water surface, ϕ_w , is proportional to the absolute surface water temperature T_w^4 . We used an surface water emissivity of $\epsilon_w = 0.97$ as suggested by Henderson-Sellers [5].

Usually a similar expression is stated for the incoming atmospheric long-wave radiation, ϕ_a , though it is evident that different atmospheric radiators at dif-

ferent heights contribute to ϕ_a . We used the "global" approach above and adopted an expression for the overall atmospheric emissivity ϵ_a as proposed by Swinbank [24], who suggest a quadratic dependence of the emissivity from the absolute temperature of the atmosphere. A correction for the cloud amount has also been included.

The short-wave radiation and the incoming long-wave radiation constitute the biggest contributions to the overall heat budget and the model proves to be very sensitive to changes of both. Marti and Imboden [13] pointed out that the simple parameterizations used above include many uncertainties but unfortunately for Lake Ammer no measured data were available.

Most formulae for the convective heat flux, ϕ_c , and evaporative heat flux, ϕ_e , at the water surface are driven by the difference of surface water temperature and air temperature or by the difference of saturated vapour pressure and actual vapour pressure, respectively. For the dependence on wind speed a vast amount of formulae have been proposed in the literature. In his extensive literature survey Sweers [23] concluded that the formulae of McMillan [14] for the wind function be the most reliable ones. We adopted his suggestion for wind measurements on land at a height of 10 meters as it was the case for Lake Ammer.

Thus the overall heat flux at the surface is

$$\phi_{\text{tot}} = \phi_w + \phi_a + \phi_c + \phi_e . \quad (5)$$

The flux of momentum through the upper surface is described by a quadratic dependence on wind speed (Henderson-Sellers [5]) and the bottom friction is parameterized by a quadratic drag law.

4 The Oxygen Model

The temporal and spatial evolution of the oxygen concentration O is described by Eq. (2). The turbulent vertical diffusion of oxygen is assumed to be equal to the turbulent diffusion of temperature as provided by the k - ϵ model. We assume that the overall production or depletion of oxygen is described by

$$P_0 = P_{\text{photo}} + R + S_{\text{BOD}} + S_{\text{SOD}} , \quad (6)$$

where P_{photo} is the production by photosynthesis, R the respiration of algae, S_{BOD} the total biochemical oxygen demand, and S_{SOD} the oxygen demand exerted by the sediment.

4.1 Production by photosynthesis

In our model we assume that photosynthesis is a first order kinetic process depending on temperature, solar radiation and nutrients. However, no explicit biological model for the algal growth is supplied. Instead, the biomass of phytoplankton is represented by measured values of the chlorophyll-a concentration implicitly including nutrient limitation, zooplankton grazing etc.

Hence, the photosynthetic production is assumed to be proportional to the chlorophyll-a concentration as in

$$P_{\text{photo}} = \nu_{\max} Y_{\text{OChla}} \Theta_P^{T-20^\circ} \tanh \left(\frac{I_{\text{PAR}}}{I_S} \right) \text{Chla}, \quad (7)$$

where the chlorophyll-a concentration Chla is specified in $\mu\text{gChla l}^{-1}$. Stefan and Fang [21] set the ratio of production to a value of $Y_{\text{OChla}} = 0.125 \text{ mgO}_2 \mu\text{gChla}^{-1}$. Since the maximum growth rate of algae is usually between $\nu_{\max} = 1-3 \text{ d}^{-1}$ we may calculate an average first order production coefficient of $k_P = \nu_{\max} Y_{\text{OChla}} = 0.25 \text{ mgO}_2 \mu\text{gChla}^{-1} \text{ d}^{-1}$ corrected by the temperature adjustment coefficient $\Theta_P = 1.036$. These values are taken from Stefan and Fang [21] fitted to the data of Megard et al. [15].

We adopted the simple model of Jassby and Platt [7] to account for the effects of light limitation. The model does not implement light inhibition. Following Harris [3], the value for I_S is mostly between $60-100 \mu\text{E m}^{-2} \text{ s}^{-1}$ PAR corresponding to $I_S \approx 12.5-25 \text{ W m}^{-2}$. We selected a value of $I_S = 20 \text{ W m}^{-2}$.

4.2 Respiration

Respiration of algae is modelled as a first-order kinetic process related only to the temperature and the concentration of chlorophyll-a

$$R = \nu_R Y_{\text{OChla}} \Theta_R^{T-20^\circ} \text{Chla}. \quad (8)$$

The assumption is made that the yield coefficient Y_{OChla} for the production and the respiration is the same. Considering a respiration rate ν_R of roughly ten percent of the growth rate (see Henderson-Sellers [5]) we use a combined coefficient

$$k_R = \nu_R Y_{\text{OChla}} = 0.025 \text{ mgO}_2 \mu\text{gChla}^{-1} \text{ d}^{-1}. \quad (9)$$

Stefan and Fang [21] report a range of $k_R = 0.0025-0.075 \text{ mgO}_2 \mu\text{gChla}^{-1} \text{ d}^{-1}$ and corrected for the temperature by a factor of $\theta_R = 1.045$. The value of Patterson et al. [17] can be converted to $k_R = 0.082 \text{ mgO}_2 \mu\text{gChla}^{-1} \text{ d}^{-1}$. However, this value seems to include also the respiration of bacteria. We restrict respiration to chlorophyll-a above the photic depth.

4.3 Biochemical oxygen demand

Biochemical oxygen demand of organic material (detritus and DOC) in a lake is a function of the mass expressed in oxygen equivalents. In the model the formulation of Thomann and Mueller [25]

$$S_{\text{BOD}} = k_B \theta_B^{T-20^\circ} \text{BOD} \quad (10)$$

is implemented, where k_B is the first-order decay coefficient, θ_B is the temperature adjustment, and BOD is the oxygen equivalent in $\text{mgO}_2 \text{l}^{-1}$. These variables are subject to model calibration.

4.4 Sedimentary oxygen demand

To account for the sedimentary oxygen demand of settled phytoplankton, dead aquatic plants, and detritus our model implements a bottom area dependend sink term according to Thomann and Mueller [25]

$$S_{\text{SOD}} = \frac{1}{A} \frac{\partial A}{\partial z} S_{b20} \theta_S^{T-20^\circ} . \quad (11)$$

S_{b20} is the constant bulk rate of SOD in $\text{gO}_2 \text{ m}^{-2}$, which is corrected only for temperature. Depending on the condition of the lake bottom Thomann and Mueller [25] suggest different values for S_{b20} . For sandy bottom, which seems to be closest related to the sediments in Lake Ammer they give a range of values of $0.2\text{--}1.0 \text{ gO}_2 \text{ m}^{-2}$. Usually a value of $\theta = 1.065$ is used for temperature adjustment. Since the hypolimnetic oxygen budget is very sensitive to S_{SOD} we refined these values further by model calibration.

4.5 Surface reareration

Surface reareration, particularly in the absence of photosynthetic production, is a major source term in the oxygen budget. We implemented it as a flux boundary condition in Eq. (2) assuming the flux to be proportional to the difference of actual and saturated oxygen concentrations at the surface

$$q_C = k_e (C_{\text{sat}} - C_{\text{surface}}) , \quad (12)$$

the saturation concentration being

$$C_{\text{sat}} = 2234.3374(T + 45.93)^{-1.31403} . \quad (13)$$

The oxygen exchange coefficient given by Wannikhof et al. [27]

$$k_e = 0.108 U_{10}^{1.64} (600/S_{ct})^{0.5} \quad (14)$$

with a dependence on the wind speed U_{10} was used in our model. Using an appropriate representation for the Schmidt number of oxygen, S_{ct} , at the surface as derived by Stefan an Fang [21] Eq. (14) can be re-written as

$$k_e = 0.02256 \left(0.10656 e^{(-0.0627T)} + 0.00495 \right)^{-0.5} U_{10}^{1.64} \quad (15)$$

now only depending on the surface temperature and the wind speed U_{10} at a height of 10 m.

With the model described above we achieved an accurate description of the temperature and oxygen profiles in Lake Ammer compared to data of the year 1996. The metalimnetic oxygen minimum of that lake could be modelled sufficiently. For a detailed discussion of the results see Jöhnk and Hutter [8].

References

- [1] W. C. Forsythe, E. J. Rykiel Jr., R. S. Stahl, H. Wu, and R. M. Schoolfield. A model comparison for daylength as a function of latitude and day of the year. *Ecol. Model.*, 80:87–95, 1995.
- [2] U. Franke, K. Hutter, and K. Jöhnk. A physical-biological coupled model for algal dynamics in lakes. *Bulletin of Mathematical Biology*, 61:239–272, 1999.
- [3] G. P. Harris. Photosynthesis, productivity, and growth: The physiological ecology of phytoplankton. *Archiv für Hydrobiologie, Beiheft 10*, 1978.
- [4] C. Häse. *Die Vorhersage der Produktivität des Phytoplanktons im Bodensee unter Berücksichtigung der Temperatur sowie der Spektralen Zusammensetzung des Unterwasser-Strahlungsfeldes*. Konstanzer Dissertationen, Vol. 514, University of Konstanz, 1996. Hartung-Gorre Verlag.
- [5] B. Henderson-Sellers. *Engineering Limnology*. Pitman Publishing, Boston, London, Melbourne, 1984.
- [6] J. Imberger and J. C. Patterson. A dynamic reservoir simulation model - DYRESM:5. In *Int. Symp. Predictive Abilities of Surface Water Flow and Transport Models, Berkeley*, 1980.
- [7] A. D. Jassby and T. Platt. Mathematical formulation of the relationship between photosynthesis and light of phytoplankton. *Limnol. Oceanogr.*, 21:540–547, 1976.
- [8] K. Joehnk and K. Hutter. Simulation der Schichtung und des Sauerstoffgehaltes im Ammersee. Final report, Institut zur Erforschung und zum Schutz der Gewässer, Konstanz, Germany, 1990.
- [9] J. Kirk. *Light and Photosynthesis in Aquatic Ecosystems*. Cambridge University Press, Cambridge, 1983.
- [10] E. B. Kraus and J. S. Turner. A one-dimensional model of the seasonal thermocline - II. The general theory and its consequences. *Tellus*, 19:98–105, 1967.
- [11] B. E. Launder, G. J. Reece, and W. Rodi. Progress in the development of Reynolds stress turbulent closure. *J. Fluid Mech.*, 68:537–566, 1975.
- [12] B. E. Launder and D. B. Spalding. The numerical computation of turbulent flow. *Comp. Meth. Appl. Mech. Eng.*, 3, 1974.
- [13] D. E. Marti and D. M. Imboden. Thermische Energieflüsse am Beispiel der Sempachersee. *Scheiz. Z. Hydrol.*, 48(2):196–228, 1986.
- [14] W. McMillan. Cooling from open water surfaces: Part 1: Lake Trawsfynydd cooling investigation. Final Report NW/SSD/RR/1204/73, Scientific Services Department, CEGB Manchester, 1973.

- [15] R. O. Megard, D. W. Tonkyn, and W. H. Senft. Kinetics of oxygenic photosynthesis in planktonic algae. *J. Plankt. Res.*, 6(2):325–337, 1984.
- [16] B. Mohammadi and O. Pironeau. *Analysis of the k-ε Turbulence Model*. Research in Applied Mathematics. John Wiley & Sons, 1994.
- [17] J. C. Patterson, B. R. Allenson, and G. N. Ivey. A dissolved oxygen budget model for Lake Erie in summer. *Freshwater Biology*, 15:683–694, 1985.
- [18] M. J. Riley and H. G. Stefan. MINLAKE: A dynamic lake water quality simulation model. *Ecol. Model.*, 43:155–182, 1988.
- [19] W. Rodi. *Turbulence Models and Their Application to Hydraulics*. IAHR Monograph Series. A. A. Balkema / Rotterdam / Brookfield, 1993.
- [20] H. G. Stefan et al. Simulation of dissolved oxygen profiles in a transparent, dimictic lake. *Limnol. Oceanogr.*, 40(1):105–118, 1995.
- [21] H. G. Stefan and X. Fang. Dissolved oxygen model for regional lake analysis. *Ecol. Model.*, 71:37–68, 1995.
- [22] U. Svenson. *A mathematical model of the seasonal thermocline*. PhD thesis, London, 1978.
- [23] H. E. Sweers. A nomogram to estimate the heat-exchange coefficient at the air-water interface as a function of wind speed and temperature; a critical survey of some literature. *Journal of Hydrology*, 30:375–401, 1976.
- [24] W. C. Swinbank. Long-wave radiation from clear skies. *Quat. J. Roy. Meteor. Soc.*, 89:339–348, 1963.
- [25] R. V. Thomann and J. A. Mueller. *Principles of surface water quality modelling and control*. Harper & Row Publ., New York, 1987.
- [26] J. S. Turner and E. B. Kraus. A one-dimensional model of the seasonal thermocline - I. A laboratory experiment and its interpretation. *Tellus*, 19:88–97, 1967.
- [27] R. Wanninkhof, J. Ledwell, and J. Crusius. Gas transfer velocities in lakes measured with sulfur hexafluoride. In S. C. Wilhelms and J. S. Gulliver, editors, *Air water mass transfer*, pages 441–458. ASCE, 1991.

A NUMERICAL STUDY ON THE EFFECT OF THE SPRING WARMING AND THE THERMAL BAR ON THE PLANKTON ECOSYSTEM OF A DEEP LAKE

Vincenzo Botte and Anthony Kay

Department of Mathematical Sciences
Loughborough University, UK

Archer (1995) has shown in a recent tutorial on the relevance of upper ocean physics on the ecosystem dynamics how phytoplankton photosynthesis is fundamentally controlled by the depth of turbulent mixing at the ocean surface coupled to the depth of sunlight penetration. Archer makes the case that, as upper ocean mixing dynamics can drive the behaviour of the plankton ecosystem, ecosystem dynamics models, used to predict the temporal variation of the plankton population, should be coupled with models of physical mixing.

In this study a finite volume formulation of the Navier-Stokes equations, adopting a parametrization of the vertical eddy-viscosity based on the Brunt-Vaisala frequency and on the strain-rate tensor, and using both a GMRES solver and a sparse multifrontal direct solver for the solution of the systems of equations, has been used to predict the temperature and velocity fields in a section of the Central Basin of Lake Baikal (figure 1) during the spring warming and the appearance of the thermal bar phenomenon. The section is 10 kilometres wide and 1200 metres deep, and has been discretised with an uniform grid with an horizontal resolution of 25 metres and a vertical resolution of 5 metres.

A plankton model based on the plankton dynamics of Franks et al. (1986), that adopts as dependent variables phytoplankton (P), herbivorous zooplankton (Z) and dissolved nutrients (N), has been coupled and solved with the Navier-Stokes equations. Although this model has been developed for the oceanographic conditions of Southern California, and therefore certainly inaccurate for the ecosystem of Lake Baikal, using the values of the biological parameters prescribed by Franks et al. allows a direct comparison of the numerical results with the results presented by Wroblewski and Richman (1987), that have used the Franks et al. model to evaluate the temporal evolution of the vertical distribution of P, Z and N for a fully stratified water column. The results presented by Wroblewski and Richman show that, starting from profiles of N, P and Z homogeneous with depth, a phytoplankton bloom is developed near the surface in the first few days, followed by a bloom in the zooplankton population and a considerable decrease in the phytoplankton from its previous bloom values.

The numerical results of the present study, show that:

(1) The currents converging towards the thermal bar convect nutrients from nutrient-rich deeper regions. A maximum in the phytoplankton population is therefore observed at the location of the thermal bar (figure 2).

(2) The vertical descending currents, generated at the thermal bar, tend to increase the concentration of phytoplankton at greater depth, but the increase in P in deeper regions disappears quite rapidly, due to the mortality and the absence of generation due to solar radiation, that is completely negligible far from the surface.

(3) The areas of transition from unstable to stable conditions act as a barrier to the diffusion of the plankton population towards deeper regions, as also observed by Parker (1991), as can be seen in figure 3. The numerical results clearly show that the increase in vertical diffusivity due to unstable conditions leads to a considerable reduction in the maximum values in the phytoplankton population compared with the data presented by Wroblewski and Richman, confirming Archer's observations on the role of vertical mixing. With the continuing warming of the upper layer of the lake, the procedure predicts a deepening of the areas of instability and, consequently, the production of the phytoplankton near the surface is diffused towards greater depths, and the maximum values achieved by the phytoplankton population are much smaller than the ones observed in the bloom condition in the results of Wroblewski and Richman. An important consequence is that the zooplankton population is kept to very low values during all the computation, as values of P high enough to start a bloom in the zooplankton are never achieved.

References:

- Archer, D., Upper ocean physics as relevant to ecosystem dynamics: a tutorial, *Ecological Applications*, 5 (3), pp. 724-739, 1995.
- Franks, P.J.S., Wroblewski, J.S. and Flierl, G.R., Behavior of a simple plankton model with food-level acclimatation by herbivores, *Marine Biology*, 91, pp. 121-129, 1986.
- Parker, R.A., Eddy diffusion of phytoplankton and nutrients: estimating coefficients from simulated and observed vertical distributions, *Journal of Plankton Research*, 13 (4), pp. 815-830, 1991.

Wroblewski, J.S., and Richman, J.G. The non-linear response of plankton to wind mixing events – implications for survival of larval northern anchovy, *Journal of Plankton Research*, 9 (1), pp. 103-123, 1987.

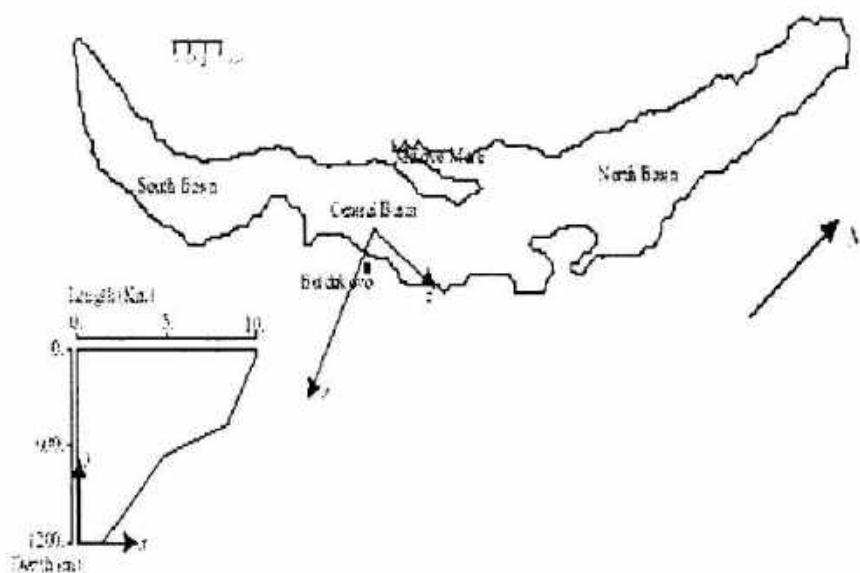


Figure 1 – Map showing the location of the section of Lake Baikal examined in this work, the location of the Cartesian axes and the geometry of the computational domain used to model the chosen section.

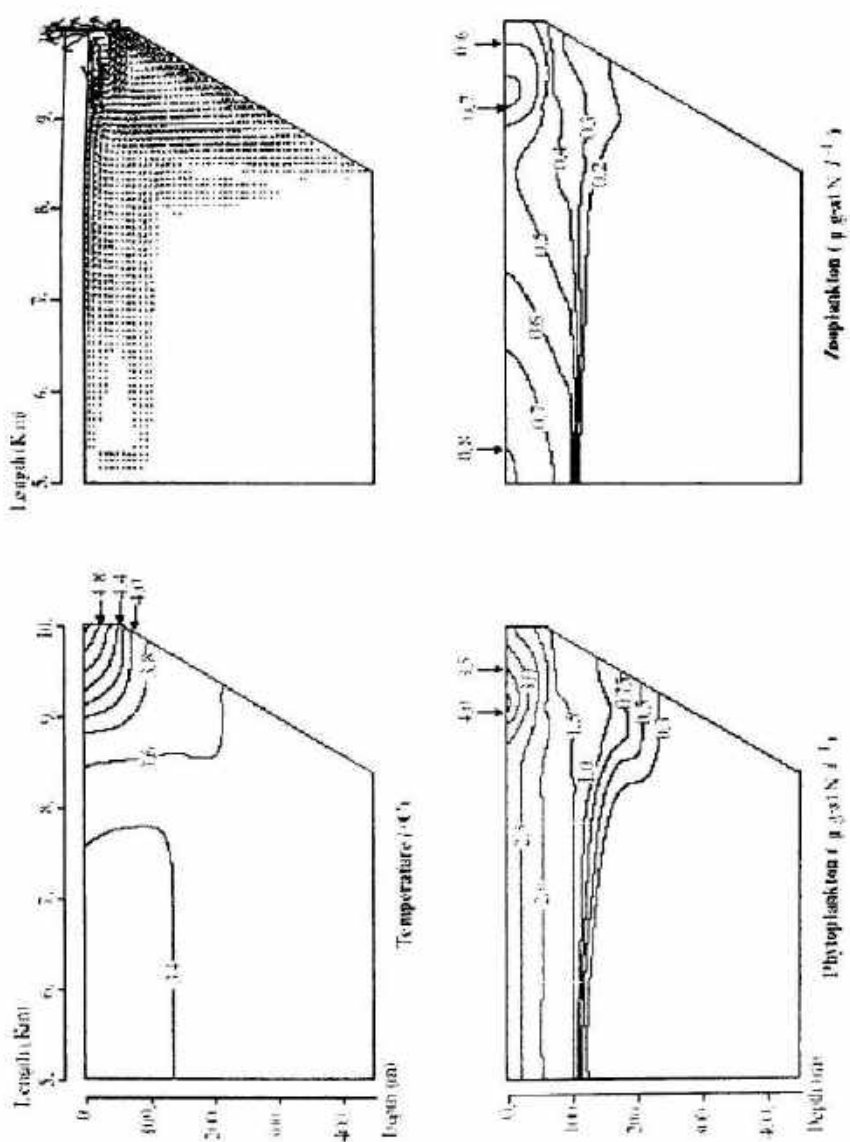


Figure 2 – Predicted results at $t=20$ days: isovalue lines of temperature, phytoplankton and zooplankton, and vector velocity field, shown at 1/3 of the resolution of the model.

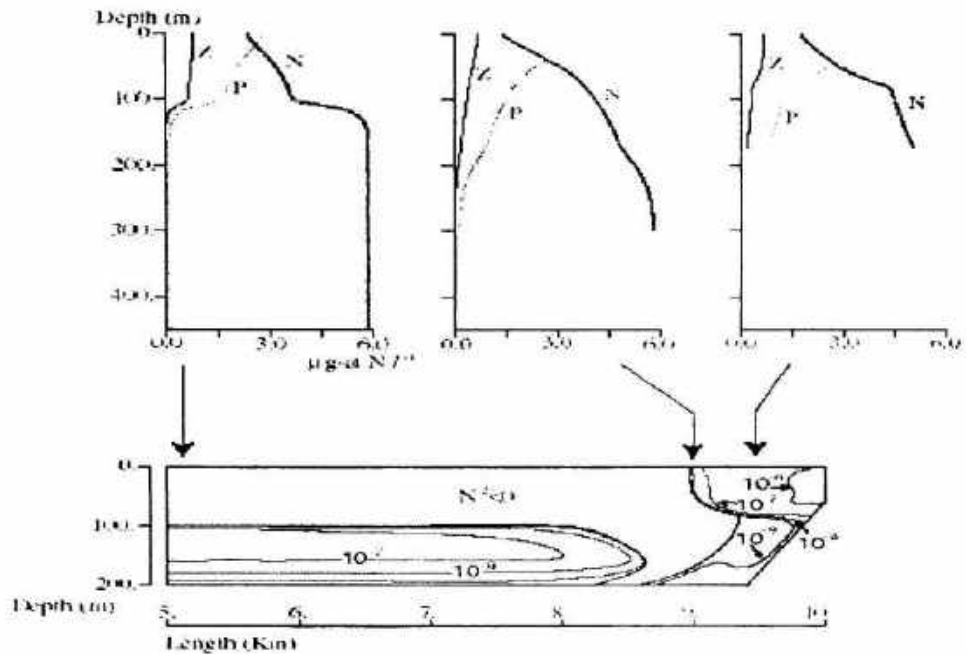


Figure 3 – Predicted results at $t=20$ days: isovalue lines of the stability frequency and vertical profiles of phytoplankton (P), zooplankton (Z) and nutrients (N) at the locations indicated by the arrows. The N, P and Z profiles are expressed in common units of nitrogen concentration.

RESULTS OF ECOHYDRODYNAMICAL INVESTIGATIONS ON LARGE SHALLOW EUTROPHIC LAKE VÖRTSJÄRV, ESTONIA IN 1995-1996

T. Nõges^{1,3}, Ä. Bilaletdin², T. Frisk², T. Huttula², A. Järvet³, H. Kaipainen², R. Kivimaa¹, O. Malve⁴, M. Möls^{1,3}, P. Nõges^{1,3}

¹ Limnological Station of Institute of Zoology and Botany, Estonian Agricultural University Rannu, 61101 Tartu County, Estonia

² Pirkanmaa Regional Environment Centre, P.O. Box 297, FIN-33101 Tampere, Finland

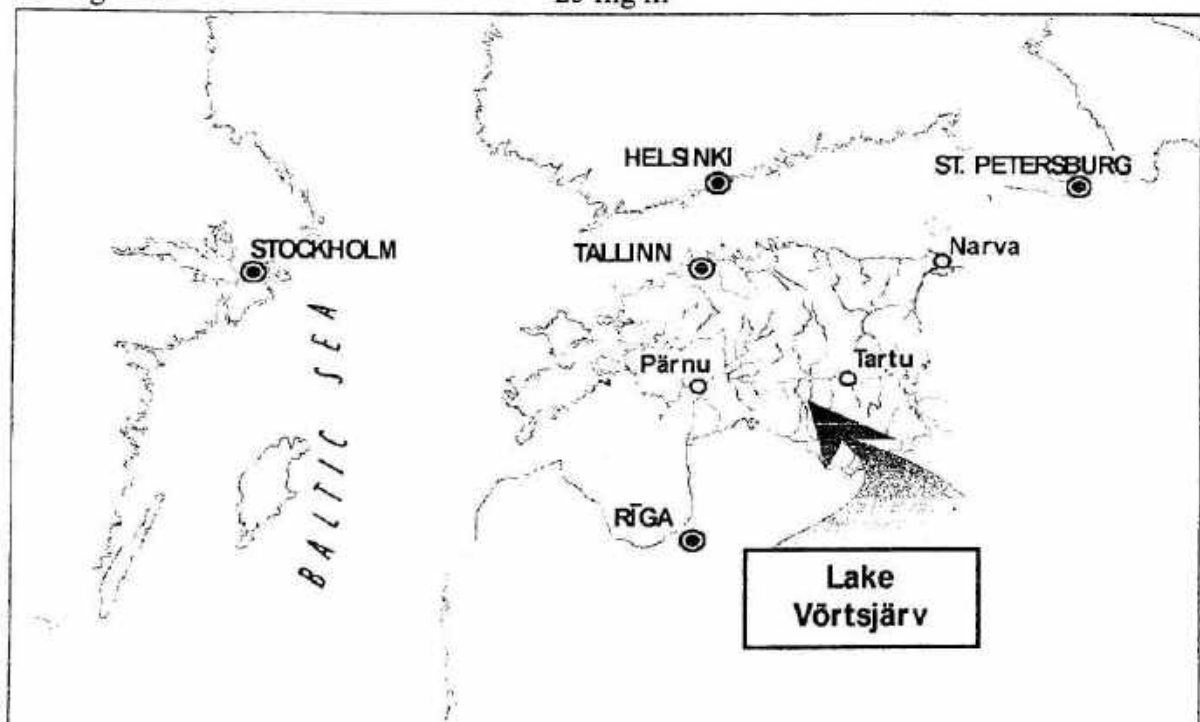
³ Tartu University, Vanemuise 46, Tartu, Estonia

⁴ Finnish Environment Institute, P.O. Box 40, FIN-00251 Helsinki, Finland

Lake Võrtsjärv is the second largest lake in the Baltic countries. It is located in the central part of Estonia in a shallow depression of preglacial origin. Through the outflowing River Emajõgi its drainage basin is connected to the watershed of Lake Peipsi-River Narva.

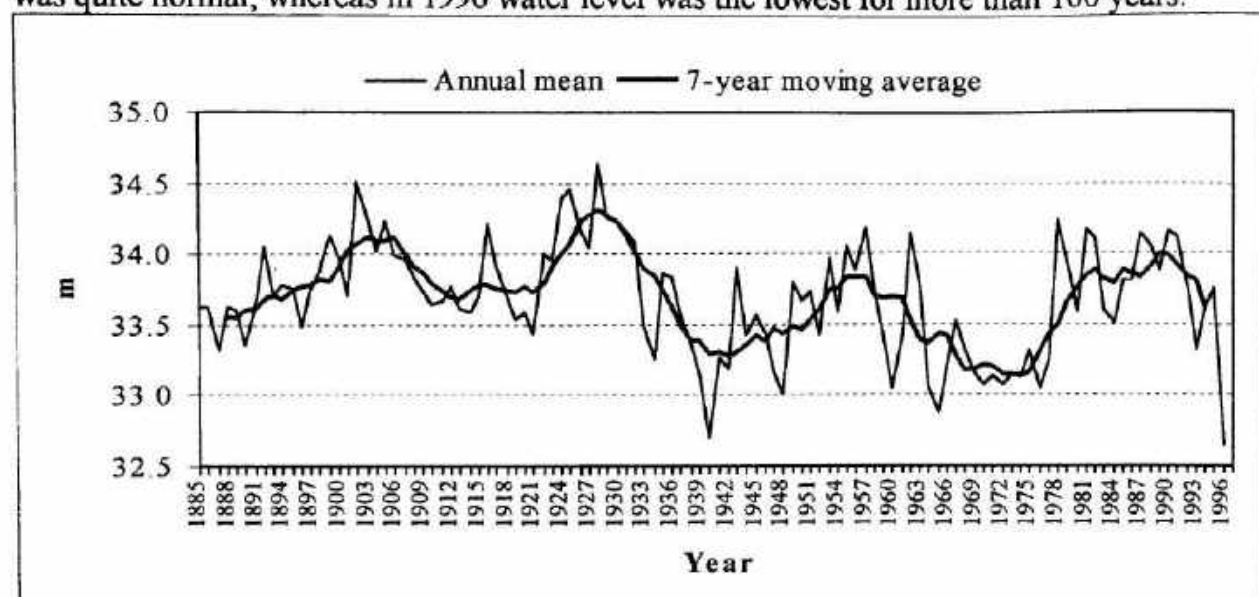
Lake Võrtsjärv

Drainage basin	3374 km ²
Area	270 km ²
Mean depth	2.8 m
Maximum depth	6 m
Annual water level fluctuations	1.4 m
Secchi Depth in summer	<1 m
Average total phosphorus	50 mg m ⁻³
Average total nitrogen	2000 mg m ⁻³
Average Chl α	25 mg m ⁻³



Location map of Lake Võrtsjärv

The hydrological conditions for investigation years were very different. Water level in 1995 was quite normal, whereas in 1996 water level was the lowest for more than 100 years:



Long-term dynamics of water level in Lake Vörtsjärv.

Ecohydrodynamical studies

- Watershed modelling

1. Steady-state modelling
2. Dynamic modelling

In runoff modelling a modification of the HBV-model (Vehviläinen, 1994) was applied. The data from 6 discharge stations, 1 water level station and 9 water equivalent stations located in L. Vörtsjärv basin were used for runoff calibration. The runoff model simulates runoff separately for open (field and bog) and forested areas, because the water quality model needs nutrient input separately from forested and agricultural areas. The calibration was done by giving extra rules for the parameters in forested and field areas. For example, the degree day component of snow melt should be greater in field area, maximum soil moisture storage is greater in forested areas and surface runoff is faster in field than in forest.

Nutrient transport model of Bilaltdin et al. (1996) was applied. In the nutrient transport calibration, the observed loading values (observed discharges and observed water quality) were explained using the constants of the nutrient transport model. The nutrient transport model simulates only the diffuse loading (agricultural and basic loading) of river basins; the point and sparse population loading were added to simulated loadings. In order to assess the proportion of bioavailable nutrient loading, the correlations between simulated total nutrients and observed nutrient fractions were calculated. The noticed fractions of nutrients were SRP and DIN.

Scenarios were formed to assess a loading situation in the future, for a period of about 10-20 years. Point source loading and basic loading were considered to be constant in the near future. Agricultural loading was assessed to increase in the future due to the rise of fertilization. Hydrological variations were taken into account in runoff scenarios as:

- dry (as 1996)
- average (as 1995)
- wet (as 1990).

9 different scenarios were developed:

Scenarios	Runoff, high (1990)	Runoff, mean (1995)	Runoff, low (1996)
Agriculture, present	x	x	x
Agriculture, 20 % increase	x	x	x
Agriculture, 50 % increase	x	x	x

- Hydrodynamical studies and modelling

1. Water velocity measurements: continuous current recording by moored current meters (Aanderaa RCM, installed at a depth of about two meters); acoustic current profiling using vessel mounted device (ADCP by RD Instruments).
2. Suspended sediment content, composition and settling velocity were studied by bottom coring, suspended sediment analyses and sedimentation traps.
3. The particle tracking technique was applied to evaluate the fate of buoyant particles from the deepest area of the lake and from the mouth of the River Tänassilma, one of the most polluted inflows, at different water level changes.
4. Hydrodynamical modelling

2D flow model was created (Podsetchine et al., 1995). Sensitivity to water level fluctuations was introduced to the model.

Particle tracking model by Jozsa et. al. (1992) was applied to the lake to simulate the fate of buoyant particles.

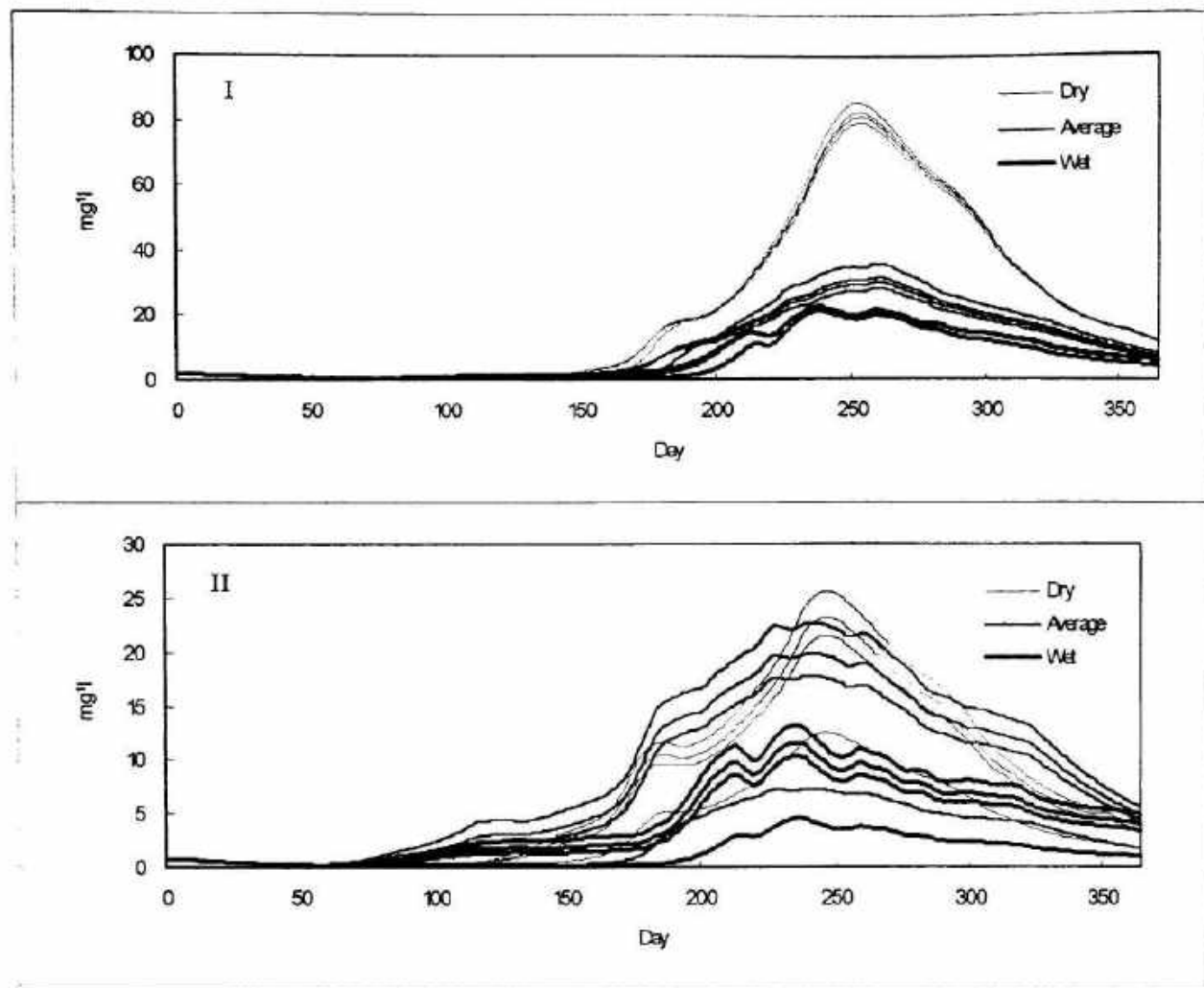
Suspended sediment transport model describes sediment as one fraction, for what the median grain size was used. 2D depth integrated description is used like in the flow model. For erosion and deposition limits, uniform values were used all over the lake. The simulated and observed daily mean SS concentrations are presented for the period May.- October. in 1995 and 1996. The model gave the highest SS peaks in May, in the middle of June and in autumn (September, October). A good agreement was found with observations in several time intervals. Also considerable discrepancies occurred. The water level impact on SS concentration and deposition (for sediment trap periods) was simulated for 1995. In lake wide scale the effect of water level change on mean SS concentrations is significant in short time scales (days and weeks), in seasonal scale it does not have so great impact. Locally the effect of water level is even more significant as can be seen from the deposition results at the deepest site of the lake. **Calculated SS concentrations were used in the water quality model to describe light limitation.**

- Ecological studies and modelling

1. Intensive data collection weekly in 1995, biweekly in 1996:
temperature, O₂, light conditions, Secchi depth,
nutrients (N, P, Si in different forms)
phyto-, zoo-, bacterioplankton (composition, biomass, productivity)

Data set was used for ecological model calibration

2. AQUASIM software was applied for ecological modelling. An ecological model was constructed using continuously stirred tank reactor (CSTR) hydraulics. Simulations using different scenarios revealed that external nutrient loading has a very small effect on biomass of cyanobacteria. The effect is clearer when diatoms are concerned. The contribution of water level to biomass is significant for both diatoms and cyanobacteria. On the basis of the simulations it can be concluded that water level is a key factor in regulating the phytoplankton biomasses of Lake Võrtsjärv.



The simulated biomasses of cyanobacteria (I) and diatoms (II) applying the different scenarios. Within each hydrological scenario the biomass curves are in logical order in relationship to loading (smaller loading - smaller biomass). In case of cyanobacteria (I) the effect of loading at the alternatives dry and average was inverse (greater loading - smaller biomass).

References

- Bilaletdin, A., Frisk, T., Vehviläinen, B., Kallio, K., Huttunen, M. & Kaipainen, H. 1996. Modelling the effects of climate change on nutrient transport from large drainage basins. In Roos, J. (Ed.): The Finnish Research Programme on Climate Change - Final Report. Publications of the Academy of Finland 7/95. pp. 173-178.
- Jozsa J., Szel S., Kontur I., 1992. Particle models for advection-dispersion-reaction phenomena in shallow lakes. In Proc. HYDROCOMP' 92, Budapest.
- Podsetchine V., Huttula T., Filatov N. 1995. Water Exchange in the Straights of Northern Ladoga: Results of Studies and Numerical Simulation. Phys. Chem. Earth, Vol 20, No 2, pp.207-213.
- Vehviläinen, B. 1994. The watershed simulation and forecasting system in the National Board of Waters and Environment. Publications of the Water and Environment Research Institute. National Board of Waters and Environment, Finland. No. 17.

OPTICAL REMOTE SENSING OF NATURAL WATERS: SOME REMARKS ON IST PRINCIBLES, POSSIBILITIES AND RESTRICTIONS

Thomas Heege

Deutsches Zentrum für Luft- und Raumfahrt (DLR)
Institut für Optoelektronik
D-82234 Weßling
Germany

1. Introduction

Spatial and temporal scales of physical and biological processes are essential properties of natural waters. Knowledge about these scales is necessary for the understanding of ecological interactions. An example is the relationship between allochthon river inputs, their distribution due to the hydrological processes and the reaction of the biological system on the permanent changing conditions of physical and chemical environment.

Remote sensing offers the best way to get spatial information on physical and biological parameters. In dependency of the repeat rate of remote sensing measurements, temporal scales of processes can be

derived. Although it is not possible to measure all relevant parameters or to derive vertical properties, many important key parameters are accessible. The following properties can be derived for natural waters:

- Surface properties and - via the surface roughness - the wind speed can be derived with radar sensors.
- Atmospheric, surface and in water optical properties are accessible using multispectral measurements from the visible to the thermal infrared wavelength region. It is possible to calculate the surface temperature, the in- and outcoming irradiances of the water body and the optical properties as weighted integral about half the euphotic zone. Using the optical properties of the water body, the concentrations of suspended matter, phytoplankton pigments and yellow substance can be calculated.

Therefore, important key parameters to characterize the biological state and the physical environment are measurable.

However, because of limited sensor or algorithm capabilities and principal restrictions, it is not always possible to derive all parameters independently. A rather obvious example is, that at cloudy conditions no information about the water body can be derived with optical measurements. Another, more complicated example is to estimate the influence of algorithm and sensor limitations on the accuracy of distinguishing between yellow substance and pigment absorption, or between sunglitter, suspended matter and aerosols.

Only with the knowledge of the system capabilities and limitations, the power of remote sensing can be fully exploited.

The second chapter shall give a short insight in principles and limitations of remote sensing of water constituents using a physically based algorithm.

The third chapter will deal with some examples of water constituents and surface temperature distribution maps, derived from the airborne multispectral scanner DAEDALUS. The potential of remote sensing is discussed according to the sensor and algorithm capabilities and limitations.

2. Principles of optical remote sensing of natural waters

The fundamental principle to derive water constituents from space is based on characteristic optical properties of water constituents. The spectral shape and intensity of the upwelling radiance (as well as the underwater reflectance) is a function of phytoplankton pigment, yellow substance and suspended matter concentrations, if the specific coefficients of absorption and scattering are constant. Therefore, variations of specific coefficients will limit the comparability of optical remote sensing data and laboratory measurements of in situ samples.

The calculation of the underwater reflectance from remote sensing data requires several sophisticated corrections of the sensor measured radiance spectra: the correction of the atmospheric influence on the measured radiances and the elimination of water surface

reflections. Taking into account, that up to 90 percent of the sensed light does not interact with the water body, and that less than 0.1 percent differences of the underwater reflection should be resolved, the importance of these corrections becomes clear.

If the atmospheric conditions are known and the water surface is flat, the underwater reflectance can be calculated from the measured radiances by the use of a radiative transfer model.

The first problem is to estimate the atmospheric conditions. The most important atmospheric parameters are the aerosol type and concentration, because these are highly variable and usually unknown. Errors in assumed aerosol concentrations lead to errors in all estimated water constituent concentrations. For the estimation of these parameters directly from the image data, we use the spectral dependency of the brightening effect due to atmospheric scattering for different viewing angles.

The second problem appears, if the measurement is disturbed by surface reflections of direct sun light. Images, which are affected by these so called sunglitter effects, look extremely inhomogenous. Uncorrected, sunglitter contaminated images at least lead to an overestimation of suspended matter. The correction of sunglitter is based on the fact, that at wavelength above 1300 nm the signal from the water body is zero. Therefore, the difference between the sensed signal including sunglitter at 1500 nm and the modelled radiance for a flat surface without surface reflections of direct sun light is the direct reflected sunglitter signal. The sunglitter signal at 1500 nm is proportional to the sunglitter signal for wavelengths in the visible part of the spectrum with the transmission ratios as proportionality factors.

After the underwater reflectance has been calculated from remote sensing data, it is possible to determine the concentrations of water constituents. This is done here by using an iterative fitting algorithm to adjust modeled and measured underwater reflectances. Direct analytic calculations are not possible because of the complexity and non-linearity of the physical processes.

Limitations or difficulties to distinguish between water constituents appear, if the spectral and radiometric resolution of the sensor is insufficient. For example, the main differences of the

absorption characteristics between phytoplankton and yellow substance are found below 300 nm and above 600 nm. Without suitable data at these wavelengths, an independent calculation of phytoplankton pigment and yellow substance concentrations is not possible.

3. Application examples

Some distributions of phytoplankton pigment, suspended matter and surface temperature above Lake Constance at several dates are demonstrated as derived from airborne DAEDALUS flights (see for example the distribution at 22.July 1996, 9:40 UTC).

The discussion will focus on

1. the limitations of the used algorithm and airborne scanner regarding the calculated distribution images.
2. the possibilities to derive informations about spatial and temporal scales of physical and biological processes in natural waters.

OPTICAL REMOTE SENSING AND CONTACT MEASUREMENTS IN ESTONIAN AND FINNISH LAKES IN 1992-98

Helgi Arst, Ants Erm, Tiit Kutser and Anu Reinart

Estonian Marine Institute,
Paldiski Road 1, 10137 Tallinn, Estonia

The marine optics group of the Estonian Marine Institute has carried out hydro-optical measurements in different water bodies (Baltic Sea, Lake Peipsi) since 1987. More systematic investigations started in summer 1992, with the main investigation objects being the Gulf of Riga, Pärnu Bay, and 12 small Estonian lakes. In 1994, a joint project with the Department of Geophysics, University of Helsinki, commenced. This co-operation has been continued up to now. From 1995 to 1997 we performed joint investigations with scientists from the Võrtsjärv Limnological Station. The aim of these projects was to estimate the ecological situation of lakes using data on their bio-optical characteristics, radiation regime, and eutrophication.

During 1992-98 nineteen Estonian and nine Finnish lakes were investigated, with the number of expeditions to different lakes varying from 1 to 17. The data gathered so far are of wider interest in a comparative sense. They not only enable a comparison of Finnish and Estonian lakes, but also demonstrate a high variability of water properties in lakes located within a rather small area.

In the present short note we consider only part of results obtained from following groups of measurements:

- 1) hydro-optical measurements *in situ*; 2) determination of optical properties of water and concentrations of optically active substances from water samples in the laboratory; 3) passive optical remote sensing (on board a boat);

Some data on two parameters characterising water transparency, Secchi disk depth (z_{SD}) and PAR-region spectrometric attenuation coefficient ($c^*_{400-700}$), are presented below. The value of c^*_λ is measured from water samples as the difference between beam attenuation coefficient of natural water and that of distilled water at the wavelength λ . The results obtained are influenced by light scattered forward within a small angle, the corresponding correction depending on scattering function of each water body. For determining this

correction we had no technical possibilities. However, the analysis of the c^*_λ spectra showed that they are rather good indicators of water transparency and quality. The values of $c^*_{400-700}$ were obtained averaging c^*_λ over PAR region of spectrum (400-700 nm).

The values of c^*_λ were determined also from the samples of filtered water, the results obtained allow to estimate the optical influence of yellow substance in the water. These results were converted into values of "effective" concentration of yellow substance, $C_{y,e}$, using the method described in Mäekivi and Arst (1996). Concentrations of chlorophyll *a*, C_{chl} , and suspended matter, C_s , were measured from water samples in the laboratory.

The downwelling vector irradiance in the PAR region, $E_d(\text{PAR})$, was measured using the underwater quantum sensor LI-192 SA. The spectra of remote sensing reflectance, r_λ , were determined by means of telespectrometers *Pegasus* (up to 1996) and ST1000 (beginning in 1997). The description of the measurement methods and predominating amount of results are published in papers by Arst and Kutser (1994), Kutser et al (1995, 1998), Mäekivi and Arst (1996), Arst et al. (1996, 1998, 1999).

Considering the whole data complex, we can see that the properties of lakes under considerations vary widely. Table 1 presents the minimum and maximum values of z_{SD} , $c^*_{400-700}$, $C_{y,e}$, C_{chl} and C_s . These data show that the variability limits of water properties can be considerably different in different lakes. However, it is hard to draw the final conclusions for one concrete lake comparing it with some other lake, because the duration of observation periods was different. The investigation of correlative relationships between z_{SD} and $c^*_{400-700}$ show the value of correlation coefficient $R = 0.89$. It leads to conclusion that the mean spectrometric attenuation coefficient is suitable as an indicator of water transparency.

The correlation coefficients of C_s , C_{chl} and $C_{y,e}$ vs. z_{SD} vary from 0.64 to 0.70, its corresponding values vs. $c^*_{400-700}$ being from 0.64 to 0.77. It is rather normal result, because the water transparency is formed under simultaneous influence of all optically active substances in the water body. The power law is suitable for description of these correlative relationships.

Some typical spectra of remote sensing reflectance (r_λ) are presented in Fig. 1. As we can see, there is a correspondence between the shape of the spectrum and the limnological type of the

water body. Note that the spectrum of hypertrophic Lake Ülemiste allows to identify the blue-green algae in the water (maxima and minima of r_λ in the region 630-700 nm).

Table 1

Minimum and maximum values of some water characteristics for lakes under investigation in 1992-98 (surface layer).

Lake	Z_{SD} m	$C^*_{400-700}$ l/m	C_{chl} mg/m ³	$C_{y,e}$ mg/L	C_s mg/L	Number of measure- ments
Estonian lakes						
Äntu Sinijärv	(15)*	0.2-1.0	0.3-0.8	1.2-4.7	2.0-7.2	5
Piigandi	4.7-6.0	1.6-1.7	1.5-2.0	4.2-5.8	2.0-5.0	3
Nohipalu Valgjärv	3.5-7.0	0.6-4.7	0.6-30	1.7-8.0	1.0-7.0	17
Kurtna Liivajärv	3.5-5.6	1.2-2.7	1.3-7.1	4.5-11	2.0-5.0	5
Kurtna Valgejärv	3.3-5.1	1.4-3.2	0.7-2.6	8.4-14.4	2.0-7.0	5
Kurtna Nõmmjärv	2.5-4.5	0.9-4.3	0.7-3.3	4.0-14.1	1.5-10	13
Koorküla Valgjärv	2.9-5.1	0.9-4.7	0.6-11.5	2.7-14	1.5-7.0	7
Rõuge Suurjärv	2.5-4.2	1.5-3.2	2.6-3.2	6.1-9.1	2.0-5.0	5
Pühajärv	2.2-3.1	1.9-3.4	2.2-10.1	6.6-7.3	1.5-7.0	4
Jõksi	2.4-3.2	2.7-3.3	4.3-11.2	10-13	3.8-6.0	5
Pangodi	2.0-2.4	2.3-3.2	2.8-15.3	4.6-7.0	3.5-8.0	5
Nõuni	1.4-2.7	2.1-4.7	2.4-8.3	5.7-8.0	5.0-7.5	5
Tamula	1.7-2.0	2.8-3.7	5.7-10.7	7.1-13	5.5-8.0	4
Verevi	0.6-3.7	1.5-8.7	4.4-108	8.1-13.8	1.0-13	17
Uljaste	1.0-3.4	1.1-6.7	1.0-46.5	8.9-18.4	3.0-16.5	9
Võrtsjärv	0.15-1.0	3.3-28.2	25-102	9.7-18	5.0-145	11
Nohipalu Mustjärv	0.4-0.8	13.7-20.1	1.7-46.5	68-150	2.0-16	14
Paukjärv	4.5-5.5	0.8-1.0	4.2-7.4	1.2-2.7	1.3-3.8	6
Ülemiste	0.5-1.75	4.2-18	13-121	6.1-30	7.6-34	76
Finnish lakes						
Puujärvi	3.0-6.0	0.7-1.8	3.6-6.1	3.8-5.5	0.6-2.3	4
Päijanne	3.5-6.5	1.3-1.9	1.3-1.7	6.7-9.6	1.4-1.5	3
Vesijärvi	1.2-3.7	1.2-5.9	1.7-26	3.4-14	1.5-10	18
Lammi Pääjärvi	1.6-3.0	2.5-5.4	3.3-13	14.6-25.2	1.0-5.2	12
Lohjanjärvi	0.7-1.75	2.1-8.4	8.5-64.5	9.5-20	2.0-18	11
Valkeakotinen	0.8-1.1	5.1-7.5	7.8-8.4	26.2-32.7	3.0-10	2
Tuusulanjärvi	0.3-0.9	8.6-18.3	8.0-68	10.8-30.6	12-37.5	6
Keravanjärvi	1.2	5.3	13.8	33.3	1.7	1
Enäjärvi	1.0	5.8	39.2	5.2	12.9	1

*) Determined in horizontal direction (the bottom was clearly seen)

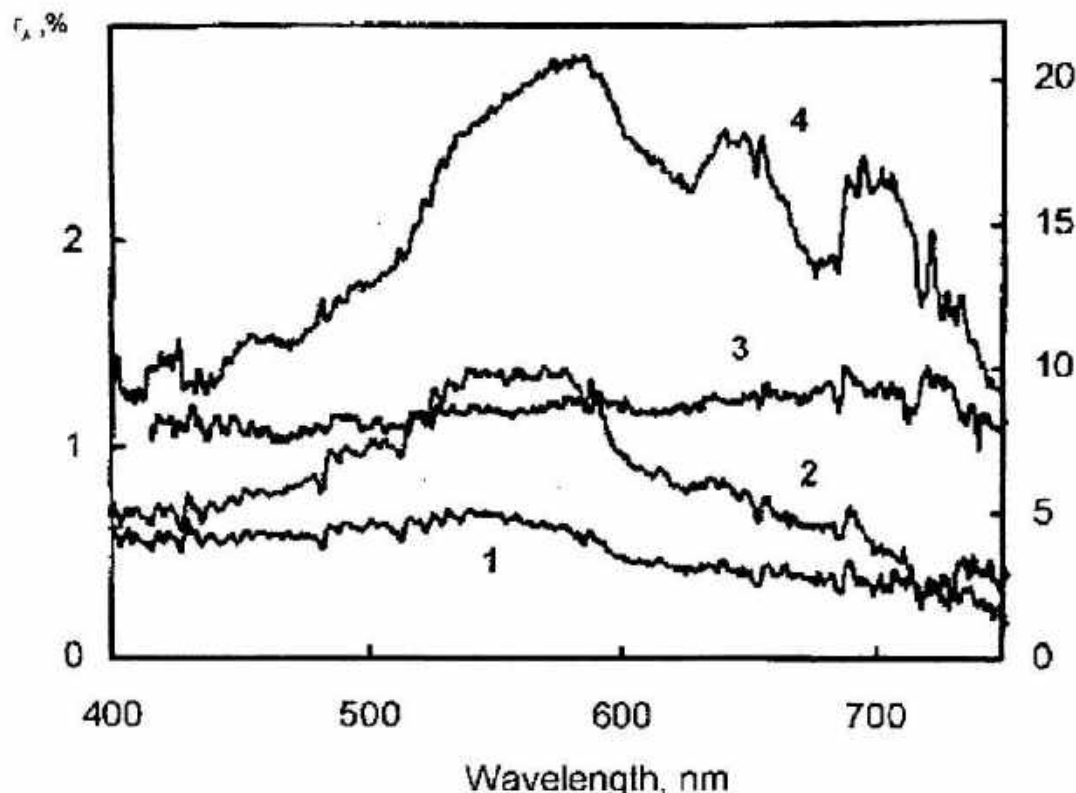


Fig.1. Some examples of remote sensing reflectance spectra for lakes belonging in different limnological types: 1 - Lake Paukjärv (oligotrophic), 11 Aug.1998; 2 - Lake Vesijärvi, station 5 (mesotrophic), 20.Aug.1998; 3 - Lake Lammi Pääjärvi, station 5 (brown-water lake), 13 Aug.1997; 4 - Lake Ülemiste, station Kurna (hypertrophic), 1 July 1997 (respective scale is in the right side of Fig.1).

General conclusions made relying on this study :

1. The investigation objects, Estonian and Finnish lakes, are very different in their optical properties. Measurements of hydro-optical, radiative, and other characteristics revealed a great variability of these characteristics, the differences being sometimes high even for lakes situated very near to each other (e.g. Nohipalu Mustjärv and Nohipalu Valgjärv). According to our measurements the chlorophyll *a* content changed from 0.3 to 121 mg m⁻³, effective amount of yellow substance from 1.2 to 150 mg L⁻¹, concentration of suspended matter from 1.1 to 145 mg L⁻¹, beam attenuation coefficient averaged over the PAR region from 0.2 to 28.2 m⁻¹, and Secchi disk depth from 0.15-7 m. Probably the range of variation of these properties (from Äntu Sinijärv to Tuusulanjärvi and Nohipalu Mustjärv) describes the variability limits for all other Estonian and Finnish lakes.
2. The spectrometric light attenuation coefficient, determined from water samples in the laboratory, and its value averaged over the PAR range are good characteristics of water

transparency. They have especially high practical importance, if measurements by Secchi disk are impossible (strong undulation, in darkness, etc.).

3. The relative amount of light energy at different depths varies remarkably from lake to lake: if in Lake Antu Sinijärv 75% of subsurface light (PAR region) penetrates to a depth of 1 m, then in Lake Verevi about 40%, in Lake Võrtsjärv -7%, and in Lake Nohipalu Mustjärv practically no light reaches this depth.
4. Comparison of the spectra of irradiance attenuation coefficient $K_d(\lambda)$ for Estonian and Finnish lakes with those for Jerlov's oceanic and coastal water types shows that only one lake is comparable with oceanic type III and only the clearest from these lakes have lower $K_d(\lambda)$ values than Jerlov's "darkest" coastal water type 9. Rather a big number of lakes show $K_d(\lambda)$ values exceeding 2-8 times those for Jerlov's type 9. It implies a necessity to elaborate a classification for lakes, additionally to ocean and coastal water classifications.
5. Correlative connections between the concentrations of optically active substances in the water and optical (including remote sensing) characteristics are mostly nonlinear and can be described by the power law. As can be expected, the correlation coefficient is higher for the sum of concentrations than for each optically active substance separately.
6. Qualitative analysis of the remote sensing spectra is able to give information for the general characterization of the water bodies (e.g. even blue-green algae can be identified). Optical classification of the water bodies, made relying on these spectra, is rather similar to limnological classification of waters.
7. Results obtained from remote sensing spectra when applying correlation method are to some extent depending on the synoptic situation and other measurement conditions. Using correlation method we derived algorithms suitable for approximate estimating the values of water transparency and concentrations of optically active substances in Estonian and Finnish waters.
8. In optically stratified lakes the remote sensing, that is being able to get information only from the surface layer of the water body, cannot describe the whole water column and give the averaged picture on the lake. Disturbing factor is also the algae bloom on the water surface. From the other side, optical remote sensing is an effective method for identification of the "blooming" areas in the sea.

9. There is a group of lakes in which extremely high concentration of yellow substance causes very strong absorption of light in these waters. As the result, the backscattering from water light is nearly zero up to the red region of spectrum (information, coming from the water is practically missing) and the shape of the remote sensing reflectance spectrum is almost entirely determined by light reflected from the water surface. For these lakes the "normal" remote sensing algorithms are not applicable.
10. In multicomponent, turbid waters the remote sensing data show very clearly large contrasts in water properties, but the relative error increases with the decrease in substance under investigation. The concentration of some substance, if it is small in comparison with others, is often impossible to determine.
11. Solving the optical remote sensing inverse problem by the method of modelling of the remote sensing spectra needs adequate data on the spectral values of the light backscattering coefficient for different type of water bodies. In coastal and inland waters these values can vary in great extent and their measuring is complicated. According to our data the values of backscattering coefficient in turbid waters can be up to two orders higher in comparison of those for clear waters.

Acknowledgements. The authors are indebted to the Estonian Science Foundation (grants 252, 751, 1804) and to the Academy of Finland for financial support to this investigation.

References.

- H.Arst, T.Kutser, 1994. Data processing and interpretation of sea radiance factor measurements. *Polar Res.*, **13**, 3-12.
- T.Kutser, H.Arst, T.Miller, L.Käärman, A.Milius, 1995. Telespectrometrical estimation of water transparency, chlorophyll-a and total phosphorus concentration of Lake Peipsi. *Int.J.Remote Sensing*, **16**, 3069-3085.
- S.Mäekivi, H.Arst, 1996. Estimation of the concentration of yellow substance in natural waters by beam attenuation coefficient spectra. *Proc. Estonian Acad. Sci., Ecology*, **6**, 108-123.
- H.Arst, S.Mäekivi, T.Kutser, A.Reinart, A.Blanco-Sequeiros, J.Virta, P.Nõges, 1996. Optical investigation of Estonian and Finnish lakes. *Lakes. Reserv. Manage.* **2**, 187-198.
- H.Arst, S.Mäekivi, A.Reinart, T.Kutser, K.Kallaste, A.Blanco-Sequeiros, P.Nõges, T.Nõges, 1998. Water properties in some regions of the Baltic Sea and in different type of lakes in Estonia and Finland. In: *Report Series in Geophysics*, No 38, 7-21.
- T.Kutser, H.Arst, S.Mäekivi, K.Kallaste, 1998. Estimation of the water quality of the Baltic Sea And Lakes in Estonia and Finland by passive optical remote sensing measurements on board vessel. *Lakes Reserv. Manage.* **3**, 53-66.
- H.Arst, A.Erm, K.Kallaste, S.Mäekivi, A.Reinart, A.Herlevi, P.Nõges, T.Nõges, 1999. Investigation of Estonian and Finnish lakes by optical measurements in 1992-97, *Proc. Estonian Acad. Sci., Biol. Ecol.*, **46**, 5-24.

SEASONAL DYNAMICS OF PHYTOPLANKTON, SUSPENDED SOLIDS AND CHEMICAL OXYGEN DEMAND IN LAKE VÖRTSJÄRV AND THEIR REFLECTION IN HYDRO-OPTICAL PARAMETERS

Peeter Nõges and Tiina Nõges

Limnological Station of Institute of Zoology and Botany, Estonian Agricultural University Rannu,
61101 Tartu County, Estonia

Introduction

The present paper is based on investigations made in 1995 on the shallow eutrophic Lake Võrtsjärv (Estonia). The lake area is 270 km² and the mean depth 2.8 m. The water level in the lake is strongly fluctuating: the difference between the seasonal maximum (usually at flood peak in April - May) and minimum (usually in September) makes up one half of the lakes mean depth (1.4 m). The runoff waters in spring often enrich the lake with humic substances turning the water color yellow or brown. Phytoplankton development starts at the time of ice-break and reaches its seasonal maximum in autumn in September or October. The late biomass maximum can be explained, on one hand, by the improvement of light conditions in the water column when the water level is low, but, on the other hand, the stronger resuspension of sediments in shallow water intensifies nutrient cycling and prevents sedimentation of algae. We studied, in which way the different seasonal behaviour of dissolved and suspended matter was reflected in diffuse attenuation coefficient and in beam attenuation coefficient spectra of nonfiltered and filtered water.

Material and methods

Data were collected weekly in 1995 from the main monitoring station in L. Võrtsjärv. Chemical oxygen demand (COD) was measured in unfiltered water using two different oxydizers: potassium permanganate and potassium bichromate resulting in COD_{Mn} and COD_{Cr}, accordingly. The amount of total suspended solids (TSS) was measured by weight difference of dried at 105°C glass-fiber filters (Watman GFF) before and after filtering of a certain amount of lake water. Phytoplankton biomass (Bfp) was determined microscopically by cell count and volume calculations (the specific weight was taken equal to 1 g/ml). Chlorophyll a (Chl a) as the most common biomass equivalent was measured spectrophotometrically in acetone extract using the equations of Jeffrey and Humphrey (1975). The beam attenuation coefficient (E) in unfiltered (UF) and filtered (F) water was measured spectrophotometrically in 5 cm cuvettes at wave lengths from 340 to 400 nm. The change in beam attenuation caused by filtration (UF-F) was analysed as an independent variable. The diffuse attenuation coefficient (K_d) was measured using a spherical photometer FM1 constructed at Tartu University according to the drawings by Williams & Jenkinson (1980).

Results

Both indices of chemical oxygen demand (COD_{Cr} and COD_{Mn}), which characterize the organic matter content of water, were the most stable among all measured variables (Cvar accordingly 20% and 14%, see Table 1). COD_{Cr} demonstrated no seasonal trend. Almost equal peaks (46-47 mgO/l) occurred in May, October and November. It was significantly positively correlated with TSS and Chl a, but with none of the measured optical variables.

COD_{Mn} formed on the average 38% of COD_{Cr} and had its maximum in March at the time of the first flood peak. No correlation was found between these two indices of organic

matter. COD_{Mn} correlated significantly with beam attenuation coefficient of filtered water, although the correlation was not very strong ($r=0.48$, see Fig. 1).

The amount of TSS reached its maximum in the second half of the year. It correlated positively with Chl a and phytoplankton biomass and negatively with the water level in the lake. As could be expected, the change in beam attenuation caused by filtration of water was in good accordance with the content of suspended solids in it (Fig. 2).

Diatoms from the genus *Aulacoseira* were dominating in the biomass of phytoplankton from March until the end of May. After that cyanobacteria got the leading position: first *Limnothrix redekei* in June which was overcome by *L. planctonica* since the middle of July. The latter kept its leading role until the end of the year. Both the phytoplankton biomass and Chl a as its chemical equivalent reached their maxima in October. The correlation between these variables was strong ($r=0.90$). Forming one part of total suspended solids, phytoplankton had a similar but weaker relation with the UF-F difference in beam attenuation.

Table 1. General statistics of measured variables

Variable	Unit	MIN	MAX	AVG	STD	Cvar %
COD _{CR}	mgO/l	21	47	36	7	20
COD _{Mn}	mgO/l	10	17	13	2	14
Bfp	mgWW/l	1	57	18	12	67
Chla	µg/l	5	64	31	13	42
TSS	mg/l	4	33	16	7	47
S	m	0.6	1.8	0.90	0.28	30
K _d	1/m	1.33	3.17	2.05	0.49	24
E340 F	1/m	3.28	15.00	6.10	2.45	40
E350 F	1/m	2.92	11.40	5.45	2.15	40
E360 F	1/m	2.34	10.00	4.68	1.92	41
E370 F	1/m	1.78	8.60	3.95	1.67	42
E380 F	1/m	1.38	7.44	3.28	1.44	44
E390 F	1/m	1.04	6.68	2.76	1.26	46
E400 F	1/m	0.50	6.00	2.29	1.16	51
E340 UF	1/m	5.90	15.18	10.89	2.14	20
E350 UF	1/m	5.50	13.84	10.21	2.15	21
E360 UF	1/m	5.00	12.50	9.29	1.97	21
E370 UF	1/m	4.42	11.78	8.43	1.91	23
E380 UF	1/m	3.94	11.38	7.67	1.85	24
E390 UF	1/m	3.58	10.88	7.06	1.86	26
E400 UF	1/m	3.26	10.44	6.51	1.88	29
E340 UF-F	1/m	0.06	10.10	4.79	2.51	52
E350 UF-F	1/m	0.22	10.06	4.77	2.45	51
E360 UF-F	1/m	0.24	9.84	4.61	2.35	51
E370 UF-F	1/m	0.68	9.62	4.48	2.30	51
E380 UF-F	1/m	0.82	9.32	4.39	2.27	52
E390 UF-F	1/m	0.76	9.22	4.27	2.28	53
E400 UF-F	1/m	0.82	9.10	4.21	2.27	54

The diffuse attenuation coefficient K_d was directly related with none of the nonoptical parameters, but a rather good accordance could be observed in the seasonal patterns of K_d and the beam attenuation in unfiltered water ($r=0.68$, Fig. 3). Both of these optical

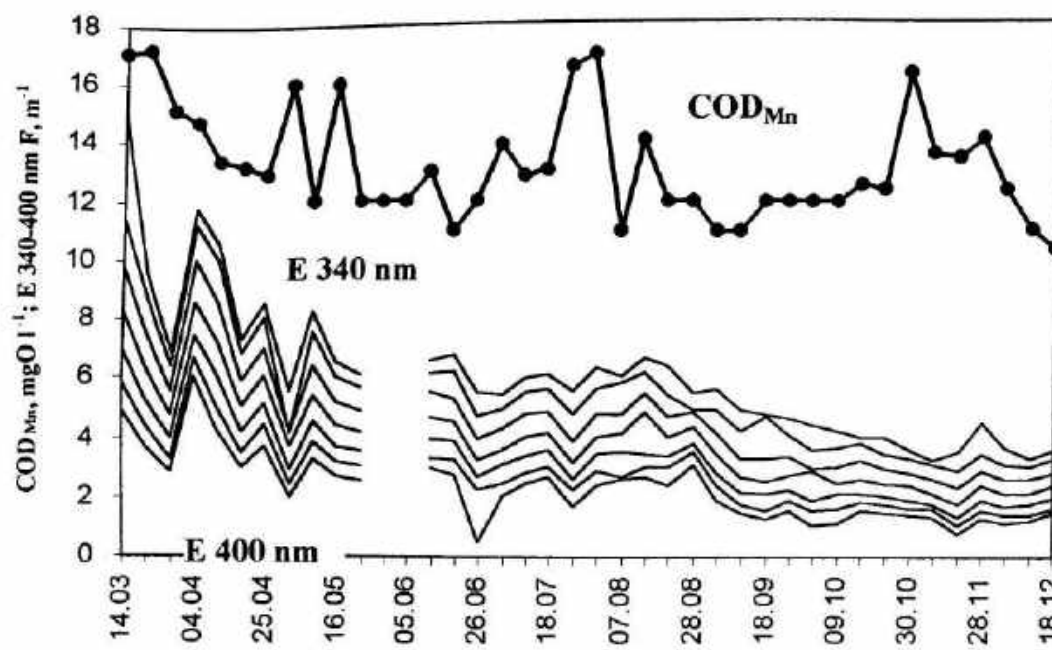


Figure 1. Permanganate oxygen demand and beam attenuation in filtered water

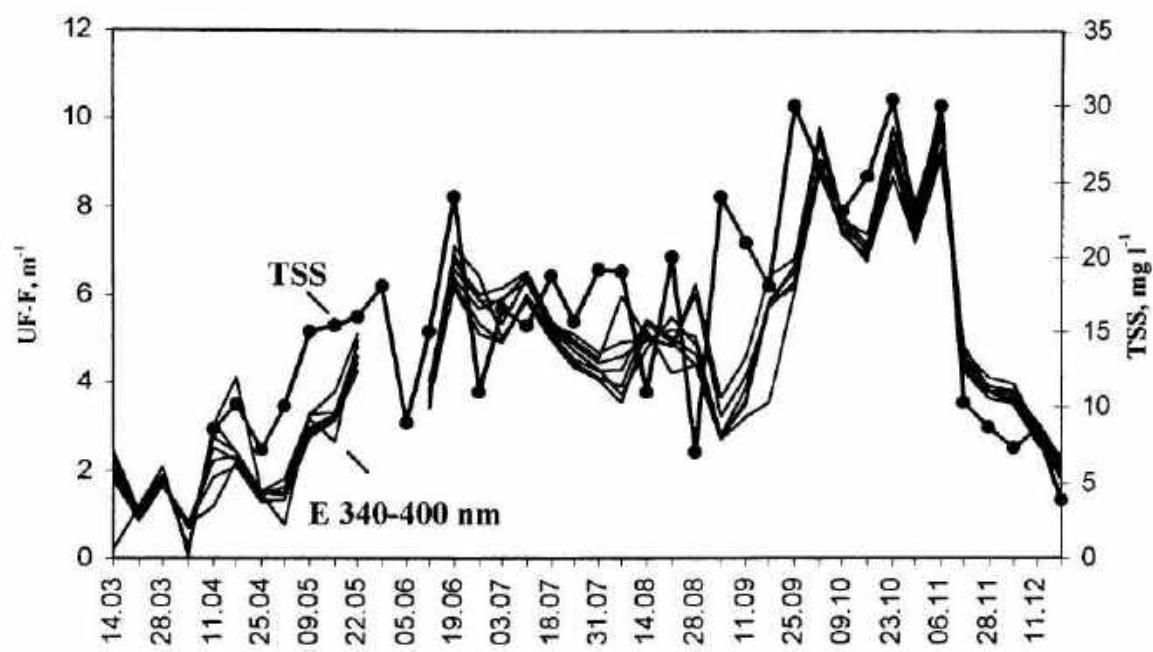


Figure 2. Total suspended solids and the change in beam attenuation coefficients caused by filtration of water

parameters as well as the Secchi depth (S) had a rather small seasonal variability in the range of 20-30% (Table 1). Among beam attenuation measurement the dependence on wave length was the strongest in filtered water (Fig. 1) while the UF-F series had almost equal spectral sensitivity (Fig. 2).

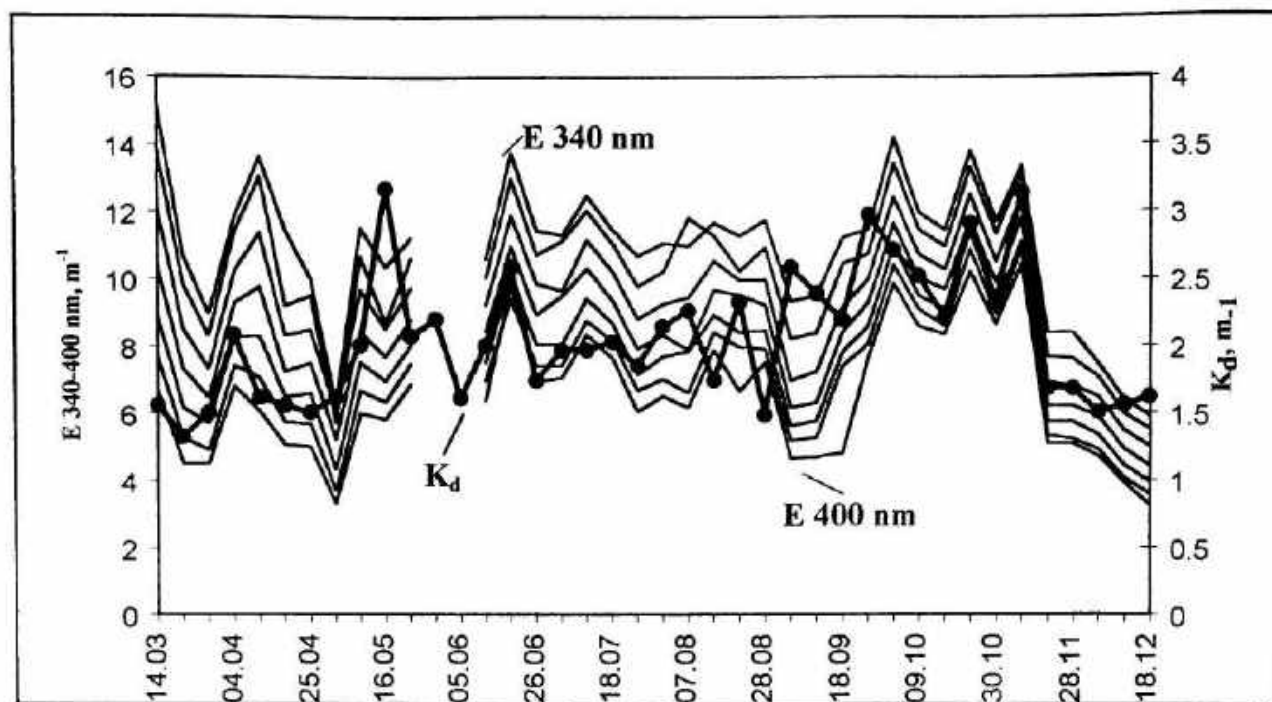


Figure 3. Diffuse vertical light attenuation coefficient (K_d) and beam attenuation coefficient in unfiltered water

Discussion

Strong seasonal polarity of dissolved and particulated matter in Lake Võrtsjärv, the first having its maximum in spring and the second in late autumn, could be detected only by appropriate optical measurements that allowed to distinguish between these different optically active components. Beam attenuation in filtered water in the blue part of the spectrum is widely used for detecting the so-called "yellow substances" in the water (Højerslev, 1980; Mäekivi & Arst, 1996). Among chemical methods the results of COD_{Mn} depend mainly on the content of humic compounds as more easily oxidised organic component in the water (Simm, 1975), but can be affected by the presence of particulate organic matter. The correlation between COD_{Mn} and beam attenuation in filtered water could have been probably stronger if also the chemical method would have been applied to filtered water. In COD_{Cr} , K_d , S or beam attenuation in filtered water, the seasonally polarised dissolved and particulate component compensate each other resulting in a more stable and smooth behaviour of these integrating variables.

References

- Højerslev, N.K. 1980. On the origin of yellow substance in the marine environment. - Univ. Copenhagen Inst. Phys., Oceanogr. Rep. 42.
- Jeffrey, S.W. & Humphrey, G.F. 1975. New spectrophotometric equations for determining chlorophylls a, b, c_1 and c_2 in higher plants, algae and natural phytoplankton. - Biochem. Physiol. Pflanzen 167: 191-194.
- Mäekivi, S. & Arst, H. 1996. Estimation of the concentration of yellow substance in natural waters by beam attenuation coefficient spectra. - Proc. Estonian Acad. Sci., Ecol. 6: 108-123.
- Simm, H. 1975. Eesti pinnavete hüdrokeemia. Valgus, Tallinn, 200 pp.

DIEL VARIABILITY OF UV ABSORPTION COEFFICIENT IN THE SEA SURFACE MICROLAYER IN THE GDAŃSK BASIN

Lucyna Falkowska¹, Sławomir Kaczmarek², Dorota Burska¹

¹ Institute of Oceanography, University of Gdańsk

² Institute of Oceanology Polish Academy of Sciences, Sopot

The vanishing ozone layer in the atmosphere and amplified solar radiation reaching the Earth surface stimulated oceanographic research on light, especially ultraviolet radiation, penetration in the sea water and on radiation effects on biological and chemical processes.

Studies and experiments carried out in the marine environment in recent years clearly pointed out that biological damage increases exponentially with decreasing wavelengths within the UV radiation band, small decreases in stratospheric ozone translate into rather large increases in biologically-damaging radiation. Sea surface microlayer absorbs a handsome part of the solar energy, though it represents only 1 part in 10^6 of the total euphotic zone. The commonly observed accumulation of DOM and the presence of many neustonic species in the sea surface microlayer are the main factors affected by light absorption and responsible for, besides thermal stratification, fundamental changes in MO cycling through DOC-included changes in light attenuation and depth distribution of planktonic organisms. DOC is an important source of carbon for bacterioplankton and the major driver of energy in the ecosystem. In relation to UV radiation, high DOC concentrations are liable to intensify the growth of bacterioplankton population by mitigating the potential UV damage and by releasing labile organic components during photobleaching. On the other hand, low concentrations of DOC and a decrease of absorption potential that lead to increased extension of UV penetration in sea water can result in photosynthesis inhibition and increased rate of respiratory breakdown of organic matter.

Environmental study of diel variability of absorption coefficients within UV and VIS bands were carried out in the open sea part of the Gdańsk Basin in May 1995 and October 1998. Three samples were collected simultaneously from the sea surface microlayer differing with the width: 10, 90 and 250 μm during the first experimental period and a sample from the subsurface (15 cm depth) layer. During the second experimental period, only one microlayer sample, 90 μm , was collected together with the subsurface sample. The samples were taken every 2 h and immediately filtered through Whatman GF/F (May 1995) or Sartorius (0.22 μm

mesh) (October 1998) filters. Absorption spectra were taken in a double-beam UV/VIS spectrometer against redistilled water (deionized on Milli-Q column).

The results of diel variations of absorption coefficient analysis from May 1995 showed that maximal coefficient values were found in the uppermost ($10\text{ }\mu\text{m}$) layer (Fig.1) and these values decreased with the layer width (Fig.2). This being an evidence of stronger accumulation of dissolved organic carbon within the surface film in comparison to subsurface layer, hence the evidence of stratified distribution of chemical substances responsible for light absorption within the sea surface microlayer.

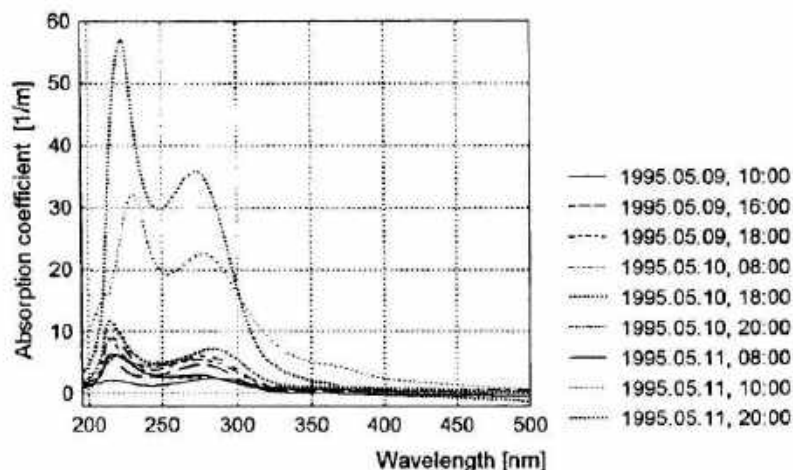


Fig.1 Differences in absorption coefficients between $10\text{ }\mu\text{m}$ sea surface microlayer and subsurface water

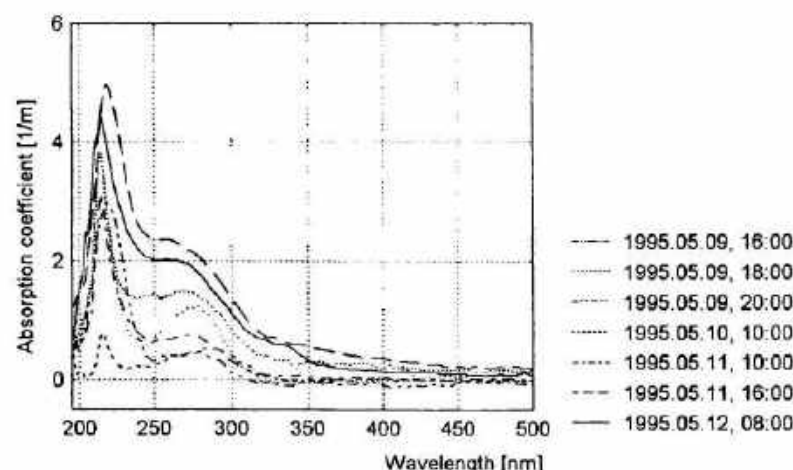


Fig.2 Differences in absorption coefficients between $250\mu\text{m}$ sea surface microlayer and subsurface water

The maximal absorption coefficients were found in the morning and in the afternoon, while around the high noon the absorption coefficients decreased considerably in each of the analysed microlayers. Simultaneously an increase of absorption coefficients was observed in

the subsurface water (Fig.3). It was found out that around noon the UV-B radiation is so strong

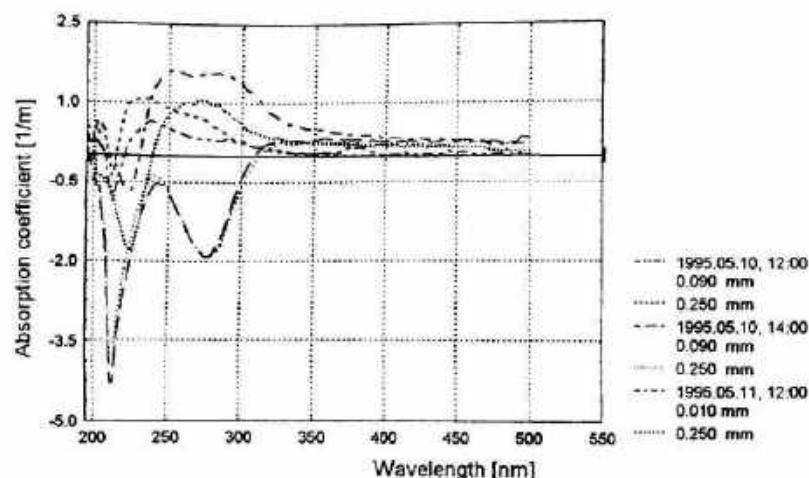


Fig.3 Differences in absorption coefficients between selected sea surface microlayer and subsurface water at noon

that photochemical oxidation of enzymes reduces the rate of photosynthesis and substances produced in photosynthesis are quickly utilized by augmented respiration. Photodegradation is the main mineralization mechanism of labile fractions of DOC in the sea surface microlayer. Biodegradation by bacterioneuston, containing e.g. carotenoids, is also possible because frequently maximal abundance of these organisms in the sea surface microlayer coincided with the maximal solar radiation period. However in general, high doses of radiation inhibit photosynthesis, chlorophyll becomes etiolated and neuston organisms phototax to deeper water layers, where the radiation is considerably attenuated. The well marked decrease of differences in absorption coefficients between 90 μ m microlayer and subsurface water was observed around the noon even in October (1998). The peak of maximal differences was shifted towards the shorter wavelengths, probably corresponding to more resistant fractions of DOC (Fig.4).

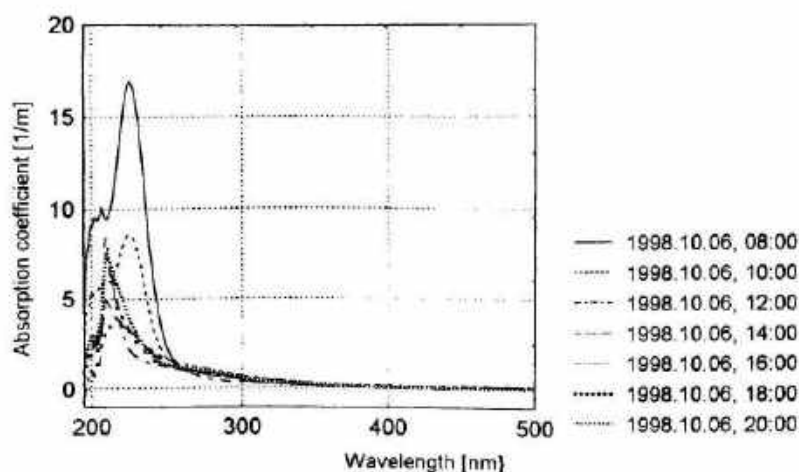


Fig.4 Differences in absorption coefficients between 90 μm sea surface microlayer and subsurface water in daytime

At night, absorption coefficients took measurements of DOC concentration supported the observation of microlayer impoverishment at night. DOC concentrations in subsurface water reached the maximum of about 69.0 mg·dm⁻³, while in the microlayers of 250, 90 and 10 μm they were 26.4, 26.0 and 17.2 mg·dm⁻³, respectively.

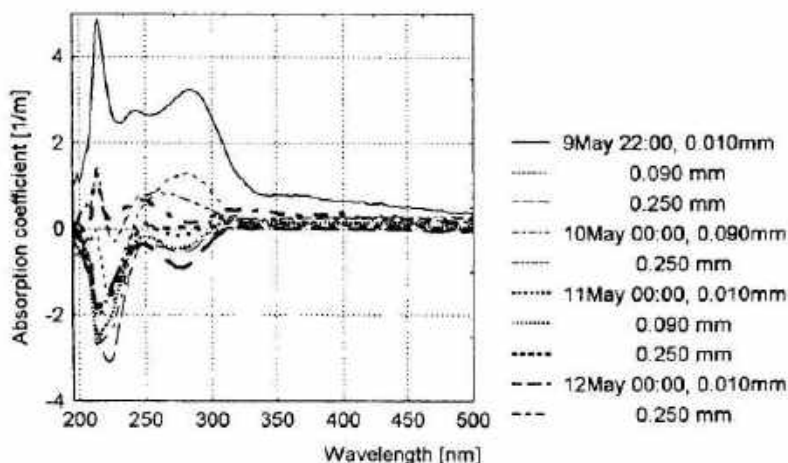


Fig.5 Differences in absorption coefficient between sea surface microlayer and subsurface water at midnight

Diel fluctuations of absorption coefficient at $\lambda = 400$ nm in the selected microlayers point out to considerable variability of this coefficient and the most intensive absorption of light within the thinnest microlayer, the one in close proximity of surface film. Absorption coefficient in surface water at wavelength 400 nm is included in algorithms used in satellite research (SeaWiFS). It seems likely that the "microlayer effect" is seen as changes in the blue part of absorption spectrum. The mean $a_{(400)}$ is 0.76 m⁻¹ in the southern Baltic water, thus taking into account the differences between absorption coefficients (Tab.1), correction of absorption coefficient in the thinnest, 10 μm , microlayer should increase its value of about 60%, excluding the high noon and midnight values.

Table 1. Statistical evaluation in differences of absorption coefficient $\lambda = 400\text{nm}$ between microlayer and subsurface water.

	May 1995			October 1998
	10 μm	90 μm	250 μm	90 μm
sample size	28	15	33	12
mean	0.459	0.153	0.106	0.133
min.	-0.271	-0.525	-0.651	0.037
max.	2.139	0.863	0.548	0.244

The greatest increments of absorption coefficient are to be expected during spring, because of the most intensive phytoplankton blooming and simultaneously the greatest increments of radiation doses within UV-B in comparison to autumn. Although in May 1995 no measurements of solar radiation were done, such measurements carried out in May and June 1998 and 1999 indicated nearly 2-fold increase in comparison to October (Fig.6).

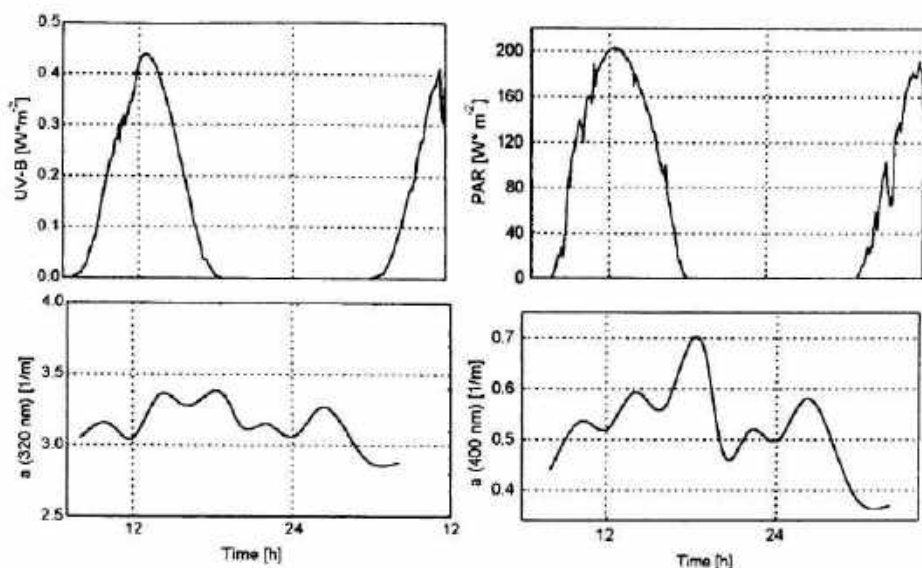


Fig.6. Diel fluctuations of absorption coefficient $a_{(400)}$ and radiation within PAR and UV-B in October 1998.

Following the suggestions of Williamson et al. (1999), absorption coefficient at $\lambda = 320 \text{ nm}$ (the boundary between UV-b and UV-A radiation) is considered a metric measure of coloured DOC (CDOC) in natural water. It reflects (much better than the $a_{(400)}$ coefficient) the important role of CDOC in mediating the impact of many anthropogenic stressors as contamination by mercury and toxic organics, input of nutrients and allochthonous matter, increase UV radiation and global warming.

LIST OF PARTICIPANTS

NAME	INSTITUTE/ ADDRESS	e-mail
Arst, Helgi, Dr	Estonian Marine Institute Paldiski road 1 10137 Tallinn, Estonia	helgi@phys.sea.ee
Bäuerle, Erich, Dr	Limnological Institute, University of Constance Mainaustrasse 212, D-78457 Konstanz Germany	erich.baeuerle@uni-konstanz.de
Boehrner, Bertram, Dr	UFZ-Gewässerforschung Brückstrasse 3a, D-39114 Magdeburg Germany	boehrner@monimo.gm.ufz.de
Elo, Aija-Riitta, Dr	Dept. of Geophysics, University of Helsinki Department of Geophysics P.o.Box 4 (Fabianinkatu 24 A) FIN-00014	Aija-Riitta.Elo@Helsinki.FI
Erm, Ants, Dr	Estonian Marine Institute Paldiski road 1 10137 Tallinn, Estonia	ants@phys.sea.ee
Hamblin, Paul, Dr	National Water Research Institute 867 Lakeshore Rd., Burlington, Ontario L7R 4A6 Canada	paul.hamblin@cciw.ca
Heege, Thomas, Dr	German Aerospace Center (DLR), Institut für optoelektronik DLR, Postfach 1116, D-82234 Wessling Germany	thomas.heege@dlr.de
Heinloo, Jaak, Dr	Estonian Marine Institute Paldiski road 1 10137 Tallinn, Estonia	jaak@phys.sea.ee
Herlevi, Antti, Dr	Dept. of Geophysics, University of Helsinki Department of Geophysics P.o.Box 4 (Fabianinkatu 24 A) FIN-00014	antti.herlevi@helsinki.fi

Ilmberger, Johan	Institut für Umweltphysik, Universität Heidelberg INF 229 Universität Heidelberg	ilm@uphys1.uphys.uni-heidelberg.de
Kaczmarek, Slawomir, Dr	Institute of Oceanology PAS ul. Powstancow Warszawy 55, 81-712 Sopot, P.O. Box 68	kaczmar@iopan.gda.pl
Kaup, Enn, Dr	Estonian Institute of Geology, Estonia 7, 10137, Estonia	kaup@gi.ee
Kay, Anthony, Dr	Department of Mathematical Sciences, Loughborough University Leicestershire, LE11 3TU, England	A.Kay@Lboro.ac.uk
Klusek, Zygmunt, Dr	Institute of Oceanology PAS Sopot, ul. Powstancow w-wy 55, Poland	klusek@iopan.gda.pl
Kushnir, Vladimir M., Dr	Marine Hydrophysical Institute. 2 Kapitanskaya st., Sevastopol 335000 Ukraine	suvorov@mhi2.sebastopol.ua
Laanearu, Janek	Estonian Marine Institute Paldiski road 1 10137 Tallinn, Estonia	janek@phys.sea.ee
Lemmin, Ulrich, Dr	LHR-DGC; EPFL CH-1015 Lausanne Switzerland	ulrich.lemmin@epfl.ch
Lilover, Madis-Jaak, Dr	Estonian Marine Institute Paldiski road 1 10137 Tallinn, Estonia	madis@phys.sea.ee
Lorke, Andreas, Dr	UFZ Centre for Environmental Research; Dept. Inland Water Research Brückstraße 3A 39114 Magdeburg Germany	lorke@gm.ufz.de

Nõges, Peeter, Dr	Institute of Zoology and Hydrobiology, Tartu University & Institute of Zoology and Botany, Estonian Agricultural University 61101, Rannu, Tartu District, Estonia	tnoges@zbi.ee
Nõges, Tiina Dr	Institute of Zoology and Hydrobiology, Tartu University & Institute of Zoology and Botany, Estonian Agricultural University 61101, Rannu, Tartu District, Estonia	tnoges@zbi.ee
Pulkkinen, Kari, Dr	Dept. of Geophysics, University of Helsinki Department of Geophysics P.o.Box 4 (Fabianinkatu 24 A) FIN-00014	kari.pulkkinen@helsinki.fi
Rannat, Kalle	Estonian Marine Institute Paldiski road 1 10137 Tallinn, Estonia	kr@teleport.ee
Reinart, Anu	Estonian Marine Institute Paldiski road 1 10137 Tallinn, Estonia	anur@physic.ut.ee
Semovski, Sergei V., Dr	Limnological Institute SB RAS Ulan-Batorskaya 3 P.O.Box 4199 Irkutsk 664033 Russia	semovsky@lin.irk.ru
Shimaraev, Michail N., Dr	Limnological Institute SB RAS Ulan-Batorskaya 3 P.O.Box 4199 Irkutsk 664033 Russia	shimarajev@lim.irk.ru
Siplegas, Liis	Estonian Marine Institute Paldiski road 1 10137 Tallinn, Estonia	liis@phys.sea.ee
Stipa, Tapani, Dr	Department of Geophysics, University of Helsinki Department of Geophysics P.o.Box 4 (Fabianinkatu 24 A) FIN-00014	Tapani.Stipa@iki.fi

Zaharov, Vladimir, Y. Dr	Udmurt State University, Universetskaja st., 1, Izhevsk, 426034, Russia	vz@eco.uni.udm.ru
Tobias, Jonas	Swiss Federal Institute of Environmental Science and Technology (EAWAG) and Swiss Federal Institute of Technology (ETH) CH-8600 Dübendorf, Switzerlan	jonas@eawag.ch
Toompuu, Aleksander, Dr	Estonian Marine Institute Paldiski road 1 10137 Tallinn, Estonia	alex@phys.sea.ee
Tsvetova, Elena, Dr	Institute of Computational Mathematics and Mathematical Geophysics SD RAS prospect Lavrent'eva 6, Novosibirsk 630090 Russia	tsvet@OMMFAO.sccc.ru
Umlauf, Lars, Dr	Institut fuer Mechanik AG 3, Fachbereich Mechanik, TU Darmstadt, Hochschulstrasse 1, 64293 Darmstadt Germany	umlauf@mechanik.tu-darmstadt.de
Virta, Hanna	Department of Geophysics, University of Helsinki Department of Geophysics P.o.Box 4 (Fabianinkatu 24 A) FIN-00014	Hanna.Virta@Helsinki.Fi
Virta, Juhani, Dr	Department of Geophysics, University of Helsinki Department of Geophysics P.o.Box 4 (Fabianinkatu 24 A) FIN-00014	Juhani.Virta@Helsinki.Fi
Wüest, Alfred, Dr	Swiss Federal Institute of Environmental Science and Technology (EAWAG) and Swiss Federal Institute of Technology (ETH) CH-8600 Dübendorf, Switzerlan	wuest@eawag.ch